

1-1-2007

Modelling the advanced oxidation of the pharmaceutical compound metronidazole in single- and multi-lamp tubular photoreactors

Melody Blythe Johnson
Ryerson University

Follow this and additional works at: <http://digitalcommons.ryerson.ca/dissertations>



Part of the [Chemical Engineering Commons](#)

Recommended Citation

Johnson, Melody Blythe, "Modelling the advanced oxidation of the pharmaceutical compound metronidazole in single- and multi-lamp tubular photoreactors" (2007). *Theses and dissertations*. Paper 243.

318'9 7000

TD
477
466
2007

MODELLING THE ADVANCED OXIDATION OF THE PHARMACEUTICAL
COMPOUND METRONIDAZOLE IN SINGLE- AND MULTI-LAMP TUBULAR
PHOTOREACTORS

by

Melody Blythe Johnson, B.Eng. (Ryerson University, 2004)

A thesis

Presented to Ryerson University

in partial fulfillment of the
requirements for the degree of
Master of Applied Science
in the Program of
Chemical Engineering

Toronto, Ontario, Canada, 2007

© Melody Johnson 2007

UMI Number: EC54190

INFORMATION TO USERS

The quality of this reproduction is dependent upon the quality of the copy submitted. Broken or indistinct print, colored or poor quality illustrations and photographs, print bleed-through, substandard margins, and improper alignment can adversely affect reproduction.

In the unlikely event that the author did not send a complete manuscript and there are missing pages, these will be noted. Also, if unauthorized copyright material had to be removed, a note will indicate the deletion.

UMI[®]

UMI Microform EC54190
Copyright 2009 by ProQuest LLC
All rights reserved. This microform edition is protected against
unauthorized copying under Title 17, United States Code.

ProQuest LLC
789 East Eisenhower Parkway
P.O. Box 1346
Ann Arbor, MI 48106-1346

ABSTRACT

MODELLING THE ADVANCED OXIDATION OF THE PHARMACEUTICAL COMPOUND METRONIDAZOLE IN SINGLE- AND MULTI-LAMP TUBULAR PHOTOREACTORS

Master of Applied Science in Chemical Engineering (2007)

Melody Blythe Johnson, B.Eng. (Ryerson University, 2004)

Department of Chemical Engineering

Ryerson University, Toronto

A model was developed to predict the removal of metronidazole utilizing the UV/H₂O₂ AOP. The rate constant for the reaction between metronidazole and the hydroxyl radical was determined to be $1.98 \times 10^9 \text{ M}^{-1}\cdot\text{s}^{-1}$. The model was able to predict an optimal initial H₂O₂ dose, and the inhibitory effects of high H₂O₂ doses and bicarbonate ions in the aqueous solution. Simulations were run for three reactors, at various influent H₂O₂ doses and reactor radii, treating a 6 μM solution of metronidazole. 4.9% to 13% removal was predicted for the single-lamp photoreactors, while 14% to 41% was predicted for the multi-lamp photoreactor. Selection of a reactor radius for maximum metronidazole removal varied with influent H₂O₂ concentration. The lowest operational cost of \$0.05 per mmol removed was projected for the multi-lamp photoreactor. Operationally, it was cost effective to utilize higher UV lamp output (36W), while keeping influent H₂O₂ concentration low (25 mg/L).

ACKNOWLEDGEMENTS

I would like to express my sincere gratitude to my advisor, Dr. Mehrab Mehrvar, who provided his guidance, support and assistance throughout the completion of this work. Thanks are also due to the faculty and staff of the Department of Chemical Engineering and the School of Graduate Studies, without whom this work would not have been possible.

TABLE OF CONTENTS

CHAPTER 1. INTRODUCTION	1
CHAPTER 2. LITERATURE SURVEY	4
2.1. Pharmaceuticals and Personal Care Products	4
2.1.1. Presence in the Environment	4
2.1.2. Target Compound – Metronidazole	6
2.1.3. Removal Options	6
2.2. AOP's for Water and Wastewater Treatment	8
2.2.1. Overview of AOP's	8
2.2.2. UV / H ₂ O ₂ Process	9
2.2.3. Fenton Process	11
2.2.4. Photo-Fenton Process	12
2.3. Use of UV/H ₂ O ₂ , Fenton, and Photo-Fenton for the Treatment of PPCP's	14
2.4. Design and Modeling of Photoreactors Utilizing the UV/H ₂ O ₂ AOP	17
CHAPTER 3. SYSTEM CONFIGURATION AND METHODOLOGY	18
3.1. Photoreactor Design	18
3.1.1. Single-Lamp UV Photoreactor	18
3.1.2. Multi-Lamp UV Photoreactor	18
3.1.3. Photoreactor Physical Properties and Operating Conditions	21
3.2. Conservation Equations	22
3.2.1. Energy Balance	22
3.2.2. Momentum Balance	23
3.2.3. Radiation Energy Balance	24

3.2.4.	Mass Balance	26
3.3.	Reaction Model.....	28
3.4.	Study Methodology.....	31
CHAPTER 4.	RESULTS AND DISCUSSION	33
4.1.	Model Calibration and Assessment	33
4.1.1.	Determination of Reaction Rate Constant for Metronidazole	33
4.1.2.	Model Predicted Removal of Clofibric Acid.....	37
4.1.3.	Effect of Inhibitors.....	41
4.2.	Modeling Metronidazole Removal in the Proposed Photoreactors	47
4.2.1.	Single Lamp Photoreactors – Reactor 1 and Reactor 2	47
4.2.2.	Multiple Lamp Reactor – Reactor 3.....	52
4.2.3.	Local Optimal Initial H ₂ O ₂ Dose and Reactor Radius.....	56
CHAPTER 5.	CONCLUSIONS AND RECOMMENDATIONS	60
5.1.	Conclusions.....	60
5.1.1.	Model Calibration and Assessment	60
5.1.2.	Behaviour of the Modeled Photoreactors	60
5.1.3.	Optimal H ₂ O ₂ Dose and Reactor Radius	61
5.2.	Recommendations.....	61
CHAPTER 6.	NOMENCLATURE	63
CHAPTER 7.	REFERENCES	65

LIST OF TABLES

Table 1. Reported Occurrences of Drug Residues in WWTP Effluents, Surface Water and Ground Water	5
Table 2. Reactions between Organic Compounds and the Hydroxyl Radical	8
Table 3. Summary of Experimental Work Conducted Utilizing the UV/H ₂ O ₂ , Fenton, and Photo-Fenton AOP's	15
Table 4. Physical Properties and Operating Conditions of the Photoreactors	22
Table 5. Model Values of Reaction Rate Constants and Extinction Coefficients	31
Table 6. Average Effluent Metronidazole Concentrations for Reactor 1 Operating in Series at Various Operating Conditions	51
Table 7. Average Effluent Metronidazole Concentrations for Reactor 2 at Various Operating Conditions.....	51
Table 8. Average Effluent Metronidazole Concentrations for Reactor 3 at Various Operating Conditions.....	55
Table 9. Operational Cost per Amount of Metronidazole Removed in Reactor 1 at Various Operating Conditions.....	57
Table 10. Operational Cost per Amount of Metronidazole Removed in Reactor 2 at Various Operating Conditions.....	57
Table 11. Operational Cost per Amount of Metronidazole Removed in Reactor 3 at Various Operating Conditions.....	58
Table 12. Local Optimal Operating Conditions in Terms of Minimum Operational Cost per mmole of Metronidazole Removed	58
Table 13. Experimental Results Used for Model Calibration – Initial H ₂ O ₂ Concentration of 25 mg/L.....	81
Table 14. Experimental Results Used for Model Calibration – Initial H ₂ O ₂ Concentration of 50	

mg/L.....	81
Table 15. Concentrations of Carbonate and Bicarbonate Ions in the Aqueous Solution.....	90
Table 16. Experimental Results Used for Model Prediction of Removal of Clofibric Acid – Initial H ₂ O ₂ Concentration of 34 mg/L.....	91
Table 17. Experimental Results Used for Model Prediction of Removal of Clofibric Acid – Initial H ₂ O ₂ Concentration of 340 mg/L.....	91
Table 18. Average Effluent Metronidazole Concentrations for Reactor 1 at Various Operating Conditions.....	99
Table 19. Average Effluent H ₂ O ₂ Concentrations for Reactor 1 at Various Operating Conditions	99
Table 20. Average Effluent Metronidazole Concentrations for Reactor 2 at Various Operating Conditions.....	102
Table 21. Average Effluent H ₂ O ₂ Concentrations for Reactor 2 at Various Operating Conditions	102
Table 22. Average Effluent Metronidazole Concentrations for Reactor 3 at Various Operating Conditions.....	114
Table 23. Average Effluent H ₂ O ₂ Concentrations for Reactor 3 at Various Operating Conditions	114

LIST OF FIGURES

Figure 1. Chemical Structure of Metronidazole	6
Figure 2. Schematic Diagram of the Single-Lamp UV Photoreactor	19
Figure 3. Schematic of Multi-Lamp UV Photoreactor	20
Figure 4. Metronidazole Concentration vs. Time – Calibrated Model	35
Figure 5. Residual Plot for the Calibrated Model	36
Figure 6. Clofibric Acid Concentration vs. Time – Performance of Model to Predict Experimental Results Reported by Andreozzi et al. (2003)	39
Figure 7. Clofibric Acid Concentration vs. Time – Performance of Modified Model to Predict Experimental Results Reported by Andreozzi et al. (2003)	40
Figure 8. Effect of $[H_2O_2]_0$ on Model Predicted Removal of Metronidazole – Optimal H_2O_2 Dose	42
Figure 9. Effect of Alkalinity as $CaCO_3$ on Model Predicted Removal of Metronidazole with $[H_2O_2]_0 = 50$ mg/L	44
Figure 10. Effect of $[H_2O_2]_0$ on Model Predicted Removal of Metronidazole with Alkalinity of 75 mg/L as $CaCO_3$ – Optimal H_2O_2 Dose	46
Figure 11. Concentration Profile of Metronidazole in Reactor 1 at Various Residence Times with $[H_2O_2]_{inf} = 100$ mg/L	48
Figure 12. Concentration Profile of Metronidazole in Reactor 2 at Various Residence Times with $[H_2O_2]_{inf} = 100$ mg/L	49
Figure 13. Metronidazole Concentration Profile for a Quadrant of Reactor 3 with $[H_2O_2]_{inf} =$ 100 mg/L and $R = 100$ mm at Two Axial Positions within the Reactor	54
Figure 14. Metronidazole Concentration Profile for a Quadrant of Reactor 3 with $[H_2O_2]_{inf} =$ 100 mg/L and $R = 100$ mm at the middle of the reactor, a distance of 1.2 m from the reactor inlet	115

Figure 15. Metronidazole Concentration Profile for a Quadrant of Reactor 3 with $[H_2O_2]_{inf} = 100$ mg/L and $R = 100$ mm at the reactor outlet, a distance of 2.4 m from the reactor inlet 116

LIST OF APPENDICES

APPENDIX A – Miscellaneous Sample Calculations.....	74
APPENDIX B – Model Calibration: Simulation Model Development, Matlab Code, and Selected Output.....	79
APPENDIX C – Single Lamp UV Reactors: Simulation Model Development, Matlab Code, and Selected Output.....	92
APPENDIX D – Multi-Lamp UV Reactor: Simulation Model Development, Matlab Code, and Selected Output.....	105
APPENDIX E – Sample Calculation for the Determination of Operating Costs Per Amount of Target Compound Removed.....	117

CHAPTER 1.

INTRODUCTION

Wastewater treatment works have, to-date, incorporated biological and chemical removal of harmful constituents from raw wastewater prior to discharge of the treated effluent to a receiving body. Over time, various processes have evolved for the removal of these constituents. Today, with more complex chemicals being discharged to wastewater collection systems, greater emphasis on removal of small amounts of micropollutants is becoming an expensive necessity. As an example, greater concern is being expressed on a daily basis regarding the amounts and occurrences of pharmaceuticals and personal care products (PPCP's) in the treated wastewater effluent being discharged to surface water bodies (Larsen et al 2004; Zwiener & Frimmel, 2000; Gagne et al., 2006; Carballa et al., 2004).

Since the early 1980's, several studies documented the presence of pharmaceuticals and related metabolites in the aquatic environment (Hernando et al., 2006; Larsen et al., 2004). Since then, with better and more sophisticated analytical methods, a large number of drugs belonging to various classes of drugs, including antibiotics, analgesics and anti-inflammatories, lipid regulator agents, β -blockers, antiepileptics, contraceptives, steroids and related hormones, have been documented in the aquatic environment (Larsen et al., 2004; Hernando et al., 2006). Pharmaceuticals are unique pollutants in that they are designed to act in specific way, that is, to target a biological effect. Due to their regular and widespread use for health benefits for both humans and animals, pharmaceuticals and their metabolites are continuously being introduced into the aquatic environment. By their nature, many of these compounds are resistant to conventional forms of biological and chemical treatment, and are therefore considered to be "pseudopersistent compounds" in the environment (Hernando et al., 2006).

In recent years, more attention has been directed to PPCP's as they most often have similar physico-chemical behaviour as other harmful chemicals that can be accumulated in living organisms. As a result of the presence of pharmaceuticals and their metabolites in surface and ground waters, investigations into methods for their removal have intensified, with advanced oxidation processes (AOP's) showing much promise for the treatment of these compounds due to

their ability to alter the chemical composition of these compounds (Zwiener & Frimmel, 2000; Andreozzi et al., 2003; Doll & Frimmel, 2005; Doll & Frimmel 2004; Emblidge & DeLorenzo, 2006; Sires et al., 2006; Feng et al., 2005; Shemer et al., 2006, Hofl et al., 1997, Perez-Estrada, 2005; Gernjak et al, 2004; Zhang et al., 2006; Arslan-Alaton & Gurses, 2004; Andreozzi et al., 2002; McDowell et al., 2005, Vogna et al., 2004).

One promising AOP for the treatment of PPCP's in aqueous solutions is the UV/H₂O₂ process. The UV / H₂O₂ process involves the formation of highly reactive hydroxyl radicals from an aqueous solution of H₂O₂ exposed to UV light with wavelengths varying between 200 to 280 nm (Metcalf & Eddy, 2003). These hydroxyl radicals react with the target compound(s) to be removed, along with other constituents of the solution known as radical scavengers. Because these radical scavengers compete with the target compound(s) for the hydroxyl radicals, they reduce the rate of removal of the target compound(s), and thus are inhibitors.

Since many water and wastewater treatment plants currently utilize UV reactors for disinfection purposes, the simple addition of H₂O₂ upstream of the UV reactors would allow many plants to be easily retrofitted to utilize this AOP. In order to effectively utilize the UV/H₂O₂ process, a means of evaluating and optimizing photoreactor design is required. While evaluation of experimental results compared with reactor specific models has been previously investigated (Shemer et al., 2006; Behnajady and Modirshahla, 2006; Aleboyeh et al., 2005; Modirshahla and Behnajady, 2006; Shu and Chang, 2005; Shu et al., 2006), very little work has been done investigating models which can be applied to various photoreactor geometries (Andreozzi et al., 2003; Beltran et al., 1999). The development of a model, which can be used to predict the behaviour of photoreactors of varying geometries and varying influent solution composition, would provide a valuable tool for the design and optimization of photoreactors using the UV/H₂O₂ process.

The focus of this study was the development of design equations for the modeling and optimization of tubular UV photoreactors for the treatment of a pharmaceutical compound, metronidazole, utilizing the UV/H₂O₂ AOP. The objectives of this study were as follows:

1. To develop a model to predict the advanced oxidation of metronidazole utilizing the

UV/H₂O₂ AOP.

2. To calibrate the model based on published experimental data.
3. To assess the ability of the model to predict the removal of another pharmaceutical compound based on published experimental data.
4. To assess the behaviour of the model by simulating the presence inhibitors in the system and examining the behaviour of the modeled system.
5. To utilize the calibrated model to determine effluent concentration profiles of the target compound and H₂O₂ for single- and multi-lamp photoreactor configurations.
6. To investigate local operating conditions for each photoreactor that provide the lowest operational cost per mmol of parent compound removed.

CHAPTER 2.

LITERATURE SURVEY

2.1. Pharmaceuticals and Personal Care Products

2.1.1. Presence in the Environment

The presence of pharmaceuticals and their metabolites in the environment is due to contaminant releases from such things as production sites, direct disposal of surplus drugs from households, excretions after drug administration to humans and animals, treatments in aquatic fish farms, other animal farms, and landfill leachate. Table 1 lists various pharmaceuticals and their metabolites that have been found in surface water, ground water, and/or wastewater treatment plant (WWTP) effluents.

Pharmaceuticals and their metabolites found in surface waters pose a risk to aquatic life, as even low doses of some of these compounds have been found to be harmful to various types of life. For example, adverse effects have been observed on rainbow trout exposed to diclofenac at a concentration of 1 $\mu\text{g/L}$, and a study on the effect of carbamazepine on invertebrates found the lowest observable effect concentration (LOEC) to be 20 $\mu\text{g/L}$ (Andreozzi et al., 2003). The presence of these compounds in potable water supplies may be a concern to human health. It has been reported that PPCP's, including some endocrine disrupting compounds, can have harmful effects on humans even at trace amounts such as irritation, toxicity, altering growth, reproduction, development and behaviour (Galindo & Kalt, 1999).

In order to avoid the presence of PPCP's in potable water supplies, treatment can be implemented as part of the potable water treatment system. To reduce the discharge of PPCP's into the environment, and subsequently into the source water for drinking water systems, WWTP effluent can be treated prior to discharge into the environment. In communities serviced by septic tank systems, this method may not be feasible.

Table 1. Reported Occurrences of Drug Residues in WWTP Effluents, Surface Water and Ground Water

Pharmaceutical Compounds	WWTP Effluents (ng/L)	Surface Water (ng/L)	Ground Water (ng/L)
Antibiotics			
Trimethoprim	154		
Sulfamethoxazole	99 - 128	50	
Erythromycin	886	34	
Metronidazole	1,800 – 9,400 ⁽¹⁾		
Roxytromycin	680		
Tylosin	128-886	2.2	
Trimethoprim	154		
Analgesics & anti-inflammatories			
Diclofenac	5 – 1,590	5 – 490	300
Ibuprofen	50 – 3,350	5 – 280	200
Naproxen	217 - 1847	266	
Ketoprofen	733		
Mefanamic Acid		68	
Acetylsalic acid	5 – 1,510	< .05	
Lipid Regulator Agents			
Bezeafibrate	2353	1100	
Fenobrate	110		
Fenofibric Acid	50 – 1,190	5 – 170	45
Gemfibrocil	84 – 2366		
Clofibric acid	361 – 1,560	5 – 300	70 – 7,300
Bezafibrate	250 – 4,560	5 – 380	
β-Blockers			
Propanolol	676	25	
Betaxolol	190	28	
Bisoprolol	190 – 777	25-2000	
Atenolol		145	
Metoprolol	777	2200	
Antiepileptics			
Carbamazepine	137 - 1625	460	
Steroid Hormones			
17-α-Ethinyl estradiol	7	2.4	
Diethylstilbestrol	20	7.5	
Diethylstilbestrol acetate	18	7.5	
Other			
Caffeine	315 – 22,000		

Notes:

Adapted from Larsen et al., 2004, and Hernando et al., 2006., Gagne et al., 2006, Gomez et al., 2006.

(1) Hospital effluent wastewater.

In Ontario, there is currently no legislation, either federal or provincial, which requires water or WWTP's to treat PPCP's. Federal regulations, if and when enacted, would likely fall within the Canadian Environmental Protection Act (CEPA). This Act currently regulates materials that are designated as toxic, and materials for which export controls are required (includes materials which are restricted and materials that are prohibited). Provincially, any changes to wastewater effluent discharge would likely be developed under the Ontario Water Resources Act (OWRA), which governs the approval and operation of all municipal and industrial wastewater systems in Ontario.

2.1.2. Target Compound – Metronidazole

Metronidazole is an antibiotic used to treat infections caused by anaerobic bacteria and various protozoans (Shemer et al., 2006). This compound was selected as the target compound for this study because this compound is widely used, highly soluble, non-biodegradable, and is a suspected carcinogen (Kummerer et al., 2000). Metronidazole has been detected in concentrations of 1.8 to 9.4 µg/L (0.011 to 0.055 µM) in hospital effluent wastewaters (Gomez et al., 2006). Figure 1 presents the chemical structure of metronidazole.

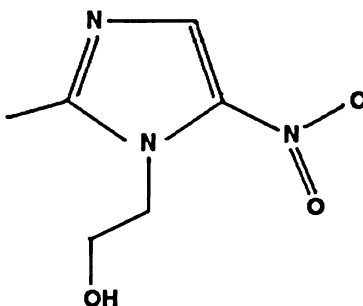


Figure 1. Chemical Structure of Metronidazole

2.1.3. Removal Options

Non-Destructive Techniques

Non-destructive removal of pharmaceuticals from aqueous solutions include such methods as steam stripping, activated carbon, and membrane filtration (Tekin et al., 2006; Jasim, 2006). In Ontario, the Walkerton Clean Water Centre (WCWC) in conjunction with the Ministry of the

Environment (MOE), have announced a project for the removal of PPCP's and endocrine disrupting compounds from drinking water using novel membrane technologies (Jasim, 2006). This study will involve bench and pilot scale experiments utilizing two (2) novel membrane preparation techniques: surface modified macromolecules (SMM), and electrospun nanofibres.

While the process can successfully remove the recalcitrant compounds from the filtrate, the waste retentate contains all the contaminants that were filtered out. Therefore, while the treated effluent may have little or no contaminants, the process waste from non-destructive treatment techniques results in a disposal problem. These concentrated retentate waste streams would then require further treatment to avoid reintroduction of the removed contaminants into the environment. Such treatment can be provided via destructive removal techniques.

In addition, conventional wastewater treatment techniques can result in the non-destructive removal of pharmaceutical pollutants via adsorption onto solid surfaces (Carballa et al., 2004).

Destructive Techniques

Destructive removal techniques are those that alter the chemical structure of the compound to be removed. Of these techniques, some of the most widely investigated are AOP's.

AOP's typically rely on the formation of the hydroxyl free radical ($\cdot\text{OH}$), which is a strong oxidant. In fact, the hydroxyl free radical is second only to fluorine with respect to oxidizing potential (Metcalf & Eddy, 2003).

Several AOP's, such as UV/H₂O₂, O₃/H₂O₂, ozonation, UV/TiO₂, Fenton, and photo-Fenton have been investigated for their use to remove pharmaceuticals and their metabolites from aqueous solutions (Andreozzi et al., 2003; Doll & Frimmel, 2004 and 2005; Zwiener & Frimmel, 2000; Shemer et al., 2006, Hofl et al., 1997, Perez-Estrada, 2005). These treatment options are attractive from the point of view of upgrading existing water and wastewater treatment facilities, since UV and ozonation use is becoming more widespread for the disinfection of both potable water and WWTP effluents.

Oxidative treatment of the PPCP's does, however, lead to the formation of various intermediate

compounds. For example, the oxidation of clofibric acid, a metabolite of the blood lipid regulating drugs clofibrate, etofibrate and etofyllinclofibrate, is known to produce sixteen (16) identified reaction intermediates, with other reaction intermediates proposed (Doll & Frimmel, 2004; Sires et al., 2006). In some cases, intermediates can themselves pose a risk to the environment and/or humans. Therefore, complete mineralization (complete conversion of the compound to CO₂ and H₂O) is desired, however due to the long reaction times required, it is likely impractical to achieve complete mineralization in a full scale treatment process.

2.2. AOP's for Water and Wastewater Treatment

2.2.1. Overview of AOP's

AOP's typically involve the formation of the hydroxyl radical, a strong oxidizing agent. Hydroxyl radicals are successful oxidizing agents due to their non-selective mode of attack and ability to react at normal temperatures and pressures (Metcalf & Eddy, 2003). The method used to form the hydroxyl radical is what separates one AOP from another. Common AOP's include UV/H₂O₂, ozonation, O₃/H₂O₂, O₃/H₂O₂/UV, UV/TiO₂, Fenton, and photo-Fenton

The hydroxyl radicals formed during advanced oxidation can react with organic compounds in a number of ways as shown in Table 2.

Table 2. Reactions between Organic Compounds and the Hydroxyl Radical

Reaction Type	Reaction Example
Radical Addition to Double Bonds or Aromatic Rings	$R-CH=CH_2 + \cdot OH \rightarrow R-C^*H-CH_2OH$
Hydrogen Abstraction from Aliphatic Carbon Atoms	$RH + \cdot OH \rightarrow R^* + H_2O$
Electron Transfer	$RX + \cdot OH \rightarrow RX^{**} + OH^-$

Notes:

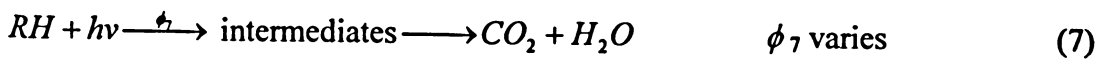
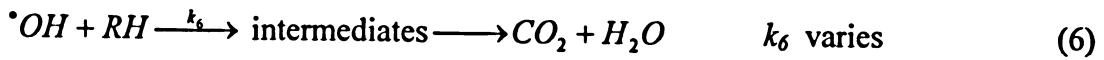
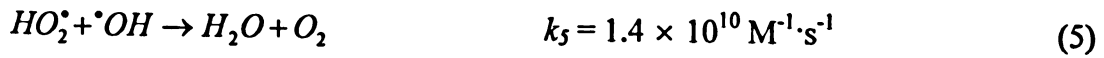
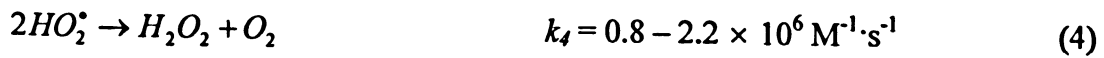
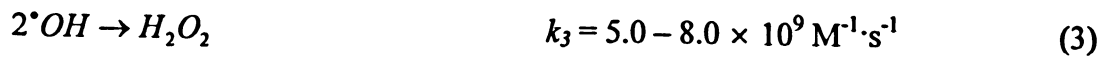
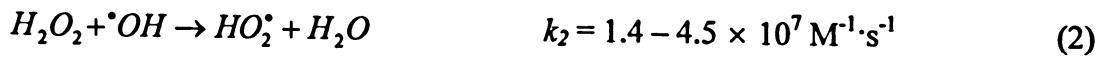
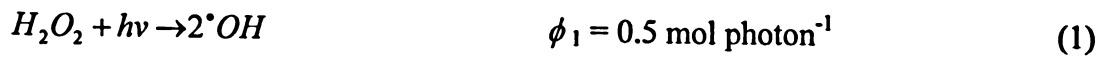
Adapted from Metcalf & Eddy, 2003, and Gernjak, 2006.

Because of the highly reactive nature of the hydroxyl radical, the presence of other normal constituents of wastewater, such as carbonate and bicarbonate can react with the hydroxyl radicals, thus acting as “radical scavengers”, reducing the overall efficiency of the oxidation process with respect to the contaminants of interest. The hydroxyl radicals themselves can inhibit their own oxidizing potential by reacting with each other to recombine into hydrogen peroxide.

Three common AOP's, namely UV/H₂O₂, Fenton, and photo-Fenton, are presented below.

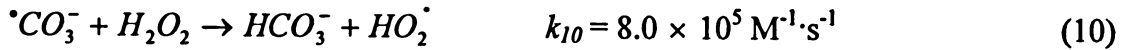
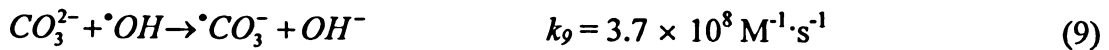
2.2.2. UV / H₂O₂ Process

The UV / H₂O₂ process involves the formation of hydroxyl radicals from an aqueous solution of H₂O₂ exposed to UV light with wavelengths varying between 200 to 280 nm (Metcalf & Eddy, 2003). The major reactions involved in the UV / H₂O₂ process are shown below, along with reported values of associated quantum yields or rate constants (Beltran et al., 1999; Gernjak, 2006):



where ϕ_i and k_i are the quantum yield (mol photon⁻¹) and reaction rate constant (M⁻¹s⁻¹) of the reactions listed in Equation (i), respectively. The values of ϕ_7 and k_6 vary, and depend on the target compound to be treated, *RH*.

The above list of reactions is by no means a comprehensive list of all the reactions that can take place in the UV / H₂O₂ process. Competing reactions with radical scavengers, such as carbonate and bicarbonate ions, can reduce the number of hydroxyl radicals in the system, reducing the removal efficiency of target compounds. Some of these reactions are shown in Equations (8) to (10) (Beltran et al, 1999):



Based on the work done by Jamal and Muaddi (1990), approximately 27% of the light energy is absorbed in the first centimeter of water. Coupled with the relatively small quantum yield of Equation (1), high H₂O₂ and UV doses may be required, making this process unsuitable for some applications (Metcalf and Eddy, 2003). This process is not suitable for wastewaters with high suspended concentrations, since the solid particles greatly reduce the UV transmittance (UVT) of the wastewater and, as a result, the production of hydroxyl radicals.

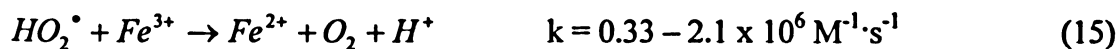
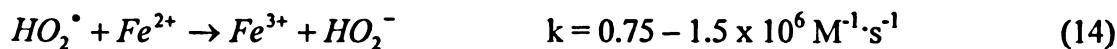
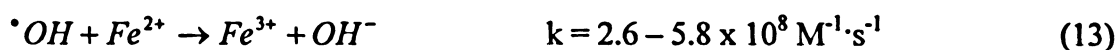
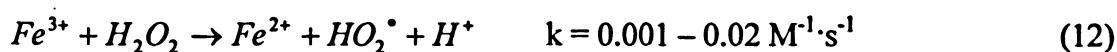
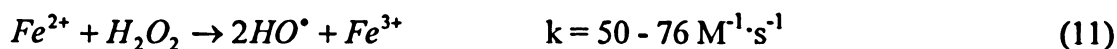
Because the dissociation of H₂O₂ into hydroxyl radicals requires UV irradiation (Equation 1), the behaviour of the system is strongly dependent on UV intensity (Mohey El-Dein et al., 2001). Removal of organic compounds has been observed to increase with increasing UV light intensity until an optimal value is reached, above which increases in removal efficiency were negligible (Shen and Wang, 2002).

The H₂O₂ dose is another important factor affecting the behaviour of the system. An increase in the rate of removal of organic compounds has been observed with increasing H₂O₂ concentration until an optimal dose is reached. Above this dose, the rate of removal of organics tends to decrease (Shen and Wang, 2002). Applications of single doses of H₂O₂ in batch systems have been found to be more effective than dosing an equivalent amount of H₂O₂ in two or more applications (Raj and Quen, 2005).

The efficiency of the UV / H₂O₂ process is affected by the pH of the wastewater to be treated. Raj and Quen (2005) reported a significant increase in organic compound removal efficiency as pH was increased to 7; increases in efficiency at higher pH values were found to be marginal.

2.2.3. Fenton Process

The Fenton process, first proposed by H.J.H. Fenton in 1894, involves the reaction of ferrous ions and hydrogen peroxide (Fenton reagent). Ferric iron and hydrogen peroxide (Fenton-like reagent) can also be used. The major reactions involved in the Fenton process include Eqs. 2 to 10, in addition to the following (Barb et al., 1951a; Barb et al., 1951b; Yoon et al., 2001; Gernjak, 2006; Neyens et al., 2003):



The above list of reactions is by no means a comprehensive list of all the reactions that can take place in the Fenton process. Competing reactions with radical scavengers, such as carbonate, bicarbonate, chloride, sulfate and nitrate ions can reduce the number of hydroxyl radicals in the system, reducing the removal efficiency of target compounds (De Laat et al., 2004).

Complete mineralization utilizing the Fenton process is generally not possible. This is because the intermediate products carboxylic acid and dicarboxylic acid form stable iron complexes with ferric ions, and cannot be further degraded by the Fenton process (Gernjak, 2006). However, carboxylic and dicarboxylic acids are readily biodegradable, and destruction of these compounds is possible utilizing biological treatment. Other compounds that resist oxidation by the Fenton process include small chlorinated alkanes (Chamarro et al., 2001), which are common disinfection by-products in water treatment processes, some of which have carcinogenic properties.

The efficiency of the Fenton process is strongly dependent on pH. Reported optimal pH values

range between 2 and 5, regardless of the composition of the wastewater being treated (Park et al., 2006; Zhang et al., 2005; Catalkaya & Kargi, 2007; Perez et al., 2002; Tambosi et al., 2006; Yang & Hwang, 2000). At low pH values (<2.5), the slowly reacting $[\text{FeOH}]^{2+}$ complex forms, and the hydroxyl radical scavenging effect of hydrogen ions becomes a significant factor (Shemer et al., 2006). At higher pH values, precipitation of ferric complexes reduces the rate of degradation of organic compounds (Shemer et al., 2006).

Because the hydroxyl radical forming reaction of the Fenton process does not require light energy, this process can be used successfully to treat wastewaters with high suspended solids concentrations, such as landfill leachate (Yoon et al., 1998; Zhang et al., 2005; Gau & Chang, 1996), livestock wastewater (Park et al., 2006), pulp and paper mill wastewater (Catalkaya & Kargi, 2007; Perez et al., 2002), oilfield wastewater (Gao et al., 2004), and textile wastewater (Mohey El-Dein et al., 2001; Garcia-Montano et al., 2006; Bae et al., 2004).

Yoon et al. (2001) investigated the effects of altering the ratio of initial ferrous iron to hydrogen peroxide, $[\text{Fe}^{2+}]_0/[\text{H}_2\text{O}_2]_0$. Researchers have found the optimal ratio to be 0.0067 for industrial pharmaceutical wastewater (Tekin et al., 2006), 0.10 for pulp and paper mill wastewater (Catalkaya & Kargi, 2007), 0.33 for livestock wastewater (Park et al., 2006), and 0.67 for landfill leachate (Zhang et al., 2005). The value of the optimal ratio varies greatly depending on the composition of the wastewater, with a decrease in the optimal ratio observed with an increase in the COD of the wastewater.

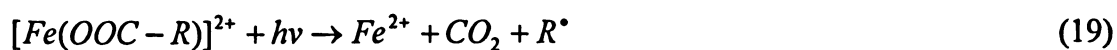
2.2.4. Photo-Fenton Process

The photo-Fenton process employs the Fenton reagent, or Fenton-like reagent, with light irradiation up to 580 nm (Bauer et al., 1999). The major reactions involved in the photo-Fenton process include Equations 1 to 15 (see Sections 2.2.2 and 2.2.3), in addition to the following (Gernjak, 2006):



where L is a ligand able to form a stable complex with ferric iron, such as H_2O , OH^- , R-COO^- , and R-NH_2 . The wavelength of light absorbed varies for different iron-ligand complexes.

Examples of reactions of specific iron-ligand complexes are shown below (Gernjak, 2006):



As can be seen in Equation (19), the iron-carboxylic acid and -dicarboxylic acid complexes dissociate in the presence of light irradiation, and the acid is oxidized. Therefore, unlike the Fenton process, complete mineralization utilizing the photo-Fenton process is possible, since oxidation of the carboxylic and dicarboxylic acid intermediates is possible.

As with the Fenton process, pH plays a very important part in the efficiency of the photo-Fenton process. Reported optimal pH values range between 2.8 and 5, regardless of the composition of the wastewater being treated (Gernjak, 2006; Park et al., 2006).

Because of the wide range of wavelengths absorbed by the iron-ligand complexes, specialized UV reactors are not always required. Studies have been done utilizing solar radiation for the photo-Fenton process (Gernjak, 2006; Bauer et al., 1999; Safarzadeh-Amiri et al., 1996; Perez-Estrada et al., 2005; Amat et al., 2004; Hincapie et al., 2005; Gernjak et al., 2004). The photo-Fenton mechanism has been recognized as essential to the auto-purification of lakes and rivers due to the naturally occurring presence of iron in surface and ground waters (Sulzberger et al., 1994). Other researchers have used UV lamps with success (Arslan et al., 2000).

As with the Fenton process, the value of the ratio of initial ferrous iron to hydrogen peroxide, $[Fe^{2+}]_0/[H_2O_2]_0$, can also have a significant impact on efficiency. For treating livestock wastewater, Park et al. (2006) found the optimal value of this ratio to be 0.1. This was lower than the optimal value of 0.33 for the Fenton process. The reduction in the required concentration of ferrous iron is likely due to the dissociation of the iron-ligand complexes in the photo-Fenton system, which frees ferrous ions which would otherwise be bound in stable complexes (Equation 16). These ferrous ions are then able to react with H_2O_2 to produce

hydroxyl radicals (Equation 11)

2.3. Use of UV/H₂O₂, Fenton, and Photo-Fenton for the Treatment of PPCP's

Table 3 provides a summary of selected experimental work done investigating the treatment of pharmaceuticals and other, chemically similar compounds utilizing the UV/H₂O₂, Fenton, and photo-Fenton AOP's. Chemically similar compounds refer to complex organic molecules that contain aromatic ring(s), and resist biological treatment, such as compounds commonly found in pulp mill effluent. This review focuses on wastewater composition and characteristics, initial hydrogen peroxide dose, and measures of the time required for removal, such as contaminant half lives.

Table 3. Summary of Experimental Work Conducted Utilizing the UV/H₂O₂, Fenton, and Photo-Fenton AOP's

Parameter	Dilute Pharmaceutical Waste (1)	Concentrated Pharmaceutical Waste (2)	Concentrated Pharmaceutical Waste (2)	Concentrated Pharmaceutical Waste (2)	Concentrated Pharmaceutical Waste (2)	Pulp Mill Effluent (4)	Livestock Wastewater (5)
Wastewater Composition	6 µM (1 mg/L) metronidazole	Effluent from a German Pharmaceutical production facility COD = 670 mg/L AOX = 3.0 mg/L	Effluent from a German Pharmaceutical production facility COD = 2,700 mg/L AOX = 5.0 mg/L	Procaïne penicillin formulation COD = 600 mg/L TOC = 450 mg/L BOD = 53 mg/L	COD = 400 mg/L TOC = 110 mg/L Initial pH of 7.8	COD = 5,320 mg/L	
Initial H ₂ O ₂ Dose	1 mg/L	2.1 g/L	11.2 g/L	25 mM	50 mM	0.2 M (Fenton) 0.1 M (photo-Fenton)	
[Fe ²⁺ /H ₂ O ₂] ₀ Ratio	0.40	0.10	0.10	0.06	0.05	0.33 (Fenton) 0.10 (photo-Fenton)	
Experimental Setup: UV / H ₂ O ₂	MP UV lamps, 200–400 nm No pH adjustment	LP UV lamps, 254 nm	LP UV lamps, 254 nm	n/a	LP UV lamps, 254 nm pH of 11	n/a	
Experimental Setup: Fenton	pH of 3.5	pH of 2.0	pH of 2.0	pH of 3	pH of 5	pH of 4	
Experimental Setup: Photo-Fenton	pH of 3.5 MP UV lamps, 200–400 nm	n/a	n/a	UV-A lamp, 300–370 nm pH of 3	LP UV lamps, 254 nm pH of 5	pH of 5	
Results: UV / H ₂ O ₂	$\tau_{1/2, \text{metro}}$ = 9.1 min	$\tau_{1/2, \text{AOX}}$ = 40 min	$\tau_{1/2, \text{AOX}}$ = 45 min	n/a	% TOC removal at 30 min = 11%	n/a	
Results: Fenton	$\tau_{1/2, \text{metro}}$ = 1.0 min	$\tau_{1/2, \text{AOX}}$ < 5 min	$\tau_{1/2, \text{AOX}}$ < 5 min	$\tau_{1/2, \text{COD}}$ = 30 min	% TOC removal at 30 min = 88%	% COD removal at 60 min = 70%	
Results: Photo-Fenton	$\tau_{1/2, \text{metro}}$ = 0.5 min	n/a	n/a	$\tau_{1/2, \text{COD}}$ = 25 min	% TOC removal at 5 min = 85%	% COD removal at 80 min = 79%	

Notes:

- n/a – not applicable
- 1. Adapted from Shemer et al., 2006.
- 2. Adapted from Hofl et al., 1997.
- 3. Adapted from Arslan-Alaton & Gurses, 2004.
- 4. Adapted from Catalkaya & Kargi, 2007.
- 5. Adapted from Park et al., 2006.

Based on the results presented in Table 3, the following observations can be made:

1. The UV/H₂O₂, Fenton, and photo-Fenton processes have been used to successfully treat pharmaceutical wastewater with both low (Shemer et al., 2006) and high (Hofl et al., 1997; Arslan-Alaton & Gurses, 2004) contaminant concentrations.
2. Multi-component wastewater was successfully treated by each of the AOP's investigated (Hofl et al., 1997; Catalkaya & Kargi, 2007; Park et al., 2006). From these results, it follows that these AOP's are likely capable of treating municipal wastewater and potable water supplies, which by their nature are composed of many different contaminants. Such a conclusion is supported by the results of Yonar et al. (2006), who had success treating domestic wastewater utilizing the UV/H₂O₂ process.
3. All three AOP's were successful in degrading the target compounds, however the UV/H₂O₂ process consistently required the longest reaction times. The fastest process was the photo-Fenton process, by an order of magnitude or more over the UV/H₂O₂ process. This has a significant impact on reactor volumes required for utilization of these processes at municipal WWTP's and potable water treatment plants.
4. The Fenton and photo-Fenton AOP's require that the solution to be treated have a low pH. This has a significant impact on pH adjustment processes that would be required for utilization of these processes at municipal WWTP's and potable water treatment plants.
5. The initial doses of hydrogen peroxide and iron, if applicable, varied from wastewater to wastewater. Because of the complexity of the interactions between the hydroxyl radicals and the wastewater constituents, and due to the fact that wastewater composition and chemistry varies significantly site to site, it is recommended that for the purposes of design, pilot testing be undertaken to determine the specific treatment requirements and technical feasibility of utilizing an AOP.

Although the UV/H₂O₂ AOP requires longer reaction times than either the Fenton or photo-Fenton processes, the proven ability of this process to treat pharmaceutical and domestic wastewaters, in addition to the ability to easily retrofit existing plants by provision of H₂O₂

upstream of existing UV reactors, make the UV/H₂O₂ process an attractive option for the treatment of PPCP's.

2.4. Design and Modeling of Photoreactors Utilizing the UV/H₂O₂ AOP

The design of photolytic oxidation reactors “requires good kinetic data and reactor models” and should optimize the use of photon energy (Yue, 1997).

While many studies have been published presenting kinetic analyses of the UV/H₂O₂ AOP for the degradation of various target compounds, many of these provide kinetic relationships that are specific to the reactor used and the unique composition of the influent stream (Shemer et al., 2006; Behnajady and Modirshahla, 2006; Aleboyeh et al., 2005; Modirshahla and Behnajady, 2006; Shu and Chang, 2005; Shu et al., 2006).

Other studies provide generalized kinetic relationships that can account for the variability in influent solution composition and reactor geometry (Andreozzi et al., 2003; Beltran et al., 1999). However, optimization of the operational costs of the modeled photoreactors by varying reactor geometry and operational conditions was not investigated.

As a result, the objectives of this study were to develop a reaction model that could be used to predict the removal of a target compound in a solution of variable composition, and in photoreactors of varying geometry. An assessment of optimization of operational costs was also undertaken.

CHAPTER 3.

SYSTEM CONFIGURATION AND METHODOLOGY

3.1. Photoreactor Design

3.1.1. Single-Lamp UV Photoreactor

The model photoreactor is a tubular reactor, of radius R , with a UV lamp with radius R_t inside a quartz sleeve with radius R_i down the centre axis. This is a single-lamp UV photoreactor since there is only a single UV lamp located at any cross section of the reactor. The aqueous solution to be treated flows upward along the z -direction in the annular space between the quartz sleeve and the outer shell of the reactor. For modeling purposes, cylindrical coordinates were used for the single-lamp UV photoreactor. A schematic diagram of the single UV lamp photoreactor is shown in Figure 2.

3.1.2. Multi-Lamp UV Photoreactor

The model photoreactor is a tubular reactor of radius R with four UV lamps, each with a radius R_t and inside a quartz sleeve of radius R_i . This is a multi-lamp UV photoreactor since there are four UV lamps located at any cross section of the reactor. The lamps are positioned parallel to the z -axis and equally spaced, each located half the reactor radius from the center of the reactor. The aqueous solution to be treated flows upwards along the z -direction in the space between the quartz sleeve and the outer shell of the reactor. For modeling purposes, Cartesian coordinates were used for the multi-lamp UV photoreactor. A schematic diagram of the multiple UV lamp photoreactor is shown in Figure 3.

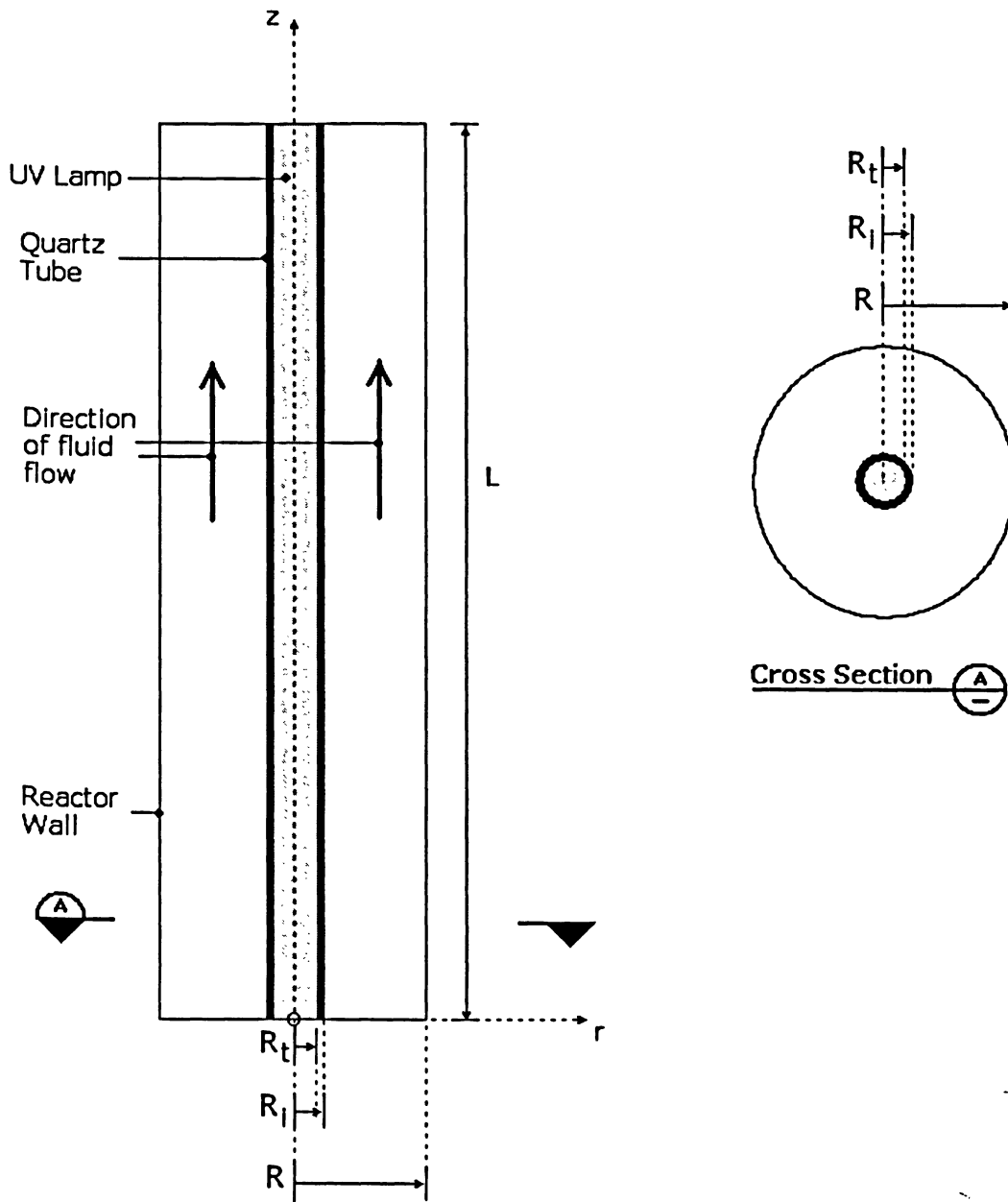


Figure 2. Schematic Diagram of the Single-Lamp UV Photoreactor
 H_2O_2 injection point not shown, but is located upstream of the photoreactor.

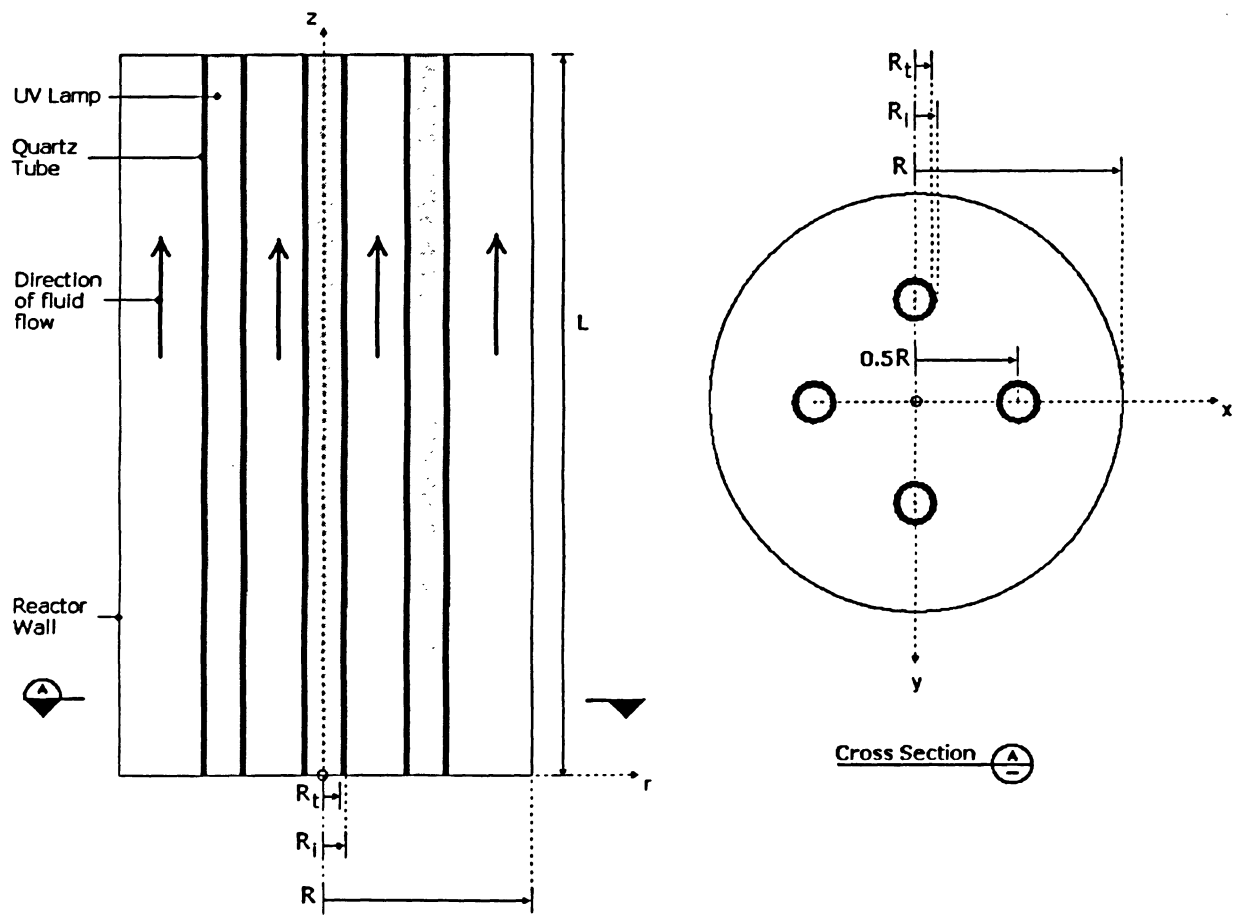


Figure 3. Schematic of Multi-Lamp UV Photoreactor
 H_2O_2 injection point not shown, but is located upstream of the photoreactor.

3.1.3. Photoreactor Physical Properties and Operating Conditions

Low pressure (LP) UV lamps were chosen as they produce nearly monochromatic light at 254 nm. Two commercially available LP UV lamps, Philips model TUV75W HO and Emperor Aquatics G48T6LVHO, were selected. A range of reactor diameters and initial H_2O_2 concentrations were chosen such that the effect of varying these operating conditions could be examined.

Reactor 1 and Reactor 2 are configured such that they are comprised of two single-lamp UV photoreactors operating in series. Hence, the overall length of Reactor 1 and Reactor 2 is equal to the sum of the length of two single-lamp UV photoreactors. Similarly, Reactor 3 is configured such that it is comprised of two multi-lamp UV photoreactors operating in series. It was assumed that plug flow was maintained along the full length of Reactors 1, 2, and 3. Physical properties and operating conditions of the system are presented in Table 4.

As shown in Table 4, the influent H_2O_2 concentration and reactor radius are represented as ranges for each reactor. For the purposes of this study, influent H_2O_2 concentrations of 25 mg/L, 50 mg/L, 75 mg/L, and 100 mg/L, and reactor radii of 50 mm, 100 mm, 150 mm, 200 mm, and 250 mm were investigated. Thus, for each reactor, 20 pairs of operating conditions were investigated, comprised of combinations of influent H_2O_2 concentrations and reactor radii.

In addition, the following assumptions were made for each reactor for the purposes of this study:

1. The photoreactors are operating at steady-state conditions;
2. The system is isothermal, and is operating at 25°C (see Section 3.2.1);
3. Flow through the reactor follows ideal plug flow (see Section 3.2.2);
4. The system is treating an aqueous solution with characteristics similar to that of tap water containing only the target compound, metronidazole, at an inlet concentration of 6 μM , pH of 6.0, and alkalinity at a concentration of 75 mg/L as CaCO_3 ; and
5. The effect of reaction intermediates in the system is neglected (see Section 3.3).

Table 4. Physical Properties and Operating Conditions of the Photoreactors

Parameter	Reactor 1	Reactor 2	Reactor 3
Reactors in Series			
Type	Single UV Lamp	Single UV Lamp	Multiple UV Lamp
Number	2	2	2
Length (overall)	2.4 m	2.4 m	2.4 m
Radius	50 – 250 mm	50 – 250 mm	50 – 250 mm
UV Lamps			
Number	2 x 1	2 x 1	2 x 4
Model	Philips TUV75W HO	Emperor Aquatics G48T6LVHO	Emperor Aquatics G48T6LVHO
Type	Low Pressure	Low Pressure	Low Pressure
Nominal Length	1.2 m	1.2 m	1.2 m
Nominal Radius (R _i)	13 mm	8.5 mm	8.5 mm
Input Current (each)	0.84 Amps	1.20 Amps	1.20 Amps
Input Watts (each)	75 W	120 W	120 W
UV Output (each)	25.5 W	36 W	36 W
Quartz Sleeve			
Outer Radius (R _i)	17 mm	17 mm	17 mm
Operating Conditions			
Flowrate to be treated	2.0 L/s	2.0 L/s	2.0 L/s
[Metronidazole] ₀	6 μM	6 μM	6 μM
[H ₂ O ₂] ₀	25 – 100 mg/L	25 – 100 mg/L	25 – 100 mg/L

3.2. Conservation Equations

3.2.1. Energy Balance

Single-Lamp UV Photoreactor

For a single UV lamp photoreactor, similar to that presented in Figure 2, Shen and Wang (2002) found that the variation of temperature in the photoreactor during photodecomposition was negligible, holding steady at around 25°C, implying that the system is nearly isothermal. As a result, it was assumed that the modeled reactors are isothermal, and at a constant and uniform

temperature of 25°C.

Multi-Lamp UV Photoreactor

It was also assumed that the multi-lamp UV photoreactor would be isothermal, and at a constant and uniform temperature of 25°C.

3.2.2. Momentum Balance

Single-Lamp UV Photoreactor

For the single lamp photoreactor presented in Figure 2, the Reynolds Number, N_R , for flow through the annular space is calculated as (Bird et al., 2002):

$$N_R = \frac{2R \left(1 - \frac{R_i}{R}\right) \bar{v}_z \rho}{\mu} \quad (20)$$

where \bar{v}_z is the average velocity of the aqueous solution through the annular space (m/s), and μ and ρ are the viscosity (Pa·s) and density (kg/m³) of the aqueous solutions, respectively. Based on the flow rate of 2.0 L/s to be treated, the calculated values of N_R for Reactor 1 and Reactor 2 are > 5,300 for reactor radii up to 250 mm, indicating turbulent flow through the reactor. Example calculations are provided in Appendix A.

According to Perry and Green (1997), “an empty tubular reactor can often be simulated as a” plug flow reactor. Shen and Wang (2002) determined that, for a single UV lamp photoreactor similar in configuration to that presented in Figure 2, the flow behaviour could be assumed to be ideal plug flow. Therefore, ideal plug flow was assumed for all modeled reactors in this work.

In ideal plug flow, $v_r = v_\theta = 0$, and $v_z = \text{constant}$ at all points in the reactor. As a result, the momentum balance can be neglected, and the residence time in the reactor, τ , is a function of axial position in the reactor, z , only.

Multi-Lamp UV Photoreactor

Based on the value of N_R calculated for Reactor 1 and Reactor 2, and due to the increase in velocity due to the volume occupied by additional UV lamps, it was assumed that flow through Reactor 3 would also be turbulent.

In ideal plug flow, $v_x = v_y = 0$, and $v_z = \text{constant}$ at all points in the reactor. As a result, the momentum balance can be neglected, and the residence time in the reactor, τ , is a function of axial position in the reactor, z , only.

3.2.3. Radiation Energy Balance

Single-Lamp UV Photoreactor

Assuming no emissivity of molecules in aqueous solution, the radiation energy balance, for a single UV lamp in a quartz sleeve parallel to the z -axis, centered at the origin, is:

$$\frac{1}{r} \frac{d(rq)}{dr} = -q(2.303\mu_s) \quad (21)$$

where q is the radiant energy flux in mol photons/(m²·s) and μ_s is the extinction coefficient of the aqueous solution (base 10) in m⁻¹. Integration yields:

$$q = q_o \frac{R_i}{r} e^{-2.303\mu_s(r-R_i)} \quad (22)$$

where q_o is the radiant energy flux at the outer surface of the quartz sleeve.

For the purposes of this study, the values of the extinction coefficient of distilled water at 254 nm, μ_w , was taken to be 0.7 m⁻¹, and for water containing alkalinity as carbonate and bicarbonate ions the value of μ_w at 254 nm is taken to be 10 m⁻¹, or that of average tap water (Gadgil, 1995). The UV absorptive properties of metronidazole and H₂O₂ can be expressed in terms of their molar absorptivities at 254 nm, ϵ_{RH} and $\epsilon_{H_2O_2}$, which are 220 mM⁻¹m⁻¹ and 1.86 mM⁻¹m⁻¹, respectively (Shemer et al., 2006; Andreozzi et al., 2003). All above extinction coefficients and molar absorptivities are to the base 10. The UV absorptive properties of reaction intermediates

were neglected since it was assumed that the concentrations of these compounds would be very small. As a result, the local extinction coefficient of the aqueous solution can be expressed as:

$$\mu_s = \mu_w + \varepsilon_{H_2O_2} C_{H_2O_2} + \varepsilon_{RH} C_{RH} \quad (23)$$

The local volumetric rate of energy absorption (LVREA), A , in mol photons/(L·s), is a function of the radiant energy flux (Mehrvar et al., 2002):

$$A = \mu_s q \quad (24)$$

Using Equations (23) and (24), the LVREA can be expressed in terms of radial position:

$$A = \mu_s q_o \frac{R_i}{r} e^{-2.303\mu_s(r-R_i)} \quad (25)$$

For any given compound, i , the fraction of photons absorbed by that compound at any given location within the reactor, f_i , can be expressed as a ratio of its local extinction coefficient, in terms of its local concentration and molar absorptivity, and the local extinction coefficient of the aqueous solution:

$$f_i = \frac{\varepsilon_i C_i}{\mu_s} \quad (26)$$

Multi-Lamp UV Photoreactor

For the purposes of modeling the multi-lamp photoreactor (Reactor 3), the expression for the LVREA was converted to Cartesian coordinates, as shown in Equation 27. This expression represents the LVREA from a lamp centered at (a, b).

$$A = \mu_s q_o \frac{R_i}{\sqrt{(x-a)^2 + (y-b)^2}} e^{-2.303\mu_s(\sqrt{(x-a)^2 + (y-b)^2} - R_i)} \quad (27)$$

The total LVREA for Reactor 3 is represented by the sum of the contributions from the four lamps centered at $(0.5R, 0)$, $(0, 0.5R)$, $(-0.5R, 0)$, and $(0, -0.5R)$. See Appendix D for details.

As with the single-lamp UV photoreactor, for any given compound, i , the fraction of photons absorbed by that compound at any given location within the reactor, f_i , can be expressed as a ratio of its local extinction coefficient, in terms of its local concentration and molar absorptivity, and the local extinction coefficient of the aqueous solution:

$$f_i = \frac{\varepsilon_i C_i}{\mu_s} \quad (26)$$

3.2.4. Mass Balance

Single-Lamp UV Photoreactor

The continuity equation in cylindrical coordinates for a compound of constant density, ρ and diffusivity, D_{AB} , is shown below (Shen and Wang, 2002):

$$\begin{aligned} \frac{\partial C_i}{\partial t} + \left(v_r \frac{\partial C_i}{\partial r} + v_\theta \frac{1}{r} \frac{\partial C_i}{\partial \theta} + v_z \frac{\partial C_i}{\partial z} \right) \\ = D_{AB} \left(\frac{1}{r} \frac{\partial}{\partial r} \left(r \frac{\partial C_i}{\partial r} \right) + \frac{1}{r^2} \frac{\partial^2 C_i}{\partial \theta^2} + \frac{\partial^2 C_i}{\partial z^2} \right) - R_{rxn,i} \end{aligned} \quad (28)$$

where C_i is the concentration of species i (M), v_r , v_θ , and v_z are velocities (m/s) in the r -, θ -, and z -directions, respectively. D_{AB} is the diffusivity of the species in the aqueous solution (m^2/s), and $R_{rxn,i}$ is the reaction rate of species i (M/s).

Since the system is considered to be at steady state conditions, the rate of change of concentration with respect to time is zero. In addition, because the flow through the reactor is assumed to be ideal plug flow (see Section 3.2.2), $v_r = v_\theta = 0$. Finally, it is assumed that the effect of diffusivity is negligible compared to that of the convective terms. As a result, Equation 19 can be simplified to (see Appendix A for details):

$$\frac{\partial C_i}{\partial \tau} = -R_{rxn,i} \quad (29)$$

where τ (s) is the reactor residence time.

Hence, the concentration profile is a function of residence time, τ , and chemical reaction rate, $R_{rxn,i}$. For photolyzed reactions, $R_{rxn,i}$ is a function of A , which is itself a function of r . Therefore, the concentration profile is a function of residence time, τ , and radial position, r .

Multi-Lamp UV Photoreactor

For Cartesian coordinates, the continuity equation can be expressed as:

$$\begin{aligned} \frac{\partial C_i}{\partial t} + \left(v_x \frac{\partial C_i}{\partial x} + v_y \frac{\partial C_i}{\partial y} + v_z \frac{\partial C_i}{\partial z} \right) \\ = D_{AB} \left(\frac{\partial^2 C_i}{\partial x^2} + \frac{\partial^2 C_i}{\partial y^2} + \frac{\partial^2 C_i}{\partial z^2} \right) - R_{rxn,i} \end{aligned} \quad (30)$$

where C_i is the concentration of species i (M), v_x , v_y , and v_z are velocities (m/s) in the x -, y -, and z -directions, respectively. D_{AB} is the diffusivity of the species in the aqueous solution (m^2/s), and $R_{rxn,i}$ is the reaction rate of species i (M/s).

Since the system is considered to be at steady state conditions, the rate of change of concentration with respect to time is zero. In addition, because the flow through the reactor is assumed to be ideal plug flow (see Section 3.2.2), $v_x = v_y = 0$. Finally, it is assumed that the effect of diffusivity is negligible compared to that of the convective terms in the z -direction. As a result, Equation 19 can be simplified to (see Appendix A for details):

$$\frac{\partial C_i}{\partial \tau} = -R_{rxn,i} \quad (29)$$

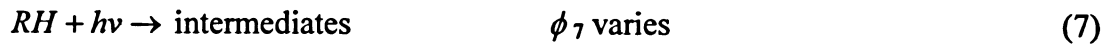
Hence, the concentration profile is a function of residence time, τ , and chemical reaction rate, $R_{rxn,i}$. For photolyzed reactions, $R_{rxn,i}$ is a function of A , which is itself a function of x and y .

Therefore, the concentration profile is a function of residence time, τ , and position in the reactor, in terms of x and y coordinates.

3.3. Reaction Model

To develop the reaction model, it was assumed that the reactions shown in Equations 2 to 6 and Equations 8 to 10 followed elementary reaction kinetics. The reactions shown in Equations 1 and 7, however, were based on the absorption of photons by the reacting species, and thus the chemical reaction rate expressions depend on the energy balance of the system.

As an example, for Equation 7:



the reaction rate can be written as the product of the photons absorbed by the target compound and the quantum yield for the reaction:

$$\frac{\partial C_{RH}}{\partial \tau} = -R_{RH} = -\phi_7 A f_{RH} \quad (31)$$

where $-R_{RH}$ is the rate of formation of the target compound (mM/s).

Using the above information, the reaction model for both the single- and multi-lamp UV photoreactors were developed, and are presented below.

Single-Lamp UV Photoreactor

The reaction model will be based on the chemical reactions shown in Equations (1) to (10). Based on these equations and the results of Section 3.2.4, the chemical reaction rates for the species in the system can be written as follows:

$$\frac{\partial C_{RH}}{\partial \tau} = -R_{RH} = -k_6 C_{RH} C_{\bullet OH} - \phi_7 A f_{RH} \quad (32)$$

$$\frac{\partial C_{H_2O_2}}{\partial \tau} = -R_{H_2O_2} = -\phi_1 A f_{H_2O_2} - k_2 C_{H_2O_2} C_{\bullet OH} + k_3 C_{\bullet OH}^2 + k_4 C_{HO_2^{\bullet}}^2 \quad (33)$$

$$\begin{aligned} \frac{\partial C_{\bullet OH}}{\partial \tau} = -R_{\bullet OH} = & -k_6 C_{RH} C_{\bullet OH} + 2\phi_1 A f_{H_2O_2} - k_2 C_{H_2O_2} C_{\bullet OH} - 2k_3 C_{\bullet OH}^2 \\ & - k_5 C_{\bullet OH} C_{HO_2^{\bullet}} - k_8 C_{HCO_3^-} C_{\bullet OH} - k_9 C_{CO_3^{2-}} C_{\bullet OH} \end{aligned} \quad (34)$$

$$\frac{\partial C_{HO_2^{\bullet}}}{\partial \tau} = -R_{HO_2^{\bullet}} = +k_2 C_{H_2O_2} C_{\bullet OH} - 2k_4 C_{HO_2^{\bullet}}^2 - k_5 C_{\bullet OH} C_{HO_2^{\bullet}} + k_{10} C_{\bullet CO_3^-} C_{H_2O_2} \quad (35)$$

$$\frac{\partial C_{HCO_3^-}}{\partial \tau} = -R_{HCO_3^-} = -k_8 C_{HCO_3^-} C_{\bullet OH} + k_{10} C_{\bullet CO_3^-} C_{H_2O_2} \quad (36)$$

$$\frac{\partial C_{CO_3^{2-}}}{\partial \tau} = -R_{CO_3^{2-}} = -k_9 C_{CO_3^{2-}} C_{\bullet OH} \quad (37)$$

$$\frac{\partial C_{\bullet CO_3^-}}{\partial \tau} = -R_{\bullet CO_3^-} = k_8 C_{HCO_3^-} C_{\bullet OH} + k_9 C_{CO_3^{2-}} C_{\bullet OH} - k_{10} C_{\bullet CO_3^-} C_{H_2O_2} \quad (38)$$

Equations (32) to (38) thus become the mathematical reaction model for the photoreactor system. As noted in Section 3.2.3, $A = A(r)$, thus the above set of equations are functions of residence time, τ , and radial position, r , for the single lamp photoreactors.

The effect of reaction intermediates formed in Equations (6) and (7) were neglected since it was assumed that the concentrations of these compounds would be very small.

Multi-Lamp UV Photoreactor

The reaction model will be based on the chemical reactions shown in Equations (1) to (10). Based on these equations and the results of Section 3.2.4, the chemical reaction rates for the species in the system can be written as follows:

$$\frac{\partial C_{RH}}{\partial \tau} = -R_{RH} = -k_6 C_{RH} C_{\bullet OH} - \phi_7 A f_{RH} \quad (32)$$

$$\frac{\partial C_{H_2O_2}}{\partial \tau} = -R_{H_2O_2} = -\phi_1 A f_{H_2O_2} - k_2 C_{H_2O_2} C_{\bullet OH} + k_3 C_{\bullet OH}^2 + k_4 C_{HO_2^{\bullet}}^2 \quad (33)$$

$$\begin{aligned} \frac{\partial C_{\bullet OH}}{\partial \tau} = -R_{\bullet OH} = & -k_6 C_{RH} C_{\bullet OH} + 2\phi_1 A f_{H_2O_2} - k_2 C_{H_2O_2} C_{\bullet OH} - 2k_3 C_{\bullet OH}^2 \\ & - k_5 C_{\bullet OH} C_{HO_2^{\bullet}} - k_8 C_{HCO_3^-} C_{\bullet OH} - k_9 C_{CO_3^{2-}} C_{\bullet OH} \end{aligned} \quad (34)$$

$$\frac{\partial C_{HO_2^{\bullet}}}{\partial \tau} = -R_{HO_2^{\bullet}} = +k_2 C_{H_2O_2} C_{\bullet OH} - 2k_4 C_{HO_2^{\bullet}}^2 - k_5 C_{\bullet OH} C_{HO_2^{\bullet}} + k_{10} C_{\bullet CO_3^-} C_{H_2O_2} \quad (35)$$

$$\frac{\partial C_{HCO_3^-}}{\partial \tau} = -R_{HCO_3^-} = -k_8 C_{HCO_3^-} C_{\bullet OH} + k_{10} C_{\bullet CO_3^-} C_{H_2O_2} \quad (36)$$

$$\frac{\partial C_{CO_3^{2-}}}{\partial \tau} = -R_{CO_3^{2-}} = -k_9 C_{CO_3^{2-}} C_{\bullet OH} \quad (37)$$

$$\frac{\partial C_{\bullet CO_3^-}}{\partial \tau} = -R_{\bullet CO_3^-} = k_8 C_{HCO_3^-} C_{\bullet OH} + k_9 C_{CO_3^{2-}} C_{\bullet OH} - k_{10} C_{\bullet CO_3^-} C_{H_2O_2} \quad (38)$$

Equations (32) to (38) thus become the mathematical reaction model for the photoreactor system, and are the same as those presented for the single-lamp UV photoreactor. However, as noted in Section 3.2.3, for the multi-lamp photoreactor $A = A(x, y)$, thus the above set of equations are functions of residence time, τ , and position within the reactor, in terms of x - and y -coordinates.

As with the single-lamp UV photoreactor, the effect of reaction intermediates formed in Equations (6) and (7) were neglected since it was assumed that the concentrations of these compounds would be very small.

Model Values of Reaction Rate Constants and Extinction Coefficients

Table 5 presents the values of reaction rate constants and extinction coefficients utilized for the

purposes of modeling the system. In the case of all constants, with the exception of k_6 and ϕ_7 , the values presented in Table 5 are those reported in the literature (see Section 2.2.2). Where a range of values has been reported, the value in the mid-point of the range was used.

Table 5. Model Values of Reaction Rate Constants and Extinction Coefficients

Values for reaction rate constants and extinction coefficients were based on values reported in Section 2.2.2, with the exception of ϕ_7 (Shemer et al., 2006).

Parameter	Value
ϕ_1	0.5 mol photon ⁻¹
k_2	$3.0 \times 10^7 \text{ M}^{-1}\cdot\text{s}^{-1}$
k_3	$6.5 \times 10^9 \text{ M}^{-1}\cdot\text{s}^{-1}$
k_4	$1.5 \times 10^6 \text{ M}^{-1}\cdot\text{s}^{-1}$
k_5	$1.4 \times 10^{10} \text{ M}^{-1}\cdot\text{s}^{-1}$
k_6	TBD
ϕ_7	$3.3 \times 10^{-3} \text{ mol photon}^{-1}$
k_8	$2.0 \times 10^7 \text{ M}^{-1}\cdot\text{s}^{-1}$
k_9	$3.7 \times 10^8 \text{ M}^{-1}\cdot\text{s}^{-1}$
k_{10}	$8.2 \times 10^5 \text{ M}^{-1}\cdot\text{s}^{-1}$

Notes:

TBD – to be determined

3.4. Study Methodology

Matlab (Version 7.1.0.246 R14), a computer software package, was used to solve the set of ordinary differential equations (ODE's) presented in Section 3.3, utilizing a predictor / corrector numerical method, ode15s, based on the numerical differentiation formulas (NDF). This particular ODE solver was chosen since the set of ODE's presented in Section 3.3 is "stiff", and hence other solvers, based on, for example, the Runge-Kutta method, were unable to solve the system of equations. Utilizing this software package allowed determination of the effluent concentration profiles for all compounds in the reaction model for each reactor configuration.

Average photoreactor effluent concentrations were determined utilizing the trapezoidal rule numerical integration method for Reactor 1 and Reactor 2 (see Appendix C).

To determine the local optimal initial H₂O₂ dose and outer reactor radius, it is desired to minimize the ratio, F (\$/mmol removed), of operational cost in terms of electrical, S_E , and chemical costs, S_C to the amount of target compound removed, $Q(\overline{C_{RH,inf}} - \overline{C_{RH,eff}})$:

$$F = \frac{S_E + S_C}{Q(\overline{C_{RH,inf}} - \overline{C_{RH,eff}})} \quad (39)$$

Electrical cost, S_E , was based on a cost of \$0.11/kWh for electricity. Chemical cost, S_C , was based on an assumed cost for H₂O₂ of \$1.10/kg (Hancu & Beckman, 2001), and an assumed cost for a 12% (w/v) solution of sodium hypochlorite of \$0.14/L. Sodium hypochlorite is required to quench the residual H₂O₂ remaining in solution after treatment in the photoreactor based on the following reaction:



Influent H₂O₂ dose, $[H_2O_2]_{inf}$, was varied from the lower and upper operating bounds, as shown in Table 4, in 25 mg/L intervals. Reactor radius, R , was varied from the lower and upper operating bounds, as shown in Table 4, in 50 mm intervals. The optimal influent H₂O₂ dose, $[H_2O_2]_{inf}^*$, and reactor radius, R^* , were determined by trial and error by calculating the value of F for each pair of set of operating conditions.

CHAPTER 4.

RESULTS AND DISCUSSION

4.1. Model Calibration and Assessment

4.1.1. Determination of Reaction Rate Constant for Metronidazole

The chemical reaction model was calibrated utilizing the experimental data reported by Shemer et al. (2006). Calibration involved determining the value of the rate constant between metronidazole and the hydroxyl radical, k_6 , which was the only value undefined in Table 5. This data was based on the UV/H₂O₂ oxidation of a 6 μ M solution of metronidazole in de-ionized water, with a pH of 6.0, under a collimated beam apparatus emitting 1.5 mW/cm² of UV light at 254 nm onto the surface of liquid held in a square Petri dish 7 cm \times 5 cm by 2.9 cm deep.

Two initial H₂O₂ doses were investigated: 25 mg/L and 50 mg/L. Since de-ionized water was used, it was possible to assume that the solution used by Shemer et al. (2006) did not contain any inhibitory compounds, and thus the extinction coefficient for distilled water was used in the determination of the solution extinction coefficient.

These conditions were simulated utilizing the chemical reaction model developed in Section 3.3. Unlike the model developed for the single and multi-lamp photoreactors, the LVREA, A , was not calculated for various positions within the Petri dish. Instead, an average value for the LVREA was calculated over the volume of the Petri dish (see simulation model development and Matlab code in Appendix B). It was assumed that the solution in the Petri dish was perfectly mixed, thus the extinction coefficient of the solution, μ_s , varied with respect to time, due to the changing concentrations of the target compound and H₂O₂. Based on reported reaction rate constants for Equation (6) for chemically similar compounds, it was assumed that the value for the reaction rate constant, k_6 , would likely lie within the range 0.5 to $10.0 \times 10^9 \text{ M}^{-1} \cdot \text{s}^{-1}$ (Beltran et al., 1999).

The value of k_6 was set to $1.0 \times 10^9 \text{ M}^{-1} \cdot \text{s}^{-1}$, which is within the range of expected values, and a simulation run was conducted with an initial H₂O₂ dose of 25 mg/L. After this run, simulation results were compared to experimental data reported by Shemer et al. (2006). If the model over-estimated the rate of removal of metronidazole, the value of k_6 was reduced; if it under-estimated

the rate of removal of metronidazole, the value of k_6 increased. This was continued until the absolute relative error between the model prediction and any experimental data point was <10%.

Using the above technique, the value of k_6 was determined to be $1.98 \times 10^9 \text{ M}^{-1}\cdot\text{s}^{-1}$, which was in the expected range, and resulted in an average absolute relative error of 3.4% between the model predictions and the reported experimental data from Shemer et al. (2006).

To test this result, a simulation was run utilizing the determined value of k_6 with an initial H_2O_2 concentration of 50 mg/L. The average absolute relative error between the model prediction and the experimental data was 1.7%.

Based on the low average absolute relative errors ($\leq 3.4\%$), the calibration of k_6 to the value of $1.98 \times 10^9 \text{ M}^{-1}\cdot\text{s}^{-1}$ was selected for all subsequent model simulations.

Results of the model calibration are shown in Figure 4. As can be seen in Figure 4, the calibrated model was able to successfully predict the concentration of metronidazole versus time for both initial H_2O_2 concentrations. In addition, the model predicted a decreasing H_2O_2 concentration with increasing time, since H_2O_2 is consumed in the oxidation process (see detailed results in Appendix B). The concentration of hydroxyl radicals, which react directly with the target compound (see Equation 6), at any time instant was quite low (on the order of 10^{12} M), since this highly reactive species tends to be consumed almost as quickly as it is produced. Detailed Matlab output for both initial H_2O_2 doses are included in Appendix B.

A residual plot was also generated, and is presented in Figure 5. The residual plot appears to indicate a random scatter of model error residual, defined as difference between the model predicted concentration and the experimentally obtained concentration, as no trends in the data points appear to be evident. A random scatter implies that the model is able to predict the experimental results very well (Mehrvar et al., 2000). It should be noted, however, that the model calibration relied on a limited number of 10 experimental data points. As a result, while the results presented in both Figure 4 and Figure 5 appear to indicate a well calibrated model, it is recommended that additional experimental work be conducted to provide additional data points for analysis.

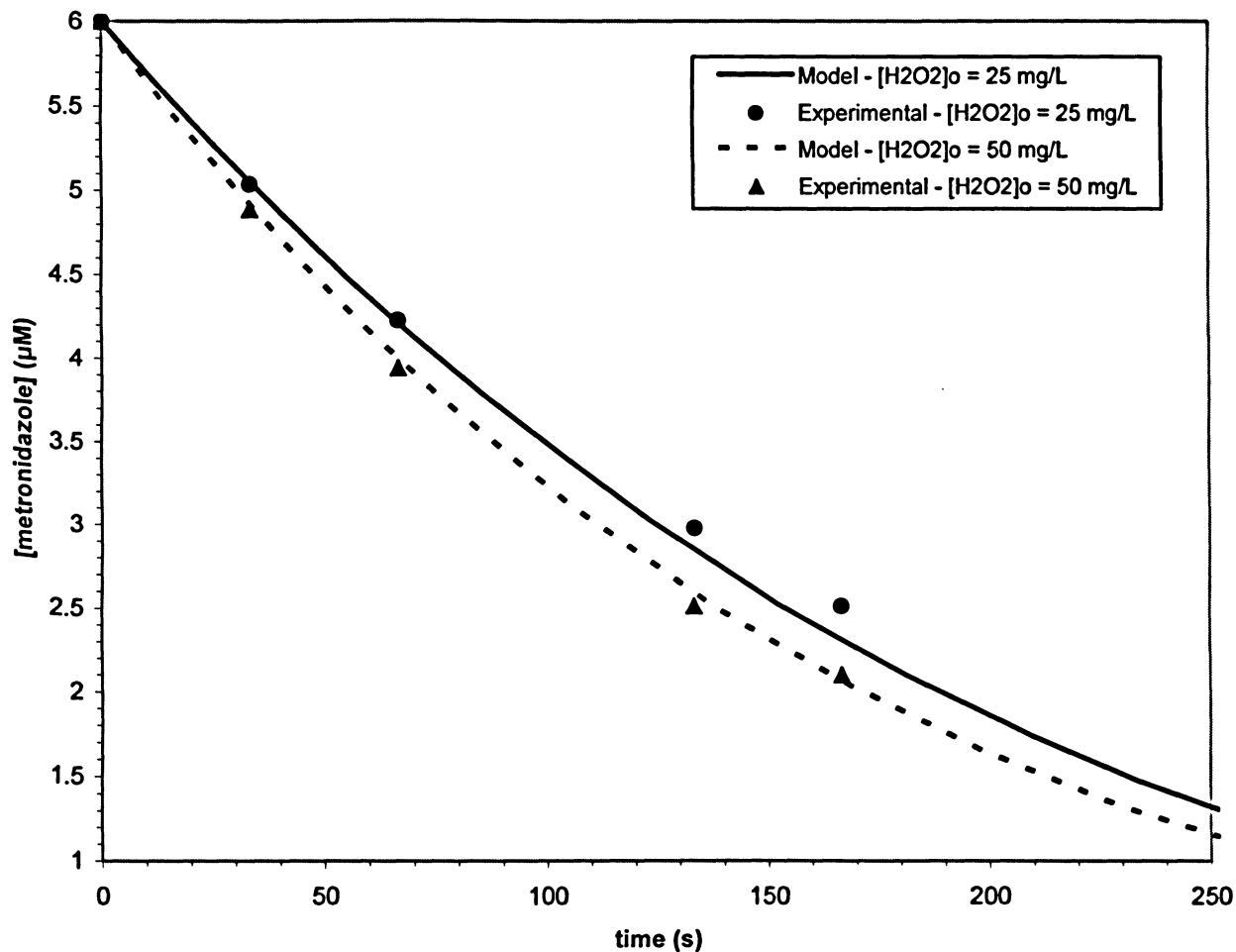


Figure 4. Metronidazole Concentration vs. Time – Calibrated Model

Model predictions obtained utilizing a value for the reaction rate constant between metronidazole and the hydroxyl radical, k_6 , of $1.98 \times 10^9 \text{ M}^{-1}\cdot\text{s}^{-1}$. All other rate constants and quantum yield values as listed in Table 5. Experimental data adapted from Shemer et al. (2006).

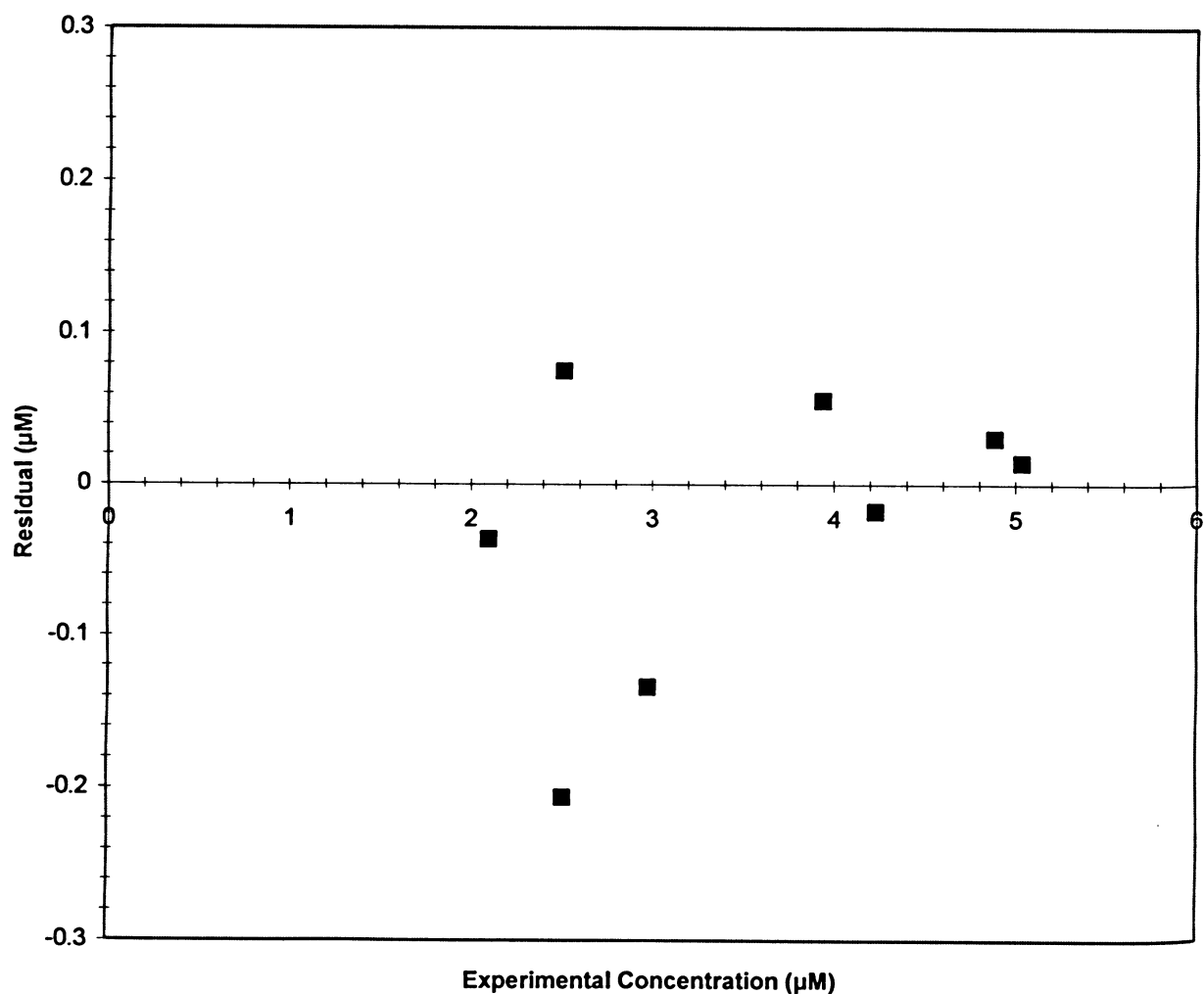


Figure 5. Residual Plot for the Calibrated Model

Residual equal to the model predicted concentration less the experimentally obtained concentration as reported by Shemer et al. (2006). Model simulations completed utilizing a value for the reaction rate constant between metronidazole and the hydroxyl radical, k_6 , of $1.98 \times 10^9 \text{ M}^{-1}\cdot\text{s}^{-1}$. All other rate constants and quantum yield values as listed in Table 5.

4.1.2. Model Predicted Removal of Clofibric Acid

Experimental data reported by Andreozzi et al. (2003) for the removal of clofibric acid, a metabolite of the lipid regulating drug clofibrate, utilizing the UV/H₂O₂ AOP was utilized to ensure the model developed would be valid for target compounds other than metronidazole.

The experimental data was based on the UV/H₂O₂ oxidation of a 0.024 to 0.0255 mM solution of clofibric acid in de-ionized water, with a pH of 5.5, in a batch cylindrical reactor with an outer diameter of 9.5 cm and a height of 28 cm. The reactor had an effective optical pathlength of 2.01 cm, volume of 0.42 L, and a LP UV lamp with an output of 2.7×10^{-6} mol photon·s⁻¹ at 254 nm. Since de-ionized water was used, it was possible to assume that the solution used by Andreozzi et al. (2003) did not contain any inhibitory compounds, and thus the extinction coefficient for distilled water was used in the determination of the solution extinction coefficient.

The reaction rate constant for the reaction between clofibric acid and the hydroxyl radical, k_6 , and the quantum yield for the direct photolysis of clofibric acid, ϕ_7 , were reported by Andreozzi et al. (2003) to be $(2.38 \pm 0.18) \times 10^9$ M⁻¹·s⁻¹ and 1.08×10^{-4} mol photon⁻¹, respectively. These values were inputted into the model developed in Section 3.3, and all other reaction rate constants and quantum yield values were kept as presented in Table 5.

Figure 6 presents the experimental data and the results of the model simulation.

As can be seen, for the simulation done for an initial H₂O₂ dose of 34 mg/L, there is good agreement between the modeled results and the experimental data. In fact, the absolute relative error remained $\leq 10\%$ for all data points up to 50% removal of the target compound (0 to 40 seconds of reaction time). At higher removal percentages (>50%), the absolute relative error remained below 52%.

For the simulation done for an initial H₂O₂ dose of 340 mg/L, there is good agreement between the modeled results and the experimental data, with an absolute relative error <15% for all data points up to 67% removal of the target compound (0 to 40 seconds of reaction time). At higher removal percentages (>67%), the absolute relative error remained below 43%.

It should be noted that, in their development of the reaction rate constant for the reaction between clofibric acid and the hydroxyl radical, Andreozzi et al. (2003) assumed a reaction rate constant for the reaction between H₂O₂ and the hydroxyl radical, k_2 , of $2.7 \times 10^7 \text{ M}^{-1}\cdot\text{s}^{-1}$. While this value is within the range of published values for this constant (see Equation 2), it is different than the value of $3.0 \times 10^7 \text{ M}^{-1}\cdot\text{s}^{-1}$ assumed in the model simulation (see Table 5). As a result, additional model simulations were run for which the value of k_2 was set to $2.7 \times 10^7 \text{ M}^{-1}\cdot\text{s}^{-1}$. Results are shown in Figure 7.

As can be seen in Figure 7, there is better agreement between the model predictions and experimental data utilizing the modified value of k_2 of $2.7 \times 10^7 \text{ M}^{-1}\cdot\text{s}^{-1}$. In fact, for the simulation done for an initial H₂O₂ dose of 34 mg/L, the absolute relative error remained below 32% for all data points; for the simulation done for an initial dose of H₂O₂ of 340 mg/L, the absolute relative error remained below 20% for all data points.

These results imply that the determination of a the rate constant for the reaction between a target compound and the hydroxyl radical (k_6) based on experimental data is dependent on the value chosen for the reaction rate constant between H₂O₂ and the hydroxyl radical (k_2).

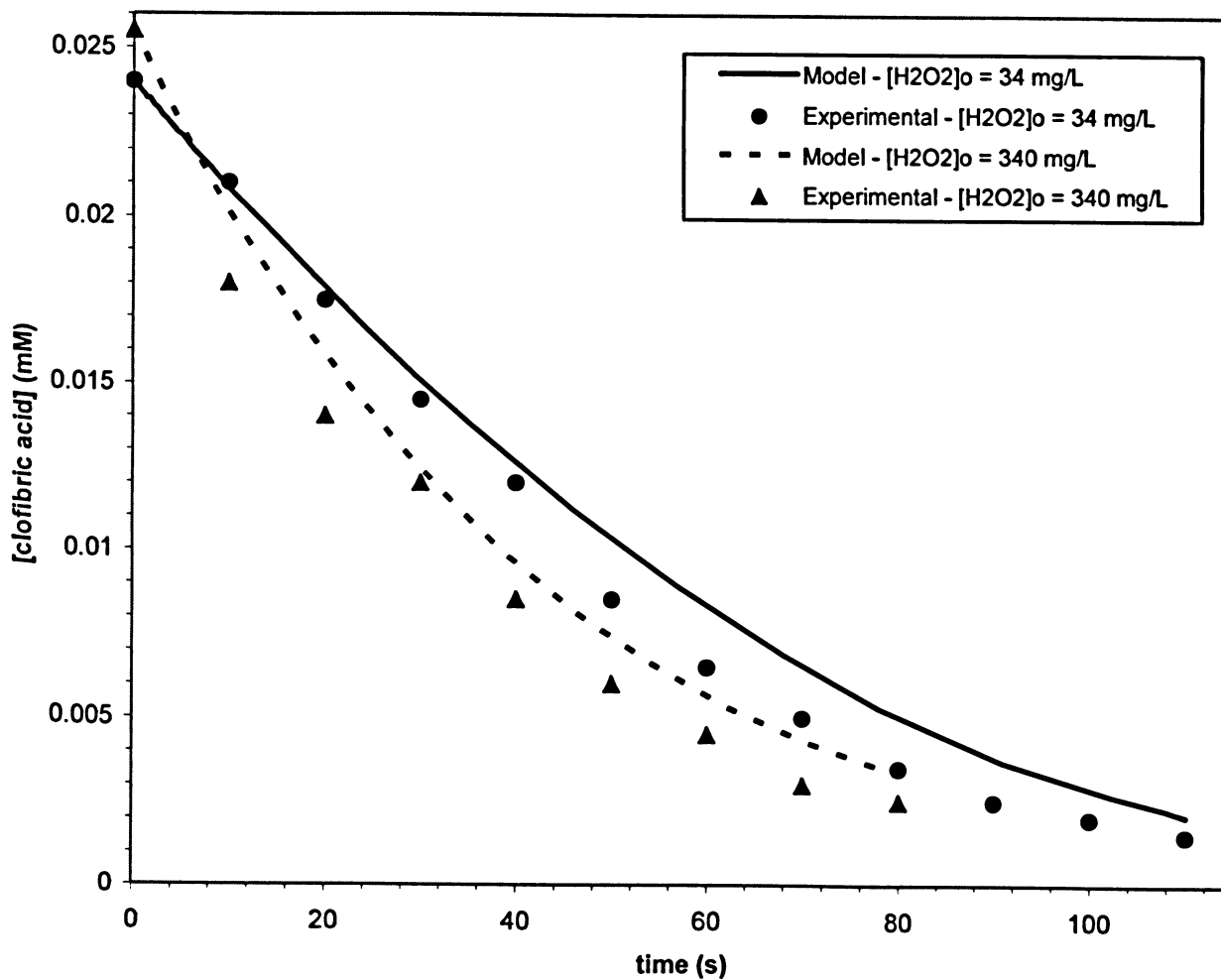


Figure 6. Clofibric Acid Concentration vs. Time – Performance of Model to Predict Experimental Results Reported by Andreozzi et al. (2003)

Utilizing a value for the reaction rate constant between clofibric acid and the hydroxyl radical, k_6 , of $2.38 \times 10^9 \text{ M}^{-1}\cdot\text{s}^{-1}$, as reported by Andreozzi et al. (2003). Value for the reaction rate constant between H_2O_2 and the hydroxyl radical, k_2 , of $3.0 \times 10^7 \text{ M}^{-1}\cdot\text{s}^{-1}$, and all other rate constants and quantum yield values as listed in Table 5.

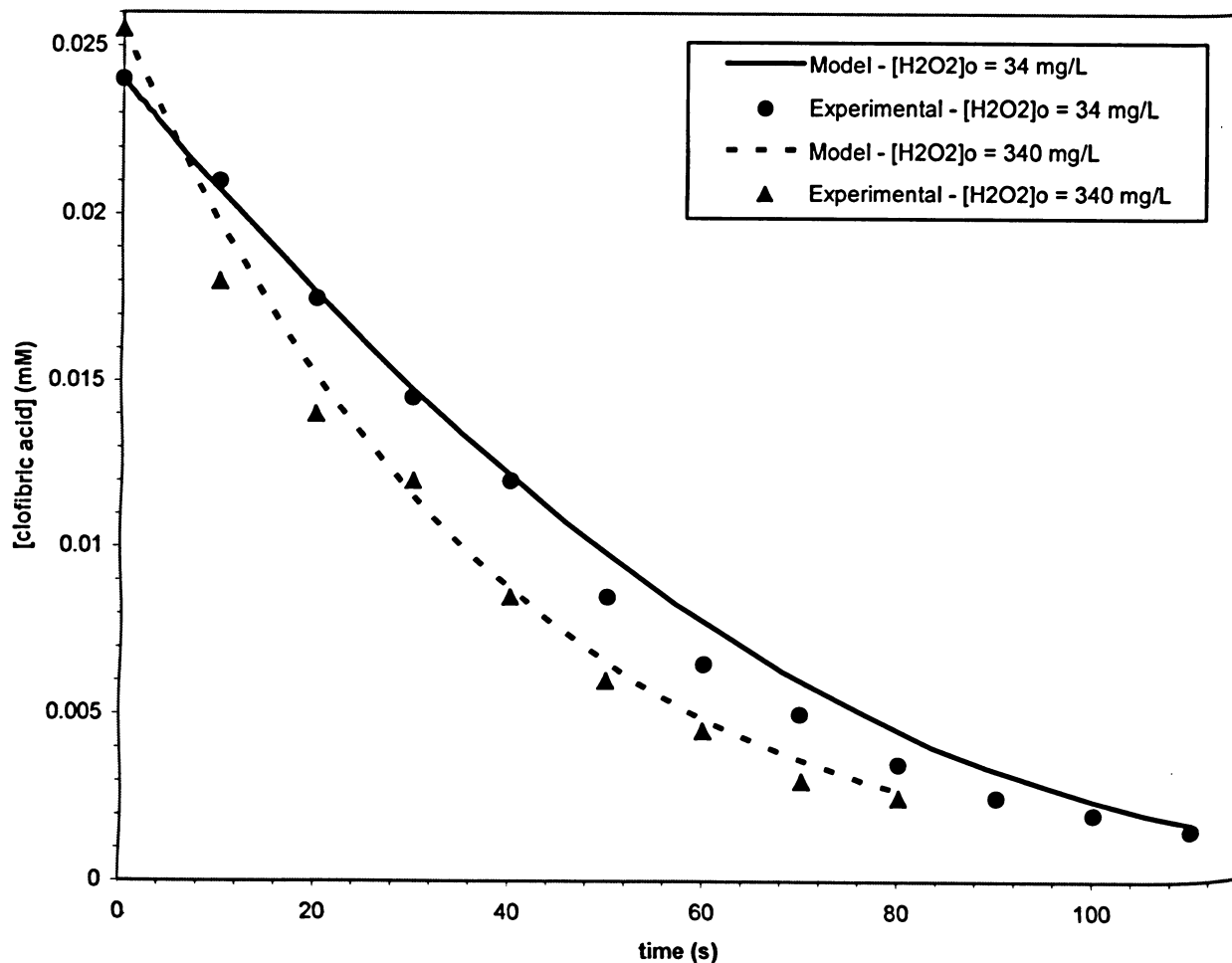


Figure 7. Clofibric Acid Concentration vs. Time – Performance of Modified Model to Predict Experimental Results Reported by Andreozzi et al. (2003)

Utilizing a value for the reaction rate constant between clofibric acid and the hydroxyl radical, k_6 , of $2.38 \times 10^9 \text{ M}^{-1}\cdot\text{s}^{-1}$, a value for the reaction rate constant between H_2O_2 and the hydroxyl radical, k_2 , of $2.7 \times 10^7 \text{ M}^{-1}\cdot\text{s}^{-1}$ as reported by Andreozzi et al. (2003). All other rate constants and quantum yield values as listed in Table 5.

4.1.3. Effect of Inhibitors

It was desired to investigate the effect of inhibitors' presence on the behaviour of the calibrated model. All simulations were run using the same simulation model developed and used in Section 4.1.1 (see Appendix B).

Effect of H₂O₂ as an Inhibitor

An increase in the rate of removal of organic compounds has been observed with increasing H₂O₂ concentration until an optimal dose is reached. Above this dose, the rate of removal of organics tends to decrease due to the hydroxyl radical scavenging behaviour of H₂O₂ (Shen and Wang, 2002).

Model simulations were run with increasing initial H₂O₂ doses to determine if the model would express a similar behaviour. The extinction coefficient for distilled water was used to determine the extinction coefficient of the aqueous solution for these simulations. The results of these runs are presented in Figure 8.

As can be seen, increasing the initial H₂O₂ dose increased the predicted removal of metronidazole up to an initial dose of approximately 50 mg/L. At dosages >50 mg/L, there was a reduction in removal efficiency, indicating the inhibitory effect of H₂O₂ at concentrations above the optimal dose.

As a result, the model is able to predict an optimal initial H₂O₂ dose, and the inhibitory effect of H₂O₂ at dosages greater than the optimal level.

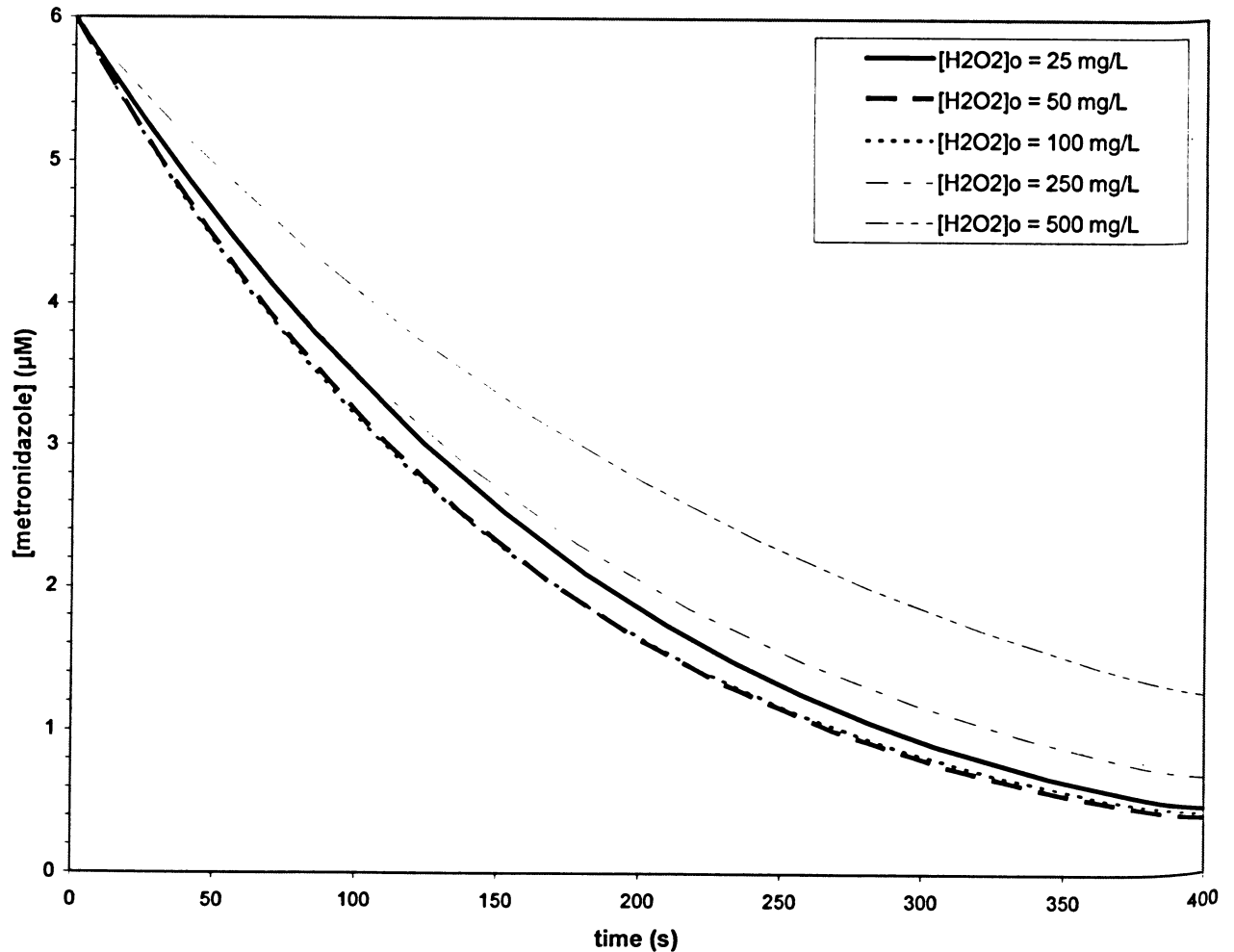


Figure 8. Effect of $[H_2O_2]_0$ on Model Predicted Removal of Metronidazole – Optimal H_2O_2 Dose

Model predictions obtained utilizing a value for the reaction rate constant between metronidazole and the hydroxyl radical, k_6 , of $1.98 \times 10^9 M^{-1} \cdot s^{-1}$. All other rate constants and quantum yield values as listed in Table 5. Extinction coefficient for distilled water was used, and it was assumed no alkalinity present. Thicker lines represent conditions at or below the optimal H_2O_2 dose; thinner lines represent conditions above the optimal H_2O_2 dose.

Effect of Alkalinity as an Inhibitor

In the UV/H₂O₂ oxidation process, carbonate and bicarbonate anions act as hydroxyl radical scavengers, reducing the number of hydroxyl radicals in the system, thus reducing the removal efficiency of target compounds. A measure of the concentration of carbonate and bicarbonate ions in an aqueous solution is known as “alkalinity”, and is reported in mg/L as CaCO₃.

For practical application, the UV/H₂O₂ AOP process could be used for the treatment of potable water supplies. Since surface and ground water potable water sources can have varying levels of alkalinity, carbonate and bicarbonate ions naturally present can have a significant impact on target compound removal. The Ontario Drinking Water Standards, Objectives, and Guidelines state an operational guideline for alkalinity of 30 to 500 mg/L (Ontario Ministry of the Environment, 2003). It was desired to model the impact of alkalinity levels within that range.

Simulations were run using the same simulation model developed and used in Section 4.1.1 (see Appendix B). Alkalinity concentrations of 75 mg/L, 150 mg/L, and 225 mg/L as CaCO₃ were used, and it was assumed that the alkalinity was due to the presence of bicarbonate ions only, since at the solution pH of 6.0, the concentration of carbonate ions would be negligible (see Appendix B). The extinction coefficient for typical tap water (10 m⁻¹) was used to determine the overall extinction coefficient of the aqueous solutions for these simulations. All simulations were run for an initial H₂O₂ concentration at 50 mg/L. All other parameters used were equal to those used in the model calibration (see Section 4.1.1). The results of these runs are shown in Figure 9.

As can be seen, increasing alkalinity levels have an inhibitory effect on the model predicted removal of metronidazole. As the concentration of alkalinity was increased, there was a decrease in the predicted removal of metronidazole.

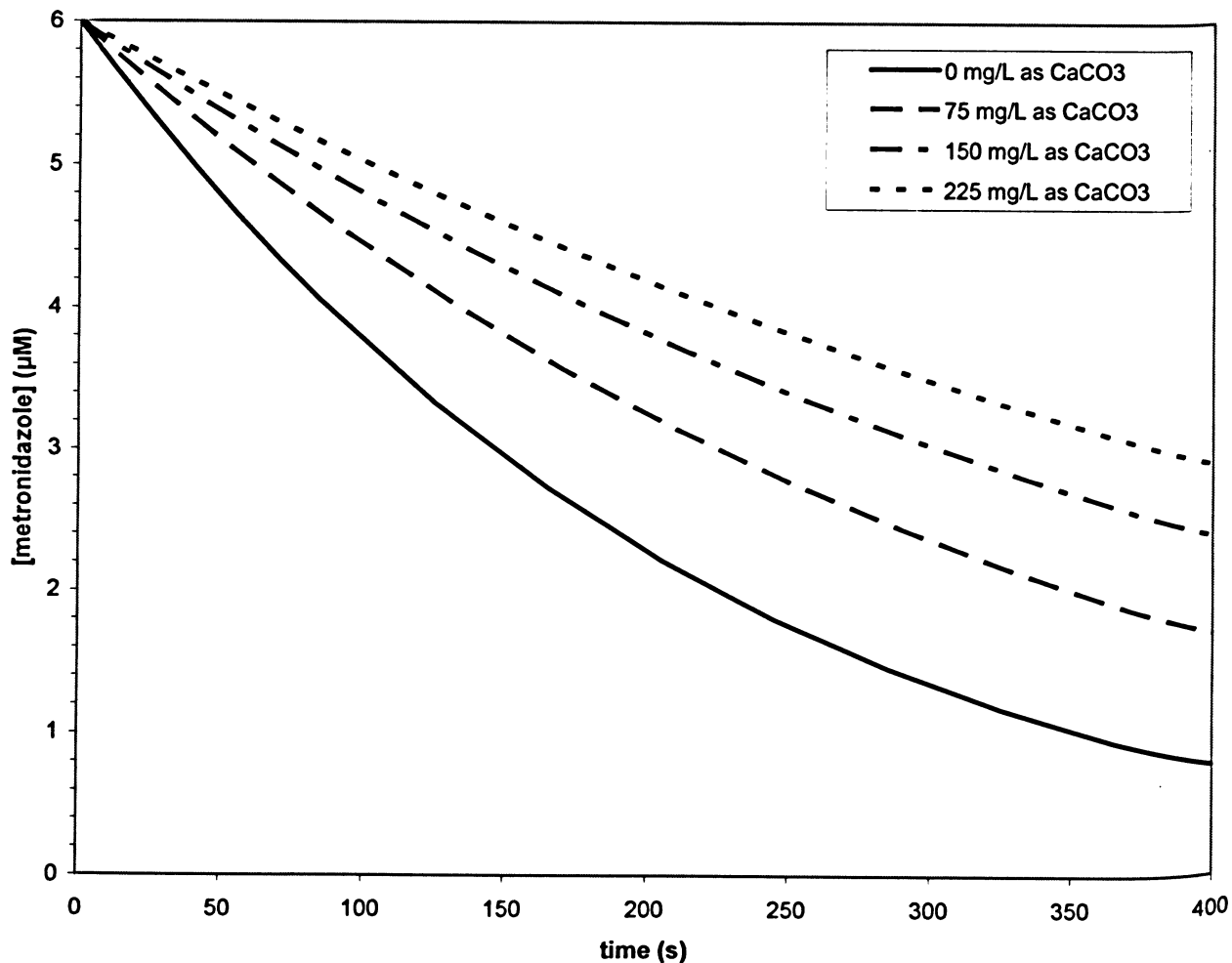


Figure 9. Effect of Alkalinity as CaCO₃ on Model Predicted Removal of Metronidazole with [H₂O₂]₀ = 50 mg/L

Model predictions obtained utilizing a value for the reaction rate constant between metronidazole and the hydroxyl radical, k_6 , of $1.98 \times 10^9 \text{ M}^{-1}\cdot\text{s}^{-1}$. All other rate constants and quantum yield values as listed in Table 5. Extinction coefficient for typical tap water was used.

Effect of Alkalinity on the Optimal H₂O₂ Dose

In order to determine if the presence of alkalinity would impact the model predicted optimal H₂O₂ dose, model simulations were run using the same simulation model developed and used in Section 4.1.1 (see Appendix B). An alkalinity concentration of 75 mg/L as CaCO₃ was used for each run, and initial H₂O₂ doses were increased to determine the predicted optimal dose. The extinction coefficient for typical tap water (10 m⁻¹) was used to determine the overall extinction coefficient of the aqueous solutions for these simulations. All other parameters used were equal to those used in the model calibration (see Section 4.1.1). The results of these runs are shown in Figure 10.

As can be seen in Figure 10, increasing the initial H₂O₂ dose increased the predicted removal of metronidazole up to an initial dose of approximately 200 mg/L. At dosages >200 mg/L, there was a reduction in removal efficiency, indicating the inhibitory effect of H₂O₂ at concentrations above the optimal dose.

It was shown that the optimal H₂O₂ dose for the system without the presence of alkalinity was approximately 50 mg/L, and that with the presence of alkalinity the optimal dose was approximately 200 mg/L. Based on these results, it appears that the presence of alkalinity increases the model predicted optimal H₂O₂ dose.

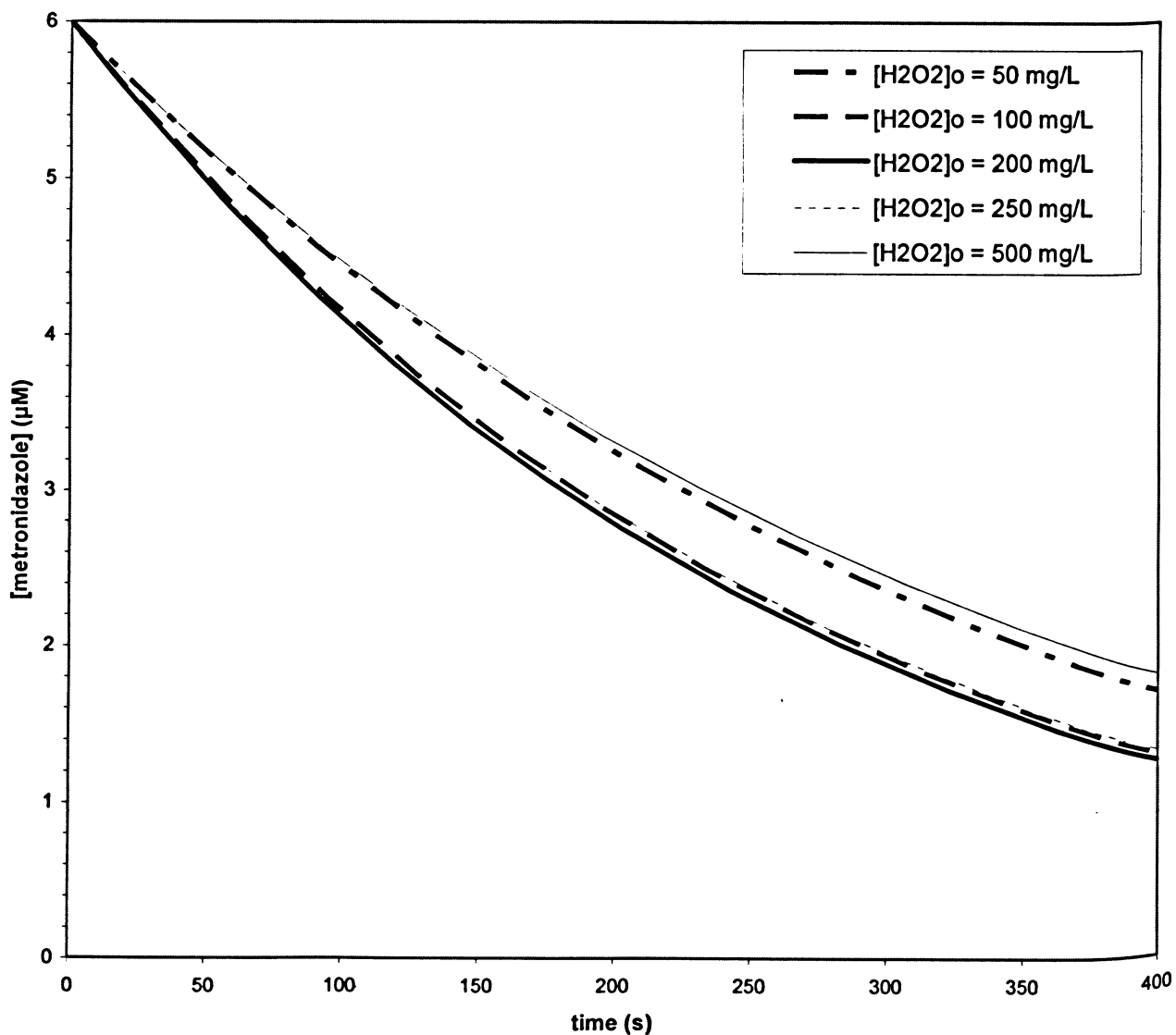


Figure 10. Effect of $[H_2O_2]_0$ on Model Predicted Removal of Metronidazole with Alkalinity of 75 mg/L as $CaCO_3$ – Optimal H_2O_2 Dose

Model predictions obtained utilizing a value for the reaction rate constant between metronidazole and the hydroxyl radical, k_6 , of $1.98 \times 10^9 M^{-1} \cdot s^{-1}$. All other rate constants and quantum yield values as listed in Table 5. Extinction coefficient for typical tap water was used. Thicker lines represent conditions at or below the optimal H_2O_2 dose; thinner lines represent conditions above the optimal H_2O_2 dose.

4.2. Modeling Metronidazole Removal in the Proposed Photoreactors

4.2.1. Single Lamp Photoreactors – Reactor 1 and Reactor 2

The reaction model calibrated and assessed in Section 4.1 was used to predict the removal of metronidazole in Reactor 1 and Reactor 2. For all modeling runs in the photoreactors, the initial concentration of metronidazole was 6 μM in an aqueous solution with an alkalinity of 75 mg/L as CaCO_3 . Reactor 1 and Reactor 2 each have identical dimensions, however each are equipped with a different lamp: the lamps in Reactor 1 each have a UV output of 25.5 W, while the lamps in Reactor 2 each have a UV output of 36 W.

These conditions were simulated utilizing the chemical reaction model developed in Section 3.3, and the radiation energy balance for the single lamp reactor developed in Section 3.2.3 (see simulation model development and Matlab code in Appendix C).

The extinction coefficient of the aqueous solution was assumed to be constant for all locations within the photoreactor, and was calculated based on the extinction coefficient of tap water and in the influent concentration of H_2O_2 . The UV absorptive properties of metronidazole were neglected due to its low influent concentration, and the influent concentration of H_2O_2 was used because it was assumed that very little H_2O_2 would be consumed, resulting in an almost uniform concentration of H_2O_2 throughout the reactor.

As a preliminary investigation, the concentration profiles of metronidazole along the reactor radius at various retention times were developed for both Reactor 1 and Reactor 2. The initial H_2O_2 dose was kept constant at 100 mg/L. Results for Reactor 1 are shown in Figure 11. Results for Reactor 2 are shown in Figure 12.

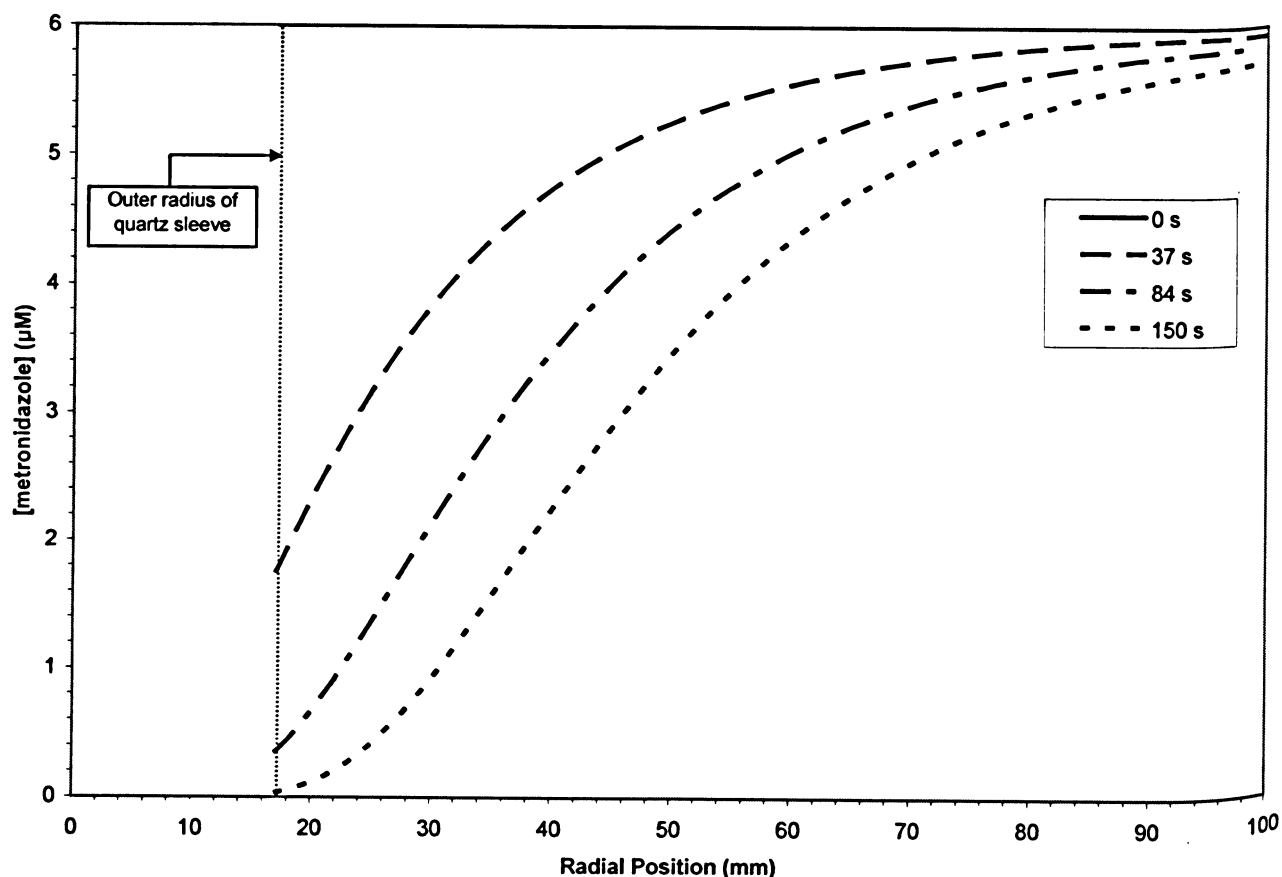


Figure 11. Concentration Profile of Metronidazole in Reactor 1 at Various Residence Times with $[H_2O_2]_{inf} = 100$ mg/L

Treating a solution of metronidazole with an initial concentration of $6 \mu\text{M}$, and an alkalinity of 75 mg/L at a flow rate of 2.0 L/s. Model predictions obtained utilizing a value for the reaction rate constant between metronidazole and the hydroxyl radical, k_6 , of $1.98 \times 10^9 \text{ M}^{-1}\cdot\text{s}^{-1}$. All other rate constants and quantum yield values as listed in Table 5. Extinction coefficient of typical tap water used. Residence time of 0 s equivalent to the inlet of the reactor, 37 s equivalent to an axial position of 2.4 m, 84 s equivalent to an axial position of 5.5 m, and 150 s equivalent to an axial position of 9.7 m.

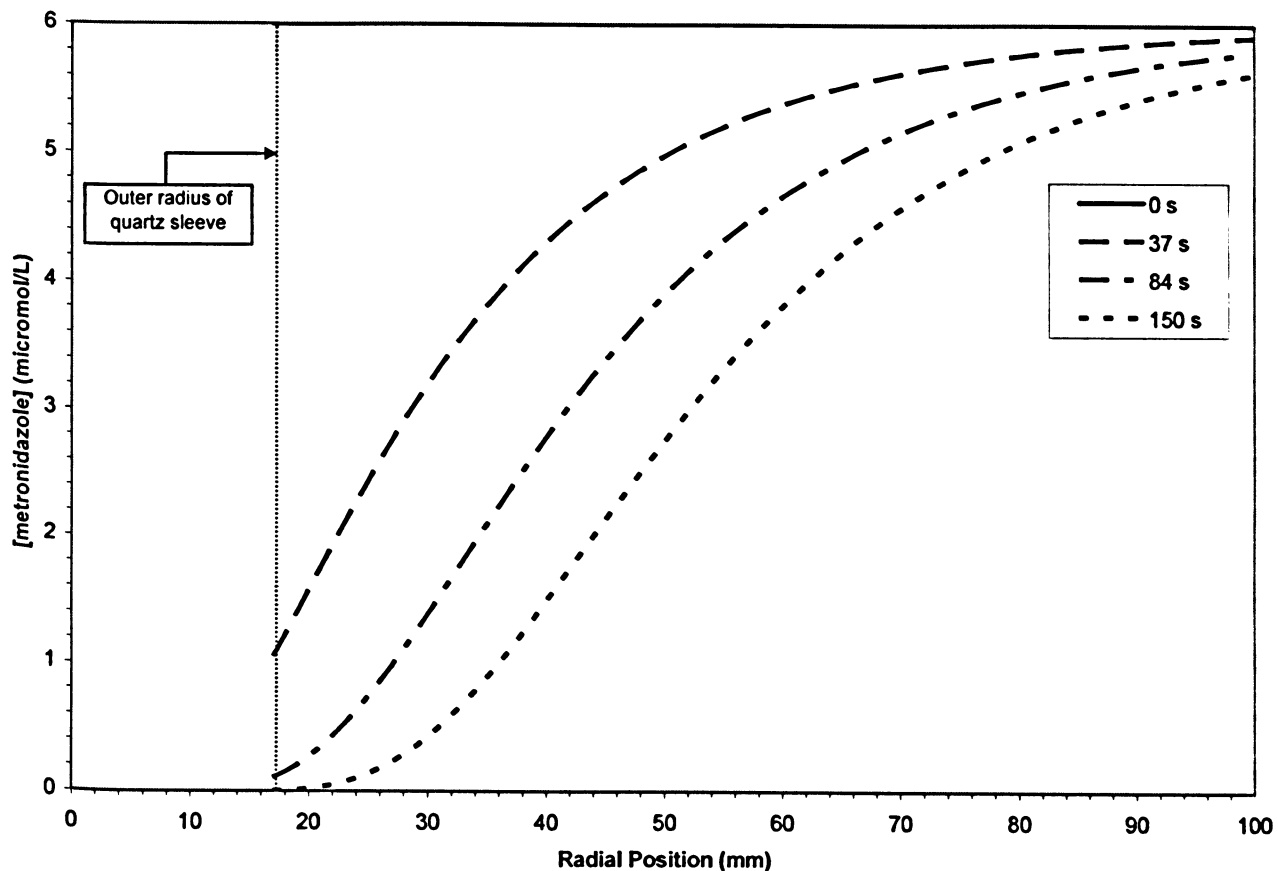


Figure 12. Concentration Profile of Metronidazole in Reactor 2 at Various Residence Times with $[H_2O_2]_{inf} = 100$ mg/L

Treating a solution of metronidazole with an initial concentration of $6 \mu\text{M}$, and an alkalinity of 75 mg/L at a flow rate of 2.0 L/s. Model predictions obtained utilizing a value for the reaction rate constant between metronidazole and the hydroxyl radical, k_6 , of $1.98 \times 10^9 \text{ M}^{-1} \cdot \text{s}^{-1}$. All other rate constants and quantum yield values as listed in Table 5. Extinction coefficient of typical tap water used. . Residence time of 0 s equivalent to the inlet of the reactor, 37 s equivalent to an axial position of 2.4 m, 84 s equivalent to an axial position of 5.5 m, and 150 s equivalent to an axial position of 9.7 m.

The results presented in Figure 11 predict that removal of metronidazole increases as residence time within the Reactor 1 increases. In addition, for any given time instant >0 s, the concentration of metronidazole increases with increasing radial position. This is due to the fact that UV irradiance decreases with increasing radial position, due to increased distance from the UV lamp and the UV radiation adsorptive properties of the aqueous solution.

Similar trends are observed for Reactor 2 (see Figure 12). However, it can be seen that the concentration profiles for Reactor 2 show lower concentrations at any given time instant >0 s and radial position that those shown for Reactor 1 (see Figure 11).

Average effluent metronidazole concentrations for Reactor 1 and Reactor 2 were determined for each set of operating conditions, and are summarized in Table 6 and Table 7. Summaries of average effluent H_2O_2 concentrations can be found in Appendix C.

Based on the average effluent concentrations presented in Table 6 and Table 7, 4.9% to 9.8% of the metronidazole was removed in Reactor 1, and 6.6% to 13% was removed in Reactor 2. Little target compound was removed, however removal was greater in Reactor 2 for each set of operating conditions (22% to 39% more removal in Reactor 2 than in Reactor 1). This is due to the fact that the UV output of the lamp used in Reactor 2 was 41% greater than that in Reactor 1. In addition, the low removal of metronidazole implies that very few reaction intermediates were formed, thus the assumption that the effect of these intermediates were negligible appears to be valid.

Based on the detailed modeling results for Reactor 1 and Reactor 2, at all points in the reactor the concentration of H_2O_2 was $\geq 80\%$ of the influent H_2O_2 concentration. As a result, the assumption that very little H_2O_2 would be consumed, resulting in an almost uniform concentration of H_2O_2 throughout the reactor, also appears to be valid.

Table 6. Average Effluent Metronidazole Concentrations for Reactor 1 Operating in Series at Various Operating Conditions

Treating a solution of metronidazole with an initial concentration of 6 μM , and an alkalinity of 75 mg/L at a flow rate of 2.0 L/s. Model predictions obtained utilizing a value for the reaction rate constant between metronidazole and the hydroxyl radical, k_6 , of $1.98 \times 10^9 \text{ M}^{-1}\cdot\text{s}^{-1}$. All other rate constants and quantum yield values as listed in Table 5. Extinction coefficient of typical tap water used. Average

Reactor Radius (mm)	Residence Time (s)	Influent H_2O_2 Concentration (mg/L)			
		25	50	75	100
50	8.3	5.71	5.60	5.55	5.53
100	37	5.58	5.46	5.42	5.41
150	84	5.58	5.48	5.47	5.48
200	150	5.61	5.54	5.54	5.56
250	235	5.65	5.60	5.60	5.62

Notes:

All reported average effluent metronidazole concentrations in μM , and were calculated utilizing the trapezoidal rule (see Appendix C).

Concentration in bold represents the lowest average effluent concentration observed.

Table 7. Average Effluent Metronidazole Concentrations for Reactor 2 at Various Operating Conditions

Treating a solution of metronidazole with an initial concentration of 6 μM , and an alkalinity of 75 mg/L at a flow rate of 2.0 L/s. Model predictions obtained utilizing a value for the reaction rate constant between metronidazole and the hydroxyl radical, k_6 , of $1.98 \times 10^9 \text{ M}^{-1}\cdot\text{s}^{-1}$. All other rate constants and quantum yield values as listed in Table 5. Extinction coefficient of typical tap water used.

Reactor Radius (mm)	Residence Time (s)	Influent H_2O_2 Concentration (mg/L)			
		25	50	75	100
50	8.3	5.60	5.45	5.38	5.35
100	37	5.43	5.27	5.23	5.22
150	84	5.44	5.33	5.31	5.33
200	150	5.50	5.42	5.42	5.45
250	235	5.56	5.50	5.51	5.54

Notes:

All reported average effluent metronidazole concentrations in μM , and were calculated utilizing the trapezoidal rule (see Appendix C).

Concentration in bold represents the lowest average effluent concentration observed.

For both reactors, the lowest average effluent metronidazole concentration was obtained with an influent H₂O₂ dose of 100 mg/L and a reactor radius of 100 mm (5.41 μM for Reactor 1, and 5.22 μM for Reactor 2).

For both reactors, the lowest average effluent metronidazole concentration for a given reactor radius was obtained at the highest modeled influent H₂O₂ concentration of 100 mg/L. This implies that the influent H₂O₂ concentrations were below the optimal dose, and no inhibitory effect was observed.

For both reactors, the lowest average effluent metronidazole concentration for a given influent H₂O₂ concentration was obtained with a reactor radius of 100 mm. This implies that, for the influent H₂O₂ concentrations modeled and the composition and flow rate of the solution to be treated, a reactor radius of 100 mm provides the most efficient use of UV light energy.

It should be noted, however, that for Reactor 1 with an influent H₂O₂ concentration of 25 mg/L, the average effluent metronidazole concentration was lowest for two reactor radii: 100 mm and 150 mm. This implies that, at lower influent H₂O₂ concentrations, the most efficient use of UV light energy may be provided with a larger reactor diameter. To test this result, simulations were run for Reactor 1 with an influent H₂O₂ concentration of 10 mg/L (see Appendix C for detailed results). Based on these simulations, the lowest average effluent metronidazole concentration was obtained with two reactor radii: 150 mm and 200 mm. Thus, it appears that, for a given influent H₂O₂ concentration, the reactor radius resulting in the lowest effluent metronidazole concentration varies with respect to the influent H₂O₂ concentration: as the influent H₂O₂ concentration is decreased, the reactor radius resulting in the lowest average effluent metronidazole concentration is increased. .

4.2.2. Multiple Lamp Reactor – Reactor 3

The reaction model calibrated and assessed in Section 4.1 was used to predict the removal of metronidazole in Reactor 3. For all modeling runs in the photoreactor, the initial concentration of metronidazole was 6 μM in an aqueous solution with an alkalinity of 75 mg/L as CaCO₃.

As discussed in Section 3.2.3, the LVREA at any point in Reactor 3, A , is the sum of the contributions of all four lamps (see Appendix D for details). The shielding of photons by the lamps and quartz tubes was neglected. Due to the symmetry of Reactor 3, it was only necessary to model one quadrant of the reactor. These conditions were simulated utilizing the chemical reaction model developed in Section 3.3, and the radiation energy balance for the multi-lamp reactor developed in Section 3.2.3 (see simulation model development and Matlab code in Appendix D).

As with Reactor 1 and Reactor 2, the extinction coefficient of the aqueous solution was assumed to be constant for all locations within the photoreactor, and was calculated based on the extinction coefficient of tap water and in the influent concentration of H_2O_2 . The UV absorptive properties of metronidazole were neglected due to its low influent concentration, and the influent concentration of H_2O_2 was used because it was assumed that very little H_2O_2 would be consumed, resulting in an almost uniform concentration of H_2O_2 throughout the reactor.

As a preliminary investigation, the concentration profile of metronidazole for a quadrant of Reactor 3 was developed at the mid-point of Reactor 3, and the effluent of Reactor 3 with an influent H_2O_2 dose of 100 mg/L and a reactor radius of 100 mm. These profiles are shown in Figure 13. See Appendix D for larger versions of each profile shown in Figure 13.

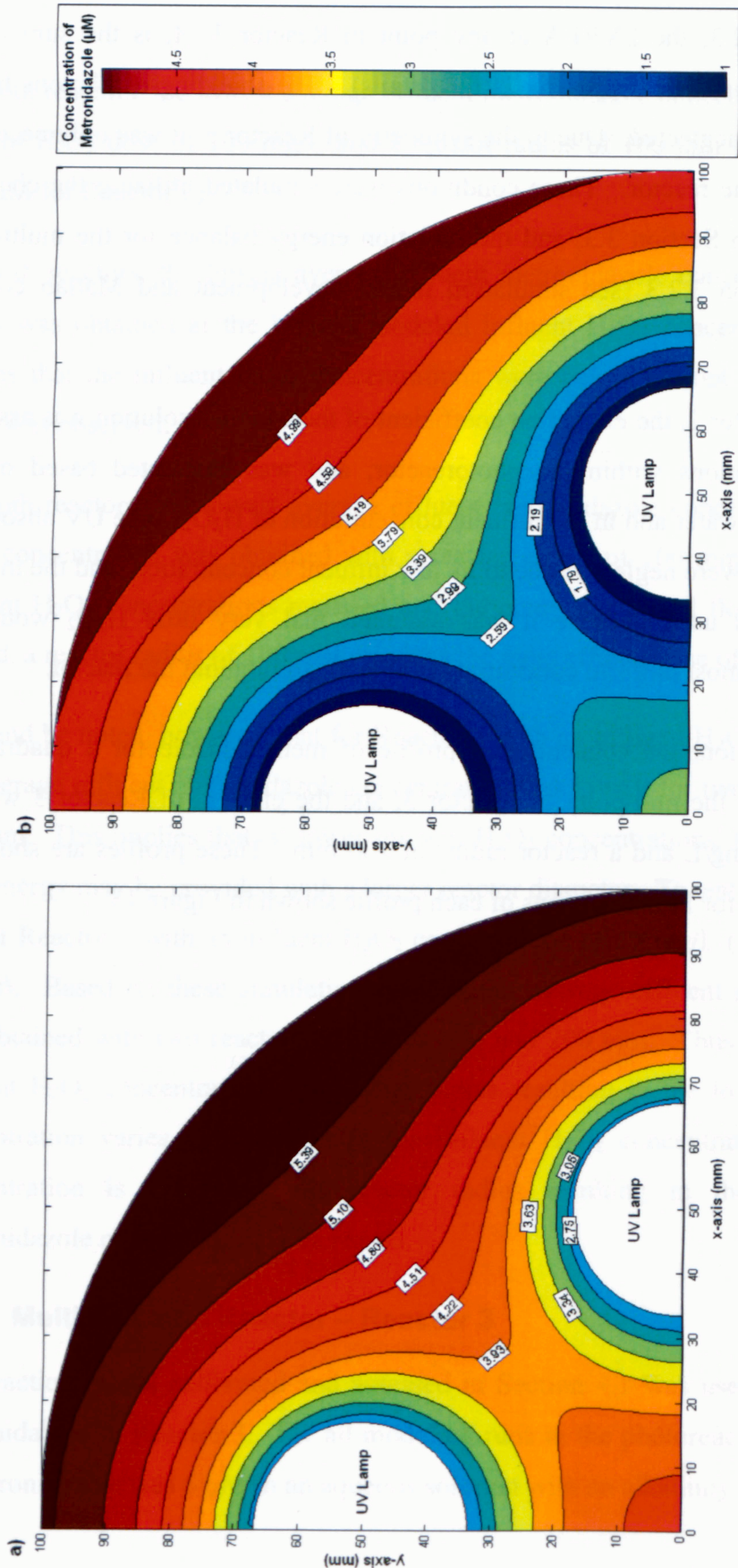


Figure 13. Metronidazole Concentration Profile for a Quadrant of Reactor 3 with $[H_2O_2]_{inf} = 100 \text{ mg/L}$ and $R = 100 \text{ mm}$ at Two Axial Positions within the Reactor

Treatment of a $6 \mu\text{M}$ metronidazole solution with an alkalinity of 75 mg/L and pH of 6 , at a flow rate of 2.0 L/s : **a)** Shown above at a distance of 1.2 m from inlet of Reactor 3, at an equivalent residence time of 17 seconds , with an average metronidazole concentration of $4.56 \mu\text{M}$, and **b)** Shown above at the outlet of Reactor 3, a distance of 2.4 m from the inlet, at an equivalent residence time of 33 seconds , with an average metronidazole concentration of $3.54 \mu\text{M}$.

The results presented in Figure 13 predict increased removal of metronidazole in the regions closest to the UV lamps. A similar result was obtained for Reactor 1 and Reactor 2. In addition, removal is enhanced in regions of the reactor that have high LVREA values due to the additive contribution of multiple UV lamps. For example, in Figure 13 (b), the effluent concentration in the region around the coordinates (22 mm, 22 mm) is approximately 2.5 μM , and approximately 3.5 μM around the coordinates (78 mm, 22 mm). These two regions are a similar distance away from the UV lamp, however the LVREA around the coordinates (22 mm, 22 mm) is enhanced due to the additive effect of the two UV lamps, resulting in a 40% increase in removal of metronidazole as compared to around the coordinates (78 mm, 22 mm).

Average effluent metronidazole concentrations for Reactor 3 were determined for various sets of operating conditions, and are summarized in Table 8. Simulations were run for a given influent H_2O_2 concentration with increasing outer reactor radius until it was ascertained that the average effluent concentration reached a minimum. Summaries of average effluent H_2O_2 concentrations can be found in Appendix D.

Table 8. Average Effluent Metronidazole Concentrations for Reactor 3 at Various Operating Conditions

Treating a solution of metronidazole with an initial concentration of 6 μM , and an alkalinity of 75 mg/L at a flow rate of 2.0 L/s. Model predictions obtained utilizing a value for the reaction rate constant between metronidazole and the hydroxyl radical, k_6 , of $1.98 \times 10^9 \text{ M}^{-1}\cdot\text{s}^{-1}$. All other rate constants and quantum yield values as listed in Table 5. Extinction coefficient of typical tap water used.

Reactor Radius (mm)	Residence Time (s)	Influent H_2O_2 Concentration (mg/L)			
		25	50	75	100
50	5.1	5.18	4.88	4.74	4.67
100	33	4.21	3.75	3.60	3.54
150	81	4.06	3.68	3.61	3.63
200	146	4.15	3.87	3.85	3.92
250	231	4.31	4.10	4.12	4.21

Notes:

All reported average effluent metronidazole concentrations in $\mu\text{mol/L}$.

Concentration in bold represents the lowest average effluent concentration observed.

Based on the average effluent concentrations presented in Table 8, 14% to 41% of the metronidazole was removed in Reactor 3. Removal was greater in Reactor 3 than in either Reactor 1 or Reactor 2. This is due to the fact that Reactor 3 is equipped with four UV lamps, each emitting 36 W of UV output, resulting in a greater UV output than in either Reactor 1 or Reactor 2. 90% removal of metronidazole was predicted for seven reactors of the same configuration as Reactor 3 operated in series.

As with Reactor 1 and Reactor 2, the lowest average effluent metronidazole concentration for Reactor 3 for a given reactor radius was obtained at the highest modeled influent H_2O_2 concentration of 100 mg/L.

The lowest average effluent concentrations of metronidazole attained for Reactor 3, 3.54 μM , was with a radius of 100 mm and an influent H_2O_2 concentration of 100 mg/L. In addition, it can be seen that, for a given influent H_2O_2 concentration, the reactor radius resulting in the lowest effluent metronidazole concentration varies with respect to the influent H_2O_2 concentration. This implies that selection of a reactor outer radius for maximum metronidazole removal varies with influent H_2O_2 concentration for the multiple UV lamp reactor.

4.2.3. Local Optimal Initial H_2O_2 Dose and Reactor Radius

It was determined in Section 4.2.1 and Section 4.2.2 that the average effluent metronidazole concentration for a given reactor radius could be lowered by increasing the UV lamp output, and increasing the influent H_2O_2 concentration. Increasing these operational parameters also increases the operational cost, hence it was desired to investigate the operational cost per mmol of metronidazole removed to determine the optimal operating conditions for each reactor studied.

Using Equation (39), operational costs per mmol of metronidazole removed were determined for various operating conditions for each reactor studied (see Appendix E for a sample calculation). These costs were based on average influent and effluent H_2O_2 concentrations, as well as the number of UV lamps in operation and their total wattage. Summaries of operational costs for each reactor are shown in Table 9, Table 10, and Table 11.

Table 9. Operational Cost per Amount of Metronidazole Removed in Reactor 1 at Various Operating Conditions

Treating a solution of metronidazole with an initial concentration of 6 μM , and an alkalinity of 75 mg/L at a flow rate of 2.0 L/s. Model predictions obtained utilizing a value for the reaction rate constant between metronidazole and the hydroxyl radical, k_6 , of $1.98 \times 10^9 \text{ M}^{-1}\cdot\text{s}^{-1}$. All other rate constants and quantum yield values as listed in Table 5. Extinction coefficient of typical tap water used.

Reactor Radius (mm)	Influent H ₂ O ₂ Concentration (mg/L)			
	25	50	75	100
50	0.33	0.47	0.61	0.77
100	0.22	0.34	0.47	0.63
150	0.22	0.36	0.52	0.70
200	0.24	0.40	0.60	0.83
250	0.27	0.46	0.70	0.98

Notes:

All reported operational costs in \$/mmol metronidazole removed.

Concentration in bold represents the lowest average effluent concentration observed.

Table 10. Operational Cost per Amount of Metronidazole Removed in Reactor 2 at Various Operating Conditions

Treating a solution of metronidazole with an initial concentration of 6 μM , and an alkalinity of 75 mg/L at a flow rate of 2.0 L/s. Model predictions obtained utilizing a value for the reaction rate constant between metronidazole and the hydroxyl radical, k_6 , of $1.98 \times 10^9 \text{ M}^{-1}\cdot\text{s}^{-1}$. All other rate constants and quantum yield values as listed in Table 5. Extinction coefficient of typical tap water used.

Reactor Radius (mm)	Influent H ₂ O ₂ Concentration (mg/L)			
	25	50	75	100
50	0.24	0.34	0.45	0.57
100	0.17	0.26	0.36	0.47
150	0.17	0.28	0.40	0.55
200	0.19	0.32	0.48	0.67
250	0.21	0.37	0.57	0.80

Notes:

All reported operational costs in \$/mmol metronidazole removed.

Concentration in bold represents the lowest average effluent concentration observed.

Table 11. Operational Cost per Amount of Metronidazole Removed in Reactor 3 at Various Operating Conditions

Treating a solution of metronidazole with an initial concentration of 6 μM , and an alkalinity of 75 mg/L at a flow rate of 2.0 L/s. Model predictions obtained utilizing a value for the reaction rate constant between metronidazole and the hydroxyl radical, k_6 , of $1.98 \times 10^9 \text{ M}^{-1}\cdot\text{s}^{-1}$. All other rate constants and quantum yield values as listed in Table 5. Extinction coefficient of typical tap water used.

Reactor Radius (mm)	Influent H_2O_2 Concentration (mg/L)			
	25	50	75	100
50	0.13	0.18	0.23	0.29
100	0.06	0.09	0.12	0.15
150	0.05	0.08	0.12	0.16
200	0.06	0.09	0.13	0.18
250	0.06	0.10	0.15	0.21

Notes:

All reported operational costs in \$/mmol metronidazole removed.

Concentration in bold represents the lowest average effluent concentration observed.

n/a – no data available. No simulation run for that combination of operating conditions.

Table 12 presents a summary of the local optimal operating conditions determined for each reactor.

Table 12. Local Optimal Operating Conditions in Terms of Minimum Operational Cost per mmole of Metronidazole Removed

Treating a solution of metronidazole with an initial concentration of 6 μM , and an alkalinity of 75 mg/L at a flow rate of 2.0 L/s. Model predictions obtained utilizing a value for the reaction rate constant between metronidazole and the hydroxyl radical, k_6 , of $1.98 \times 10^9 \text{ M}^{-1}\cdot\text{s}^{-1}$. All other rate constants and quantum yield values as listed in Table 5. Extinction coefficient of typical tap water used.

Local Optimal Parameter	Reactor 1	Reactor 2	Reactor 3
Influent H_2O_2 Concentration ($[\text{H}_2\text{O}_2]_{\text{inf}}$)	25 mg/L	25 mg/L	25 mg/L
Reactor Radius (R°)	100 – 150 mm	100 – 150 mm	150 mm
Average Effluent Metronidazole Concentration	5.58 $\mu\text{mol/L}$	5.43 – 5.44 $\mu\text{mol/L}$	4.06 $\mu\text{mol/L}$
Operational Cost per mmol Metronidazole Removed	\$0.22/mmol	\$0.17/mmol	\$0.05/mmol

As can be seen, the optimal influent H_2O_2 concentration, $[H_2O_2]_{inf}$, was the same for all three reactors, at 25 mg/L.

The lowest operational cost per mmol of metronidazole removed was projected for Reactor 3, while the highest was projected for Reactor 1. Based on the results presented in Table 9, Table 10, and Table 11, for a given set of operating conditions, the operational cost per mmol of metronidazole removed was higher for Reactor 1 than for Reactor 2. Since the only difference between Reactor 1 and Reactor 2 is the UV output of the lamp, this implies that reduced operational costs can be achieved by increasing the UV output of the lamp, in spite of the increase in electricity costs. A similar trend is observed when comparing the results for Reactor 2 and Reactor 3.

For all reactors, increasing the influent H_2O_2 concentration, while keeping the reactor radius constant, resulted in an increase in operational costs per mmol of metronidazole removed. Conversely, as seen in Section 4.2.1 and Section 4.2.2, an increase in influent H_2O_2 concentration resulted in an increase in removal of metronidazole.

These results imply that the chemical costs associated with increasing influent H_2O_2 concentration are much greater than the electrical costs associated with increasing UV lamp output. As a result, it appears that, from an operational perspective, it would be cost effective to increase the UV lamp output, while keeping influent H_2O_2 concentration low.

Such a strategy, however, would have impacts on the capital costs for such an installation. The costs associated with the purchase of a greater number of high output UV lamps could make such an approach cost prohibitive. In addition, no operational cost estimates were included for UV lamp replacement. A greater number of high output UV lamps would increase the lamp replacement costs. As a result, in order to properly assess the optimal operating conditions, a 25 year life cycle cost analysis should be conducted to provide a more realistic evaluation of total costs.

CHAPTER 5.

CONCLUSIONS AND RECOMMENDATIONS

5.1. Conclusions

5.1.1. Model Calibration and Assessment

1. The reaction rate constant for the reaction between metronidazole and hydroxyl radical was determined to be $1.98 \times 10^9 \text{ M}^{-1}\cdot\text{s}^{-1}$. This calibration was done based on experimental results published elsewhere (Shemer et al. 2006).
2. The calibrated reaction model was able to predict an optimal initial H_2O_2 dose, and the inhibitory effect of H_2O_2 doses above the optimal value.
3. The calibrated reaction model was able to predict the inhibitory effect due to the presence of alkalinity as bicarbonate ions in the aqueous solution to be treated.
4. The calibrated reaction model predicted an increase in the optimal initial H_2O_2 dose with the presence of alkalinity in the solution to be treated.
5. The reaction model was able to accurately predict the removal of clofibric acid based on experimental results published elsewhere (Andreozzi et al., 2003).
6. Based on the above, the calibrated reaction model was assumed to be valid and was used to predict the removal of metronidazole in the proposed single and multiple UV lamp photoreactors.

5.1.2. Behaviour of the Modeled Photoreactors

1. 4.9% to 9.8% of the metronidazole was removed in Reactor 1, 6.6% to 13% was removed in Reactor 2, and 14% to 41% was removed in Reactor 3.
2. Keeping the reactor radius constant, the average effluent metronidazole concentration could be lowered by increasing the UV lamp output, and increasing the influent H_2O_2 concentration.

3. Selection of a reactor radius for maximum metronidazole removal varied with influent H_2O_2 concentration.

5.1.3. Optimal H_2O_2 Dose and Reactor Radius

1. Optimal influent H_2O_2 concentration, $[H_2O_2]_{inf}^*$, and outer reactor radius, R^* , resulting in the lowest operational cost per mmol of metronidazole removed, were determined for each reactor. The lowest operational cost per mmol of metronidazole removed was projected for Reactor 3, at \$0.05/mmol, while the highest was projected for Reactor 1, at \$0.22/mmol.
2. The optimal influent H_2O_2 concentration, $[H_2O_2]_{inf}^*$, was the same for all three reactors, at 25 mg/L.
3. Based on the results of this study, it appears that, from an operational perspective, it would be cost effective to increase the UV lamp output, while keeping influent H_2O_2 concentration low.

5.2. Recommendations

1. Since the model was calibrated based on a limited number of experimental data points, it is recommended that additional batch experimental runs be performed to confirm and/or refine the value of the reaction rate constant for the reaction between metronidazole and hydroxyl radical obtained in this work.
2. Pilot scale single and multi lamp UV reactors, of similar configuration to Reactor 1, Reactor 2, and Reactor 3, could be constructed, and experimental runs performed. The resulting experimental results could be compared to simulation model predictions.
3. It is recommended that additional optimization be done with respect to the influent H_2O_2 dose, since this study considered only four influent doses.
4. It is recommended that additional optimization be done with respect to Reactor 3 to determine the optimal position of the lamps within the reactor for various operating conditions.

5. It is recommended that the effects of different flow regimes, such as laminar flow, within the reactors be investigated.
6. It is recommended that the model be expanded to predict the treatment of multiple target compounds.

NOMENCLATURE

$[H_2O_2]_{inf}$	–	local optimal influent H_2O_2 concentration (mg/L)
$[H_2O_2]_{inf}$	–	influent H_2O_2 concentration (mg/L)
$[H_2O_2]_0$	–	initial H_2O_2 concentration (mg/L)
A	–	local volumetric rate of energy absorption (mol photons/(L·s))
\bar{A}	–	average local volumetric rate of energy absorption (mol photons/(L·s))
C_i	–	concentration of species i (mM)
$C_{i,eff}$	–	effluent concentration of species i (mM)
D_{AB}	–	diffusivity of the species in the aqueous solution (m^2/s)
D_H	–	hydraulic diameter (m)
f_i	–	fraction of photons absorbed by species i (dimensionless)
F	–	operational cost per amount of target compound (\$/mmol)
k	–	reaction rate constant ($M^{-1}s^{-1}$)
L	–	reactor length (k)
N_R	–	Reynold's number (dimensionless)
Q	–	flowrate (L/s)
q	–	radiant energy flux (mol photons/($m^2 \cdot s$))
q_0	–	radiant energy flux at liquid surface (mol photons/($m^2 \cdot s$))
r	–	radial position (m)
R	–	outer reactor radius (m)
R^*	–	local optimal outer reactor radius (m)
R_i	–	inner reactor radius (m)
R_H	–	hydraulic radius (m)
$R_{rxn,i}$	–	reaction rate for species i (mM/s)
S	–	cross-sectional area (m^2)
S_C	–	chemical operating costs (\$/s)
S_E	–	electrical operating costs (\$/s)
t	–	time (s)
v	–	velocity (m/s)
V	–	volume (m^3)

x	–	position on x-axis for multi-lamp reactor (m)
y	–	position on y-axis for multi-lamp reactor (m)
z	–	axial position (m)

Greek Letters

τ	–	reactor residence time (s)
$\tau_{1/2,x}$	–	half life of contaminant x (s)
ϕ	–	quantum yield (mol photon ⁻¹)
ρ	–	density (kg/m ³)
ϵ_{RH}	–	molar absorptivity of the target compound at 254 nm (mM ⁻¹ m ⁻¹)
$\epsilon_{H_2O_2}$	–	molar absorptivity of H ₂ O ₂ at 254 nm (mM ⁻¹ m ⁻¹)
μ_s	–	solution extinction coefficient at 254 nm (m ⁻¹)
μ_w	–	extinction coefficient of water at 254 nm (m ⁻¹)

Acronyms

AOP	–	advanced oxidation process
AOX	–	adsorbable organic halogens
COD	–	chemical oxygen demand
DIC	–	dissolved inorganic carbon
LOEC	–	lowest observable effect concentration
LVREA	–	local volumetric rate of energy absorption
ODE	–	ordinary differential equation
PPCP	–	pharmaceuticals and personal care products
RH	–	target compound
TOC	–	total organic carbon

REFERENCES

- Aleboyeh, A., Moussa, Y., Aleboyeh, H. (2005). The effect of operational parameters on UV/H₂O₂ decolourisation of Acid Blue 74. *Dyes and Pigments*, **66**, 129-134.
- Amat, A.M., Arques, A., Miranda, M.A., Segui, S. (2004). Photo-Fenton reaction for the abatement of commercial surfactants in a solar pilot plant. *Solar Energy*, **77**, 559-566.
- Andreozzi, R., Marotta, R., Pinto, G., Pollio, A. (2002). Carbamazepine in water: persistence in the environment, ozonation treatment and preliminary assessment on algal toxicity. *Water Research*. **36**(11), 2869-2877.
- Andreozzi, R., Caprio, V., Marotta, R., Radovnikovic, A. (2003). Ozonation and H₂O₂/UV treatment of clofibrac acid in water: a kinetic investigation. *Journal of Hazardous Materials*, **B103**, 233-246.
- Arslan, I., Balcioglu, I.A., Bahnemann, D.W. (2000). Advanced chemical oxidation of reactive dyes in simulated dyehouse effluents by ferrioxalate-Fenton/UV-A and TiO₂/UV-A processes. *Dyes and Pigments*, **47**, 207-218.
- Arslan-Alaton, I., Gurses, F. (2004). Photo-Fenton-like and photo-fenton-like oxidation of Procaine Penicillin G formulation effluent. *Journal of Photochemistry and Photobiology*, **165**, 165-175.
- Bae, W., Lee, S.H., Ko, G.B. (2004). Evaluation of predominant reaction mechanisms for the Fenton process in textile dyeing wastewater treatment. *Water Sci. Technol.*, **49**(4), 91-96.
- Barb, W.G., Baxendale, J.H., George, P. (1951a). Reactions of ferrous and ferric ions with hydrogen peroxide. Part I – The ferrous ion reaction. *Trans. Faraday Soc.*, **47**, 462-500.

- Barb, W.G., Baxendale, J.H., George, P. (1951a). Reactions of ferrous and ferric ions with hydrogen peroxide. Part II – The ferric ion reaction. *Trans. Faraday Soc.*, **47**, 591-616.
- Bauer, R., Waldner, G., Fallman, H., Hager, S., Klare, M., Krutzler, T., Malato, S., Maletzky, P. (1999). The photo-Fenton reaction and the TiO₂/UV process for wastewater treatment – novel developments. *Catal. Today*, **53**, 131-144.
- Behnajady, M.A., Modirshahla, N. (2006). Kinetic modelin on photooxidative degradation of C.I. Acid Orange 7 in a tubular continuous-flow photoreactor. *Chemosphere*, **62**, 1543-1548.
- Beltran, J., Rivas, J., Alvarez, P.M., Alonso, M.A., Acedo, B. (1999). A kinetic model for advanced oxidation processes of aromatic hydrocarbons in water: application to phenanthrene and nitrobenzene. *Ind. Eng. Chem. Res.*, **38**, 4189-4199.
- Bird, R.B., Stewart, W.E., Lightfoot, E.N. (2002). *Transport Phenomena*, 2nd ed. John Wiley & Sons, Inc., NY.
- Carballa, M., Omil, F., Lema, J.M., Llompart, M., Garcia-Jares, C., Rodgriguez, I., Gomez, M., Ternes, T. (2004). Behaviour of pharmaceuticals, cosmetics and hormones in a sewage treatment plant. *Water Research*, **38**, 2918-2926.
- Catalkaya, E.C., Kargi, F. (2007). Color, TOC, and AOX removals from pulp mill effluent by advanced oxidation processes: a comparative study. *Journal of Hazardous Materials*, **B139**, 244-253.
- Chamarro, E., Marco, A., Esplugas, S. (2001). Use of Fenton reagent to improve organic chemical biodegradability. *Water Resources*. **35**(4), 1047-1051.

- Doll, T.E., Frimmel, F.H. (2004). Kinetic study of photocatalytic degradation of carbamazepine, clofibric acid, iomeprol and iopromide assisted by different TiO₂ materials – determination of intermediates and reaction pathways. *Water Research*, **38**, 955-964.
- Doll, T.E., Frimmel, F.H. (2005). Photocatalytic degradation of carbamazepine, clofibric acid and iomeprol with P25 and Hombikat UV100 in the presence of natural organic matter (NOM) and other organic water constituents. *Water Research*, **39**, 403-411.
- De Laat, J., Le, G.T., Legube, B. (2004). A comparative study of the effects of chloride, sulfate and nitrate ions on the rates of decomposition of H₂O₂ and organic compounds by Fe(II)/H₂O₂ and Fe(III)/H₂O₂. *Chemosphere*, **55**, 715-723.
- Emblidge, J.P., DeLorenzo, M.E. (2006). Preliminary risk assessment of the lipid-regulating pharmaceutical clofibric acid, for three estuarine species. *Environmental Research*, **100**, 216-226.
- Feng, X., Ding, S., Tu, J., Wu, F., Deng, N. (2005). Degradation of estrone in aqueous solution by photo-Fenton system. *Sci. Total Environ.*, **345**, 229-237.
- Gadgil, A. (1995). *UV Waterworks 2.0 – Answers to Ten Commonly Asked Questions about the design, operation, and economics*. Energy & Environment Division, Lawrence Berkley National Laboratory. Berkely, CA.
- Gagne, F., Blaise, C., Andre, C. (2006). Occurrence of pharmaceutical products in a municipal effluent and toxicity to rainbow trout (*Oncorhynchus mykiss*) hepatocytes. *Exotoxicology and Environmental Safety*, **64**, 329-336.
- Galindo, C., Kalt, A. (1999). UV/H₂O₂ oxidation of azodyes in aqueous media: evidence of a structure-degradability relationship. *Dyes and Pigments*, **42**(3), 199-207.

- Gao, Y.X., Yan, M., Zhang, Y., Hu, J.Y. (2004). Treatment of oilfield wastewater by Fenton's process. *Water Sci. Technol.*, 49(4), 103-108.
- Garcia-Montano, J., Ruiz, N., Munoz, I., Domenech, X., Garcia-Hortal, J.A., Torrades, F., Peral, J. (2006). Environmental assessment of different photo-Fenton approaches for commercial reactive dye removal. *Journal of Hazardous Materials*, 138(2), 218-25.
- Gau, S.-H., Chang, F.-S. (1996). Improved Fenton method to remove recalcitrant organics in landfill leachate. *Wat. Sci. Tech.*, 34(7), 455-462.
- Gernjak, W., Maldonado, M.I., Malato, S., Caceres, J., Krutzler, T., Glaser, A., Bauer, R. (2004). Pilot-plant treatment of olive mill wastewater (OMW) by solar TiO₂ photocatalysis and solar photo-Fenton. *Solar Energy*, 77, 567-572.
- Gernjak, W. (2006). Solar photo-Fenton treatment of EU priority substances – process parameters and control strategies. Ph.D. Thesis, Universitat fur Bodenkultur Wien, Vienna.
- Gomez, M.J., Petrovic, M., Fernandez-Alba, A.R., Barcelo, D. (2006). Determination of pharmaceuticals of various therapeutic classes by solid-phase extraction and liquid chromatography – tandem mass spectrometry analysis in hospital effluent wastewaters. *Journal of Chromatography A*, 1114, 224-233.
- Hancu, D., Beckman, E.J. (2001). Generation of hydrogen peroxide directly from H₂ and O₂ using CO₂ as the solvent. *Green Chemistry*, 3, 80-86.
- Hernando, M.D., Mezcua, M., Fernandez-Alba, A.R., Barcelo, D. (2006). Environmental risk assessment of pharmaceutical residues in wastewater effluents, surface waters and sediments. *Talanta*, 69, 334-342.

- Hincapie, M., Maldonado, M.I., Oller, I., Gernjak, W., Sanchez-Perez, J.A., Ballesteros, M.M., Malato, S. (2005). Solar photocatalytic degradation and detoxification of EU priority substances. *Catalysis Today*, **101**, 203-210.
- Hofl, C., Sigl, G., Specht, O., Wurdack, I., Wabner, D. (1997). Oxidative degradation of AOX and COD by different advanced oxidation processes: a comparative study with two samples of pharmaceutical wastewater. *Wat. Sci. & Tech.*, **35(4)**, 257-264.
- Jamal, M.A., Muaddi, J.A. (1990). Solar energy at various depths below a water surface. *Int. J. of Energy Research*, **14**, 859-867.
- Jasim, S. (2006). Drinking Water Centre Announces Partnership. *Environmental Science and Engineering Magazine*, **19(3)**, 50.
- Kummerer, K., Al-Ahmad, A., Mersch-Sundermann, V. (2000). Biodegradability of some antibiotics, elimination of the genotoxicity and affection of wastewater bacteria in a simple test. *Chemosphere*, **40**, 701-710.
- Larsen, T.A., Lienert, J., Joss, A., Siegrist, H. (2004). How to avoid pharmaceuticals in the aquatic environment. *Journal of Biotechnology*, **113**, 295-304.
- McDowell, D.C., Huber, M.M, Wagner, M., Gunten, U., Ternes, T.A. (2005). Ozonation of carbamazepine in drinking water: identification and kinetic study of major oxidation products. *Environmental Science & Technology*, **39(20)**, 8014-8022.
- Mehrvar, M., Anderson, W.A., Moo-Young, M., Reilly, P.M. (2000). Non-linear parameter estimation for a dynamic model in photocatalytic reaction engineering. *Chemical Engineering Science*, **55**, 4885-4891.

- Mehrvar, M., Anderson, W.A., Moo-Young, M. (2002). Comparison of the photoactivities of two commercial titanium dioxide powders in the degradation of 1,4-dioxane. *International Journal of Photoenergy*, 4, 141-146.
- Metcalf & Eddy (2003). *Wastewater Engineering Treatment and Reuse*, 4th ed. McGraw-Hill, NY.
- Mohey El-Dein, A., Libra, J.A., Wiesmann, U. (2001). Kinetics of decolorization and mineralization of the azo dye Reactive Black 5 by hydrogen peroxide and UV light. *Wat. Sci. & Tech.*, 44(5), 295-301.
- Mordirshahla, N., Behnajady, M.A. (2006). Photooxidative degradation of Malachite Green (MG) by UV/H₂O₂: Influence of operational parameters and kinetic modeling. *Dyes and Pigments*, 70, 54-59.
- Neyens, E., Baeyens, J. (2003). A review of classic Fenton peroxidation as an advanced oxidation technique, *J. Hazard. Mater.* B98, 33-50.
- Ontario Ministry of the Environment (2003). *Technical Support Document for Ontario Drinking Water Standards, Objectives and Guidelines*. www.ene.gov.on.ca.
- Park, J.-H., Cho, I.-H., Chang, S.-W. (2006). Comparison of Fenton and photo-Fenton processes for livestock wastewater treatment. *Journal of Environmental Science and Health Part B*, 41, 109-120.
- Perez, M., Torrades, F., Garcia-Hortal, J.A., Domenech, X., Peral, J. (2002). Removal of organic contaminants in paper pulp treatment effluents under Fenton and photo-Fenton conditions. *Applied Catalysis B: Environmental*, 36, 63-74.

- Perez-Estrada, L.A., Maldonado, M.I., Gernjak, W., Aguera, A., Fernandez-Alba, A.R., Ballesteros, M.M., Malato, S. (2005). Decomposition of diclofenac by solar driven photocatalysis at pilot plant scale. *Catalysis Today*, **101**, 219-226.
- Perry, R.H., Green, D.W. (1997). *Perry's Chemical Engineers' Handbook*, 7th ed., McGraw-Hill, NY.
- Raj, C.B.C., Quen, H.L. (2005). Advanced oxidation processes for wastewater treatment: optimization of UV/H₂O₂ process through a statistical technique. *Chemical Engineering Science*, **60**, 5305-5311.
- Safarzadeh-Amiri, A., Bolton, J.R., Cater, S.R. (1996). Ferrioxalate-mediated solar degradation of organic contaminants in water. *Solar Energy*, **5**, 439-443.
- Shemer, H., Kunukcu, Y.K., Linden, K.G. (2006). Degradation of the pharmaceutical Metronidazole via UV, Fenton, and photo-Fenton processes. *Chemosphere*, **63**, 269-276.
- Shen, Y.-S., Wang, D.K. (2002). Development of photoreactor design equation for the treatment of dye wastewater by UV/H₂O₂ process. *Journal of Hazardous Materials*, **B89**, 267-277.
- Shu, H.-Y., Chang, M.-C. (2005). Pilot scale annular plug flow photoreactor by UV/H₂O₂ for the decolorization of azo dye wastewater. *Journal of Hazardous Materials*, **B125**, 244-251.
- Shu, H.-Y., Fna, H.-J., Chang, M.-C., Hsieh, W.-P. (2006). Treatment of MSW landfill leachate by a thin gap annular UV/H₂O₂ photoreactor with multi-UV lamps. *Journal of Hazardous Materials*, **B129**, 73-79.

- Sires, I., Cabot, P.L., Centellas, F., Garrido, J.A., Rodriguez, R.M., Arias, C., Brillas, E. (2006). Electrochemical degradation of clofibric acid in water by anodic oxidation – comparative study with platinum and boron-doped diamond electrodes. *Electrochimica Acta*, **52**, 75-85.
- Sulzburger B., Laubscher H. and Karametaxas G., (1994). Photoredox reactions at the surface of iron(III)(hydr-)oxides. Aquatic and surface photochemistry. Lewis Publishers, Boca Raton, 53-74
- Tambosi, J.L., Di Domenico, M., Schirmer, W.N., Humberto, J., Moreira, R. (2006). Treatment of pulp and paper wastewater and removal of odorous compounds by a Fenton-like process at the pilot scale. *Journal of Chemical Technology and Biotechnology*, **81**(8), 1426-1432.
- Tekin, H., Bilkay, O., Ataberk, S.S., Balta, T.H., Ceribasi, I.H., Dilek Sanin, F., Dilek, F.B., Yetis, U. (2006). Use of Fenton oxidation to improve the biodegradability of a pharmaceutical wastewater. *Journal of Hazardous Materials*, **B136**, 258-265.
- Vogna, D., Marotta, R., Andreozzi, R., Napolitano, A., d'Ishcia, M. (2004). Kinetic and chemical assessment of the UV/H₂O₂ treatment of antiepileptic drug carbamazepine. *Chemosphere*, **54**(4), 497-505.
- Yang, Y.W., Hwang, K.-Y. (2000) Effects of reaction conditions on the oxidation efficiency in the Fenton Process, *Water Res.*, **34**, 2786-2790
- Yonar, T., Kestioglu, K, Azbar, N. (2006). Treatability studies on domestic wastewater using UV/H₂O₂ process. *Applied Catalysis B: Environmental*, **67**, 223-228.
- Yoon, J., Cho, S., Cho, Y., Kim, S. (1998). The characteristics of coagulation of Fenton reaction in the removal of landfill leachate organics. *Wat. Sci. Tech.*, **38**(2), 209-214.

- Yoon, J., Lee, Y., Kim, S. (2001). Investigation of the reaction pathway of OH radicals produced by Fenton oxidation in the conditions of wastewater treatment. *Water and Sci. Tech.* 44(5), 15-21.
- Yue, P.L. (1997). Oxidation Reactors for Water and Wastewater Treatment. *Wat. Sci. Tech.*, 4, 189-196.
- Zhang, H., Choi, H.J., Huang, C.-P. (2005). Optimization of Fenton process for the treatment of landfill leachate. *Journal of Hazardous Materials*, B125, 166-174.
- Zhang, G., Shulan, J, Xib, B. (2006). Feasibility of treatment of amoxillin wastewater with a combination of extraction, Fenton oxidation and reverse osmosis. *Desalination*, 196, 32-42.
- Zwiener, C., Frimmel, F.H. (2000). Oxidative treatment of pharmaceuticals in water. *Water Research*, 34(6), 1181-1885.

APPENDIX A – Miscellaneous Sample Calculations

A.1. Reynolds Number Calculation

Reynolds number, N_R , is calculated as follows:

$$N_R = \frac{D_H \bar{v}_z \rho}{\mu} \quad (\text{A.1})$$

where D_H is the hydraulic diameter of the annular space (m), \bar{v}_z is the average velocity of the aqueous solution through the annular space (m/s), and μ and ρ are the viscosity (Pa·s) and density (kg/m³) of the aqueous solutions, respectively.

D_H is defined as follows:

$$D_H = 4R_H = 4 \frac{\pi(R^2 - R_i^2)}{\pi(2R + 2R_i)} = 4 \frac{(R - R_i)(R + R_i)}{2(R + R_i)} = 2(R - R_i) = 2R \left(1 - \frac{R_i}{R}\right) \quad (\text{A.2})$$

Therefore, Equation A.1 can be written:

$$N_R = \frac{2R \left(1 - \frac{R_i}{R}\right) \bar{v}_z \rho}{\mu} \quad (20)$$

An example calculation is presented below for the Reynolds number in Reactor 1, with a radius of 250 mm, at an aqueous solution flowrate of 2.0 L/s at 25°C.

$$\bar{v}_z = \frac{Q}{S} = \frac{2.0 \text{ L/s}}{\pi \left((350 \times 10^{-3})^2 - (17 \times 10^{-3})^2 \right) \text{ m}^2} \frac{\text{m}^3}{1000 \text{ L}} = 1.02 \times 10^{-2} \text{ m/s} \quad (\text{A.3})$$

$$N_R = \frac{2(250 \times 10^{-3} \text{ m}) \left(1 - \frac{17 \times 10^{-3} \text{ m}}{250 \times 10^{-3} \text{ m}}\right) (1.02 \times 10^{-2} \text{ m/s})(997 \text{ kg/m}^3)}{8.9 \times 10^{-4} \text{ Pa}\cdot\text{s}} = 5,325 \quad (\text{A.4})$$

A.2. Mass Balance Simplification

Cylindrical Coordinates

For cylindrical coordinates, the mass balance can be expressed as:

$$\begin{aligned} \frac{\partial C_i}{\partial t} + \left(v_r \frac{\partial C_i}{\partial r} + v_\theta \frac{1}{r} \frac{\partial C_i}{\partial \theta} + v_z \frac{\partial C_i}{\partial z} \right) \\ = D_{AB} \left(\frac{1}{r} \frac{\partial}{\partial r} \left(r \frac{\partial C_i}{\partial r} \right) + \frac{1}{r^2} \frac{\partial^2 C_i}{\partial \theta^2} + \frac{\partial^2 C_i}{\partial z^2} \right) - R_{rxn,i} \end{aligned} \quad (28)$$

where C_i is the concentration of species i (M), v_r , v_θ , and v_z are velocities (m/s) in the r -, θ -, and z -directions, respectively. D_{AB} is the diffusivity of the species in the aqueous solution (m²/s), and $R_{rxn,i}$ is the reaction rate of species i (M/s).

Since the system is considered to be at steady state conditions, the rate of change of concentration with respect to time is zero. In addition, because the flow through the reactor is assumed to be ideal plug flow (see Section 3.2.2), $v_r = v_\theta = 0$. Finally, it is assumed that the effect of diffusivity is negligible compared to that of the convective terms.

As a result, Eq. 17 can be simplified as follows:

$$\begin{aligned} \cancel{\frac{\partial C_i}{\partial t}} + \left(\cancel{v_r} \frac{\partial C_i}{\partial r} + \cancel{v_\theta} \frac{1}{r} \frac{\partial C_i}{\partial \theta} + v_z \frac{\partial C_i}{\partial z} \right) \\ = \cancel{D_{AB}} \left(\frac{1}{r} \frac{\partial}{\partial r} \left(r \frac{\partial C_i}{\partial r} \right) + \frac{1}{r^2} \frac{\partial^2 C_i}{\partial \theta^2} + \frac{\partial^2 C_i}{\partial z^2} \right) - R_{rxn,i} \end{aligned} \quad (A.5)$$

$$\left(v_z \frac{\partial C_i}{\partial z} \right) = -R_{rxn,i} \quad (A.6)$$

The reactor to be modeled is of constant volume, V , and cross-sectional area, S , therefore the residence time, τ , can be expressed as:

$$\tau = \frac{V}{v_z} = \frac{S \cdot z}{S \cdot v_z} = \frac{z}{v_z} \quad (\text{A.7})$$

From Equation A.7, and the fact that v_z is constant throughout the reactor, it follows that:

$$\partial \tau = \partial \left(\frac{z}{v_z} \right) = \frac{\partial z}{v_z} \quad (\text{A.8})$$

Combining Equations A.5 and A.7, the simplified mass balance can be expressed as:

$$\frac{\partial C_i}{\partial \tau} = -R_{rxn,i} \quad (29)$$

Cartesian Coordinates

For Cartesian coordinates, the mass balance can be expressed as:

$$\begin{aligned} \frac{\partial C_i}{\partial t} + \left(v_x \frac{\partial C_i}{\partial x} + v_y \frac{\partial C_i}{\partial y} + v_z \frac{\partial C_i}{\partial z} \right) \\ = D_{AB} \left(\frac{\partial^2 C_i}{\partial x^2} + \frac{\partial^2 C_i}{\partial y^2} + \frac{\partial^2 C_i}{\partial z^2} \right) - R_{rxn,i} \end{aligned} \quad (30)$$

where C_i is the concentration of species i (M), v_x , v_y , and v_z are velocities (m/s) in the x -, y -, and z -directions, respectively. D_{AB} is the diffusivity of the species in the aqueous solution (m^2/s), and $R_{rxn,i}$ is the reaction rate of species i (M/s).

Since the system is considered to be at steady state conditions, the rate of change of concentration with respect to time is zero. In addition, because the flow through the reactor is assumed to be ideal plug flow (see Section 3.2.2), $v_x = v_y = 0$. Finally, it is assumed that the effect of diffusivity is negligible compared to that of the convective terms in the z -direction.

As a result, Equation A.9 can be simplified as follows:

$$\begin{aligned} \frac{\partial C_i}{\partial t} + \left(v_x \frac{\partial C_i}{\partial x} + v_y \frac{\partial C_i}{\partial y} + v_z \frac{\partial C_i}{\partial z} \right) \\ = D_{AB} \left(\frac{\partial^2 C_i}{\partial x^2} + \frac{\partial^2 C_i}{\partial y^2} + \frac{\partial^2 C_i}{\partial z^2} \right) - R_{rxn,i} \end{aligned} \quad (\text{A.9})$$

$$\left(v_z \frac{\partial C_i}{\partial z} \right) = -R_{rxn,i} \quad (\text{A.6})$$

which is the same result obtained for the cylindrical coordinates.

Using the relationship presented in Equation A.8, which is also valid for Cartesian coordinates, the simplified mass balance can be expressed as:

$$\frac{\partial C_i}{\partial \tau} = -R_{rxn,i} \quad (29)$$

**APPENDIX B – Model Calibration: Simulation Model Development,
Matlab Code, and Selected Output**

B.1. Background Calculations and Information

For the collimated beam apparatus and Petri dish, as described by Shemer et al. (2006), the LVREA at any depth, x , in the Petri dish can be presented as:

$$A = \mu_s q_o e^{-\mu_s x} \quad (\text{B.1})$$

The average LVREA throughout the Petri dish, \bar{A} , can be expressed as:

$$\bar{A} = \frac{\int_0^L \mu_s q_o e^{-\mu_s x} dx}{\int_0^L dx} = \frac{\mu_s q_o}{L} \int_0^L e^{-\mu_s x} dx = \frac{\mu_s q_o}{L} \frac{e^{-\mu_s x} \Big|_0^L}{-\mu_s} = \frac{q_o}{L} (1 - e^{-\mu_s L}) \quad (\text{B.2})$$

The radiant energy flux at the liquid surface, q_o , was calculated based on the reported UV light intensity of 1.5 mW/cm² (Shemer et al., 2006):

$$q_o = \left(\frac{1.5 \text{ mW}}{\text{cm}^2} \right) \left(\frac{W}{1,000 \text{ mW}} \right) \left(\frac{J/s}{W} \right) \left(\frac{\text{mol photon}_{254\text{nm}}}{4.713 \times 10^5 J} \right) \left(\frac{100^2 \text{ cm}^2}{\text{m}^2} \right) = 3.183 \times 10^{-5} \frac{\text{mol photon}}{\text{m}^2 \cdot \text{s}} \quad (\text{B.3})$$

The solution extinction coefficient, μ_s (m⁻¹), for the solution in the Petri dish, assuming uniform reactant concentration throughout, is:

$$\mu_s = \mu_w + \varepsilon_{H_2O_2} C_{H_2O_2} + \varepsilon_{RH} C_{RH} = 0.7 + 1.86 C_{H_2O_2} + 2.2 \times 10^2 C_{RH} \quad (\text{B.4})$$

where μ_w is the extinction coefficient of distilled water (m⁻¹), ε_{RH} and $\varepsilon_{H_2O_2}$, are the molar absorptivities (mM⁻¹m⁻¹) of metronidazole and H₂O₂, respectively, and C_{RH} and $C_{H_2O_2}$ are the concentrations (mM) of metronidazole and H₂O₂, respectively.

The depth of the liquid in the Petri dish, L , as reported by Shemer et al. (2006), is 2.9×10^{-2} m.

The experimental results used for the model calibration were adapted from graphed results as reported by Shemer et al. (2006), and are presented in Table 13 and Table 14.

Table 13. Experimental Results Used for Model Calibration – Initial H₂O₂ Concentration of 25 mg/L

Adapted from in Shemer et al. (2006)			
UV Dose	ln(C/C ₀)	Time	Concentration
0 mJ/cm ²	0	0 s	6.00 μM
50 mJ/cm ²	-0.175	33.3 s	5.04 μM
100 mJ/cm ²	-0.35	66.7 s	4.23 μM
200 mJ/cm ²	-0.7	133 s	2.98 μM
250 mJ/cm ²	-0.87	167 s	2.51 μM

Table 14. Experimental Results Used for Model Calibration – Initial H₂O₂ Concentration of 50 mg/L

Adapted from Shemer et al. (2006)			
UV Dose	ln(C/C ₀)	Time	Concentration
0 mJ/cm ²	0	0 s	6.00 μM
50 mJ/cm ²	-0.205	33.3 s	4.89 μM
100 mJ/cm ²	-0.42	66.7 s	3.94 μM
200 mJ/cm ²	-0.87	133 s	2.51 μM
250 mJ/cm ²	-1.05	167 s	2.10 μM

B.2. Matlab Code Development

Presented below is code for Matlab file “main.m”, which calls the predictor/corrector method to solve the set of ODE’s in file “model.m”. The code for “model.m” is also provided.

For reference, concentrations of compounds in the reaction model are represented as follows:

- C_{RH} is represented as y(1);
- $C_{H_2O_2}$ is represented as y(2);
- C_{OH} is represented as y(3);
- C_{HO_2} is represented as y(4);
- $C_{HCO_3^-}$ is represented as y(5);
- $C_{CO_3^{2-}}$ is represented as y(6);
- C_{CO_2} is represented as y(7).

The reaction rate constants and extinction coefficients are represented as follows:

- ϕ_1 is represented as phi1, and ϕ_7 is represented as phi7.
- k_2 is represented as k2, k_3 is represented as k3, etc.; and

Other parameters, as outlined in Section B.1, are represented as follows in the Matlab code:

- \bar{A} is represented as A;
- q_o is represented as q0;
- μ_s is represented as mu.

In the file “model.m”, the final seven lines of code represent the chemical reaction model

equations presented in Section 3.3. As an example, Equation 32 in Section 3.3, incorporating the relationship presented in Equation 26, can be written as:

$$\frac{\partial C_{RH}}{\partial \tau} = -R_{RH} = -k_6 C_{RH} C_{\bullet OH} - \phi_7 A f_{RH} = -k_6 C_{RH} C_{\bullet OH} - \phi_7 A \frac{\varepsilon_{RH}}{\mu_s} C_{RH} \quad (B.5)$$

This equation appears as follows in the file “model.m”:

$$y(1) = -k6*y(1)*y(3) - phi7*A*2.2E2/mu*y(1) \quad (B.6)$$

All initial concentrations, as represented in the vector y0 in the file “main.m”, are reported in mM. As such, initial H₂O₂ concentrations were converted from mg/L to mM using the molar mass of H₂O₂ of 34 mg/mmol.

Before providing output, the concentration of metronidazole, y(1) (or the first column of the answer matrix Y), is converted to μM in the file “main.m”.

All simulation runs took less than 5 seconds of CPU time to complete using an AMD Athlon 64 Processor 3200+.

File "main.m"

```
clear  
clc
```

```
span = [0 400]    %span of duration of simulation  
y0 = [0.006 0.735 0 0 0 0 0] %vector of initial conditions in mmol/L
```

```
options = odeset('RelTol',1e-6,'AbsTol',[1e-6 1e-6 1e-6 1e-6 1e-6 1e-6 1e-6]);  
[t, Y]=ode15s(@model, span, y0, options);
```

```
Y(:,1)=Y(:,1)*1000; %convert concentration of metro into micromol/L and  
output solution matrix Y
```

```
t  
Y
```

```
figure(1); plot(t,Y(:,1),'-')
```

File "model.m"

```
function dy = model(t,y)
dy = zeros(7,1);    % a column vector

k2 = 3.0E4; %in mM-1*s-1
k3 = 6.5E6; %in mM-1*s-1
k4 = 1.5E3; %in mM-1*s-1
k5 = 1.4E7; %in mM-1*s-1
k6 = 1.98E6; %k of metro - to be varied
k8 = 2.0E4; %in mM-1*s-1
k9 = 3.7E5; %in mM-1*s-1
k10 = 8.0E2; %in mM-1*s-1

phi1 = 0.5; %in mmol photon-1
phi7 = 0.0033; %in mmol photon-1

mu = (0.7+1.86*y(2)+2.2E2*y(1)); %in m-1, Equation B.4
q0 = 3.183E-5; %in mol photon/(m2*s)
L = 2.9E-2; %in m
A = q0/L*(1-exp(-2.303*muE*L)); %in mol photon/(m3*s) = mmol photon/(L*s),
Equation B.2

dy(1) = -k6*y(1)*y(3)-phi7*A*2.2E2/mu*y(1); %Equation 32

dy(2) = -phi1*A*1.86/mu*y(2)-k2*y(2)*y(3)+k3*y(3)*y(3)+k4*y(4)*y(4);
%Equation 33

dy(3) = -k6*y(1)*y(3)+2*phi1*A*1.86/mu*y(2)-k2*y(2)*y(3)-2*k3*y(3)*y(3)-
k5*y(3)*y(4)-k8*y(5)*y(3)-k9*y(6)*y(3); %Equation 34

dy(4) = k2*y(2)*y(3)-2*k4*y(4)*y(4)-k5*y(3)*y(4)+k10*y(7)*y(2); %Equation 35

dy(5) = -k8*y(5)*y(3)+k10*y(7)*y(2); %Equation 36

dy(6) = -k9*y(6)*y(3); %Equation 37

dy(7) = k8*y(5)*y(3)+k9*y(6)*y(3)-k10*y(7)*y(2); %Equation 38
```

B.3. Matlab Output

Run 1 – with initial H₂O₂ dose of 25 mg/L.

Note that time (t) is in seconds, and output Y concentrations are in mM, with the exception of y1, which is in μM.

span =

0 400

y0 =

0.0060 0.7350 0 0 0 0 0

t =

0
0.0006
0.0013
0.0019
0.0084
0.0149
0.0214
0.0863
0.1511
0.2160
0.7866
1.1729
1.5591
1.9454
3.2166
4.1920
5.1674
6.1428
7.1183
8.4687
9.8191
11.1695
15.9104
20.6513
25.3922
40.2727
55.1532
70.0337
84.9141
123.3541
152.2400

181.1260
210.0119
233.7057
257.3995
281.0933
304.7871
344.7871
384.7871
400.0000

Y =

6.0000	0.7350	0	0	0	0	0
6.0000	0.7350	0.0000	0.0000	0	0	0
6.0000	0.7350	0.0000	0.0000	0	0	0
5.9999	0.7350	0.0000	0.0000	0	0	0
5.9997	0.7350	0.0000	0.0000	0	0	0
5.9995	0.7350	0.0000	0.0000	0	0	0
5.9993	0.7350	0.0000	0.0000	0	0	0
5.9973	0.7350	0.0000	0.0000	0	0	0
5.9952	0.7350	0.0000	0.0000	0	0	0
5.9932	0.7350	0.0000	0.0000	0	0	0
5.9754	0.7349	0.0000	0.0000	0	0	0
5.9635	0.7349	0.0000	0.0001	0	0	0
5.9516	0.7348	0.0000	0.0001	0	0	0
5.9399	0.7348	0.0000	0.0001	0	0	0
5.9015	0.7347	0.0000	0.0001	0	0	0
5.8724	0.7346	0.0000	0.0001	0	0	0
5.8434	0.7346	0.0000	0.0001	0	0	0
5.8146	0.7345	0.0000	0.0001	0	0	0
5.7859	0.7344	0.0000	0.0001	0	0	0
5.7463	0.7343	0.0000	0.0001	0	0	0
5.7070	0.7342	0.0000	0.0001	0	0	0
5.6678	0.7341	0.0000	0.0001	0	0	0
5.5321	0.7337	0.0000	0.0001	0	0	0
5.3986	0.7334	0.0000	0.0001	0	0	0
5.2673	0.7330	0.0000	0.0001	0	0	0
4.8681	0.7319	0.0000	0.0001	0	0	0
4.4897	0.7307	0.0000	0.0001	0	0	0
4.1326	0.7296	0.0000	0.0001	0	0	0
3.7966	0.7284	0.0000	0.0001	0	0	0
3.0229	0.7253	0.0000	0.0001	0	0	0
2.5277	0.7229	0.0000	0.0001	0	0	0
2.1007	0.7205	0.0000	0.0001	0	0	0
1.7360	0.7181	0.0000	0.0001	0	0	0
1.4793	0.7161	0.0000	0.0001	0	0	0
1.2568	0.7140	0.0000	0.0001	0	0	0
1.0648	0.7120	0.0000	0.0002	0	0	0
0.9000	0.7099	0.0000	0.0002	0	0	0
0.6748	0.7065	0.0000	0.0002	0	0	0
0.5040	0.7030	0.0000	0.0002	0	0	0
0.4505	0.7016	0.0000	0.0002	0	0	0

Run 2 – with initial H₂O₂ dose of 50 mg/L.

Note that time (t) is in seconds, and output Y concentrations are in mM, with the exception of y1, which is in μM.

span =

0 400

y0 =

0.0060 1.4700 0 0 0 0 0

t =

0
0.0004
0.0007
0.0011
0.0047
0.0084
0.0120
0.0485
0.0850
0.1215
0.3906
0.6048
0.8190
1.0332
1.5209
2.0086
2.4963
2.9841
3.7370
4.4900
5.2429
5.9959
6.7488
9.3013
11.8538
14.4063
16.9588
31.5479
46.1370
60.7261
75.3152
105.9821
136.6489
167.3158

197.9826
 228.6495
 268.6495
 308.6495
 348.6495
 388.6495
 400.0000

Y =

6.0000	1.4700	0	0	0	0	0
6.0000	1.4700	0.0000	0.0000	0	0	0
6.0000	1.4700	0.0000	0.0000	0	0	0
6.0000	1.4700	0.0000	0.0000	0	0	0
5.9998	1.4700	0.0000	0.0000	0	0	0
5.9997	1.4700	0.0000	0.0000	0	0	0
5.9996	1.4700	0.0000	0.0000	0	0	0
5.9982	1.4700	0.0000	0.0000	0	0	0
5.9969	1.4700	0.0000	0.0000	0	0	0
5.9956	1.4700	0.0000	0.0000	0	0	0
5.9858	1.4699	0.0000	0.0001	0	0	0
5.9781	1.4699	0.0000	0.0001	0	0	0
5.9704	1.4698	0.0000	0.0001	0	0	0
5.9628	1.4698	0.0000	0.0001	0	0	0
5.9456	1.4697	0.0000	0.0001	0	0	0
5.9285	1.4696	0.0000	0.0002	0	0	0
5.9115	1.4695	0.0000	0.0002	0	0	0
5.8946	1.4694	0.0000	0.0002	0	0	0
5.8687	1.4693	0.0000	0.0002	0	0	0
5.8428	1.4692	0.0000	0.0002	0	0	0
5.8170	1.4691	0.0000	0.0002	0	0	0
5.7914	1.4690	0.0000	0.0002	0	0	0
5.7658	1.4689	0.0000	0.0002	0	0	0
5.6797	1.4685	0.0000	0.0002	0	0	0
5.5946	1.4681	0.0000	0.0002	0	0	0
5.5105	1.4677	0.0000	0.0002	0	0	0
5.4274	1.4673	0.0000	0.0002	0	0	0
4.9711	1.4650	0.0000	0.0002	0	0	0
4.5459	1.4627	0.0000	0.0002	0	0	0
4.1508	1.4603	0.0000	0.0002	0	0	0
3.7846	1.4580	0.0000	0.0002	0	0	0
3.1031	1.4530	0.0000	0.0002	0	0	0
2.5308	1.4480	0.0000	0.0002	0	0	0
2.0544	1.4429	0.0000	0.0002	0	0	0
1.6610	1.4378	0.0000	0.0002	0	0	0
1.3383	1.4326	0.0000	0.0002	0	0	0
1.0056	1.4259	0.0000	0.0002	0	0	0
0.7528	1.4191	0.0000	0.0002	0	0	0
0.5619	1.4123	0.0000	0.0002	0	0	0
0.4184	1.4055	0.0000	0.0002	0	0	0
0.3845	1.4036	0.0000	0.0002	0	0	0

B.3. Calculation of Concentrations of Carbonate and Bicarbonate Ions

For the effect alkalinity on the calibrated reaction model, the concentrations of carbonate and bicarbonate ions were calculated for alkalinity levels of 75 mg/L, 150 mg/L, and 225 mg/L as CaCO₃. Total alkalinity in milliequivalents per litre (meq/L), can be defined as:

$$\text{Alkalinity} = [\text{HCO}_3^-] + 2[\text{CO}_3^{2-}] + [\text{OH}^-] - [\text{H}^+] \quad (\text{B.7})$$

where concentrations of ions are in mM.

For a solution at a pH of 6.0, dissolved inorganic carbon (DIC) would be in the form of HCO₃⁻ and H₂CO₃, with no DIC in the form of CO₃²⁻. In addition, it was assumed that the concentration of H⁺ and OH⁻ would be negligible compared to the concentration of HCO₃⁻. Hence Equation B.7 can be reduced to:

$$\text{Alkalinity} \cong [\text{HCO}_3^-] \quad (\text{B.8})$$

It is also known that, to convert alkalinity from meq/L to mg/L as CaCO₃ the relation 50 mg as CaCO₃/meq can be used. The concentration of HCO₃⁻ in mM is equivalent to the concentration in meq/L. Based on the above, the concentrations of carbonate and bicarbonate ions for the three alkalinity levels investigated were determined and are summarized in Table 15.

Table 15. Concentrations of Carbonate and Bicarbonate Ions in the Aqueous Solution

Parameter	Value		
	75 mg/L	150 mg/L	225 mg/L
Alkalinity Level (as CaCO ₃)	75 mg/L	150 mg/L	225 mg/L
Alkalinity Level	1.5 meq/L	3.0 meq/L	4.5 meq/L
(CO ₃ ²⁻)	0.0 meq/L	0.0 meq/L	0.0 meq/L
[CO ₃ ²⁻]	0.0 mM	0.0 mM	0.0 mM
(HCO ₃ ⁻)	1.5 meq/L	3.0 meq/L	4.5 meq/L
[HCO ₃ ⁻]	1.5 mM	3.0 mM	4.5 mM

B.4. Data for Model Prediction of Removal of Clofibric Acid

Below are shown the experimental data adapted from Andreozzi et al. (2003) that was used to assess the model's ability to predict the removal of another pharmaceutical compound.

Table 16. Experimental Results Used for Model Prediction of Removal of Clofibric Acid – Initial H₂O₂ Concentration of 34 mg/L

Adapted from Andreozzi et al. (2003)	
Time	Concentration
0 s	0.024 mM
10 s	0.021 mM
20 s	0.0175 mM
30 s	0.0145 mM
40 s	0.012 mM
50 s	0.0085 mM
60 s	0.0065 mM
70 s	0.005 mM
80 s	0.0035 mM
90 s	0.0025 mM
100 s	0.002 mM
110 s	0.0015 mM

Table 17. Experimental Results Used for Model Prediction of Removal of Clofibric Acid – Initial H₂O₂ Concentration of 340 mg/L

Adapted from Andreozzi et al. (2003)	
Time	Concentration
0 s	0.0255 mM
10 s	0.018 mM
20 s	0.014 mM
30 s	0.012 mM
40 s	0.0085 mM
50 s	0.006 mM
60 s	0.0045 mM
70 s	0.003 mM
80 s	0.0025 mM

**APPENDIX C – Single Lamp UV Reactors: Simulation Model
Development, Matlab Code, and Selected Output**

C.1. Background Calculations

For the single UV lamp reactor, as described in Section 3.1.1, the LVREA at any radial position, r , in the reactor can be presented as:

$$A = \mu_s q_o \frac{R_i}{r} e^{-2.303\mu_s(r-R_i)} \quad (25)$$

The outer radius of the quartz sleeve, R_i , was taken to be 17×10^{-3} m for both Reactor 1 and Reactor 2.

The radiant energy flux at the outer surface of the quartz sleeve, q_o , was calculated based on the UV lamp output of 25.5 W for Reactor 1, and 36 W for Reactor 2, and the outer surface area of the quartz sleeve:

Surface area of quartz sleeve:

$$S = 2\pi R_i L = 2\pi(17 \times 10^{-3} \text{ m})(1.2 \text{ m}) = 0.128 \text{ m}^2 \quad (C.1)$$

For Reactor 1:

$$q_o = \left(\frac{25.5 \text{ W}}{0.128 \text{ m}^2} \right) \left(\frac{\text{J/s}}{\text{W}} \right) \left(\frac{\text{mol photon}_{254 \text{ nm}}}{4.713 \times 10^5 \text{ J}} \right) = 4.22 \times 10^{-4} \frac{\text{mol photon}}{\text{m}^2 \cdot \text{s}} \quad (C.2)$$

For Reactor 2:

$$q_o = \left(\frac{36 \text{ W}}{0.128 \text{ m}^2} \right) \left(\frac{\text{J/s}}{\text{W}} \right) \left(\frac{\text{mol photon}_{254 \text{ nm}}}{4.713 \times 10^5 \text{ J}} \right) = 5.97 \times 10^{-4} \frac{\text{mol photon}}{\text{m}^2 \cdot \text{s}} \quad (C.3)$$

The extinction coefficient of the aqueous solution was assumed to be constant for all locations within the photoreactor, and was calculated based on the extinction coefficient of tap water and in the influent concentration of H_2O_2 . The UV absorptive properties of metronidazole were

neglected due to its low influent concentration, and the influent concentration of H₂O₂ was used because it was assumed that very little H₂O₂ would be consumed, resulting in an almost uniform concentration of H₂O₂ throughout the reactor. Based on the above assumptions, the solution extinction coefficient, μ_s (m⁻¹), for the solution in the reactor can be written as:

$$\mu_s = \mu_w + \varepsilon_{H_2O_2} C_{H_2O_2,inf} = 10.0 + 1.86C_{H_2O_2,inf} \quad (C.4)$$

where μ_w is the extinction coefficient of average tap water, in m⁻¹, and $\varepsilon_{H_2O_2}$ is the molar absorptivity (mM⁻¹m⁻¹) of H₂O₂, and $C_{H_2O_2,inf}$ is the influent concentration (mM) of H₂O₂.

C.2. Matlab Code Development – Reactor 1 and Reactor 2

Presented below is code for Matlab files “reactor1main.m”, which calls the predictor/corrector method to solve the set of ODE’s in file “reactor1model.m”. The code for “reactor2main.m” and “reactor2model.m” is not shown. This is because the code for the simulation of Reactor 1 and Reactor 2 is identical, with the exception of the value of the flux at the outer surface of the quartz sleeve, q_o .

For reference, concentrations of compounds in the reaction model are represented as follows:

- C_{RH} is represented as y(1);
- $C_{H_2O_2}$ is represented as y(2);
- C_{OH} is represented as y(3);
- C_{HO_2} is represented as y(4);
- C_{HCO_3} is represented as y(5);
- $C_{CO_3^{2-}}$ is represented as y(6);
- C_{CO_2} is represented as y(7).

The reaction rate constants and extinction coefficients are represented as follows:

- ϕ_1 is represented as phi1, and ϕ_7 is represented as phi7.
- k_2 is represented as k2, k_3 is represented as k3, etc.; and

Other parameters, as outlined in Section B.1, are represented as follows in the Matlab code:

- A is represented as A;
- q_o is represented as q0;
- μ_s is represented as mu.

In the file “reactor1model.m”, the final seven lines of code represent the chemical reaction model equations presented in Section 3.3. As an example, Equation 32 in Section 3.3, incorporating the relationship presented in Equation 26, can be written as:

$$\frac{\partial C_{RH}}{\partial \tau} = -R_{RH} = -k_6 C_{RH} C_{\bullet OH} - \phi_7 A f_{RH} = -k_6 C_{RH} C_{\bullet OH} - \phi_7 A \frac{\varepsilon_{RH}}{\mu_s} C_{RH} \quad (C.5)$$

This equation appears as follows in the file “reactor1model.m”:

$$y(1) = -k6*y(1)*y(3) - phi7*A*2.2E2/mu*y(1) \quad (C.6)$$

All initial concentrations, as represented in the vector y_0 in the file “reactor1main.m”, are reported in mM. As such, initial H_2O_2 concentrations were converted from mg/L to mM using the molar mass of H_2O_2 of 34 mg/mmol. Initial concentrations of carbonate and bicarbonate ions are based on an alkalinity of 75 mg/L as $CaCO_3$ (see Appendix B, Section B.3).

In the file “reactor1main.m”, the value of the vector span is set to cover the retention time of within the reactor, $[0, \tau]$. The predictor/corrector method is called to solve the set of ODE’s in the file “reactor1model.m” for each 1 mm increment along the radius of the reactor, from the quartz sleeve to the reactor wall. The matrix Y is created each time the predictor/correct method is called, providing the concentration profiles vs. retention time for all modeled compounds at a particular location along the radius of the reactor. The matrix Ans is used to hold the values of the effluent concentrations of metronidazole and H_2O_2 for each increment along the reactor radius. Before storing the effluent concentrations in the matrix Ans , the concentration of metronidazole, $y(1)$ (or the first column of the answer matrix Y), is converted to μM .

The results provided in matrix Ans cannot be used to directly calculate the average effluent concentrations of metronidazole and H_2O_2 . As a result, a numerical integration technique was utilized, and is summarized in Section C.3.

All simulation runs took less than 5 seconds of CPU time to complete using an AMD Athlon 64 Processor 3200+.

File "reactor1main.m"

```
clear
clc

global raxis Router

Router = 250e-3

%span = [0 ##] <- residence time
span = [0 234.5] %span of duration of simulation

%y0 = [0.006 #### 0 0 0 ... <- Y2 initial value
y0 = [0.006 .735 0 0 1.5 0.0 0] %vector of initial conditions in mmol/L

options = odeset('RelTol',1e-6,'AbsTol',[1e-6 1e-6 1e-6 1e-6 1e-6 1e-6 1e-6]);

i = 0;

for raxis = 17:Router*1000; %move along r-axis from quartz sleeve to reactor
wall using 1 mm increments

    i = i + 1;
    [t, Y]=ode15s(@reactor1model, span, y0, options);

    Y(:,1)=Y(:,1)*1000; %convert concentration of metro into micromol/L

    [m,n] = size(Y);

    Ans(i,1)=raxis; %position on raxis
    Ans(i,2)=Y(m,1); %effluent metronidazole concentration in micromol/L
    Ans(i,3)=Y(m,2); %effluent peroxide concentration in mmol/L

end

Ans
```

File "reactor1model.m"

```
function dy = reactor1model(t,y)
dy = zeros(7,1);    % a column vector

global raxis Router

r = raxis/1000;

k2 = 3.0E4; %in mM-1*s-1
k3 = 6.5E6; %in mM-1*s-1
k4 = 1.5E3; %in mM-1*s-1
k5 = 1.4E7; %in mM-1*s-1
k6 = 1.98E6; %k of metro from model calibration in mM-1*s-1
k8 = 2.0E4; %in mM-1*s-1
k9 = 3.7E5; %in mM-1*s-1
k10 = 8.0E2; %in mM-1*s-1

phil = 0.5; %in mmol photon-1
phi7 = 0.0033; %in mmol photon-1

%mu = (10+1.86*###) <-Initial H2O2 concentration
mu = (10+1.86*.735); %in m-1, Equation C.4
q0 = 4.22E-4; %in mmol photon/(m2*s)

A = mu*q0*17E-3/r*exp(-2.303*mu*(r-17E-3)); %in mmol photon/(m2*s) = mmol
photon/(L*s), Equation 25

dy(1) = -k6*y(1)*y(3)-phi7*A*2.2E2/mu*y(1); % Equation 32

dy(2) = -phil*A*1.86/mu*y(2)-k2*y(2)*y(3)+k3*y(3)*y(3)+k4*y(4)*y(4); %
Equation 33

dy(3) = -k6*y(1)*y(3)+2*phil*A*1.86/mu*y(2)-k2*y(2)*y(3)-2*k3*y(3)*y(3)-
k5*y(3)*y(4)-k8*y(5)*y(3)-k9*y(6)*y(3); % Equation 34

dy(4) = k2*y(2)*y(3)-2*k4*y(4)*y(4)-k5*y(3)*y(4)+k10*y(7)*y(2); % Equation 35

dy(5) = -k8*y(5)*y(3)+k10*y(7)*y(2); % Equation 36

dy(6) = -k9*y(6)*y(3); % Equation 37

dy(7) = k8*y(5)*y(3)+k9*y(6)*y(3)-k10*y(7)*y(2); % Equation 38
```

C.3. Summarized Matlab Output for Reactor 1

Table 18. Average Effluent Metronidazole Concentrations for Reactor 1 at Various Operating Conditions

Treating a solution of metronidazole with an initial concentration of 6 μM , and an alkalinity of 75 mg/L at a flow rate of 2.0 L/s. Model predictions obtained utilizing a value for the reaction rate constant between metronidazole and the hydroxyl radical, k_6 , of $1.98 \times 10^9 \text{ M}^{-1}\cdot\text{s}^{-1}$. All other rate constants and quantum yield values as listed in Table 5. Extinction coefficient of typical tap water used.

Reactor Radius (mm)	Residence Time (s)	Influent H ₂ O ₂ Concentration (mg/L)				
		10	25	50	75	100
50	8.3	5.85	5.71	5.60	5.55	5.53
100	37	5.76	5.58	5.46	5.42	5.41
150	84	5.75	5.58	5.48	5.47	5.48
200	150	5.75	5.61	5.54	5.54	5.56
250	235	5.77	5.65	5.60	5.60	5.62

Notes:

All reported average effluent metronidazole concentrations in μM . Average effluent concentration calculated utilizing the trapezoidal rule.

Concentration in bold represents the lowest average effluent concentration observed.

Table 19. Average Effluent H₂O₂ Concentrations for Reactor 1 at Various Operating Conditions

Treating a solution of metronidazole with an initial concentration of 6 μM , and an alkalinity of 75 mg/L at a flow rate of 2.0 L/s. Model predictions obtained utilizing a value for the reaction rate constant between metronidazole and the hydroxyl radical, k_6 , of $1.98 \times 10^9 \text{ M}^{-1}\cdot\text{s}^{-1}$. All other rate constants and quantum yield values as listed in Table 5. Extinction coefficient of typical tap water used.

Reactor Radius (mm)	Residence Time (s)	Influent H ₂ O ₂ Concentration (mg/L)				
		10	25	50	75	100
50	8.3	0.294	0.734	1.47	2.20	2.94
100	37	0.294	0.734	1.47	2.20	2.93
150	84	0.294	0.734	1.47	2.20	2.93
200	150	0.294	0.734	1.47	2.20	2.93
250	235	0.294	0.734	1.47	2.20	2.93

Notes:

All reported average effluent H₂O₂ concentrations in mM. Average effluent concentration calculated utilizing the trapezoidal rule.

Reactor 1 – Example Matlab Output for Radius = 50 mm and Influent H₂O₂ = 100 mg/L

Note that “span” is in seconds, and output Y concentrations are in mM, with the exception of y1, which is in μM. The columns of the matrix “Ans” correspond to radial position, y1, and y2, respectively.

Router =

0.0500

span =

0 8.3000

y0 =

0.0060 2.9400 0 0 1.5000 0 0

Ans =

17.0000	4.5568	2.9254
18.0000	4.6663	2.9266
19.0000	4.7655	2.9278
20.0000	4.8555	2.9288
21.0000	4.9374	2.9297
22.0000	5.0122	2.9305
23.0000	5.0804	2.9312
24.0000	5.1430	2.9319
25.0000	5.2004	2.9325
26.0000	5.2532	2.9330
27.0000	5.3018	2.9335
28.0000	5.3466	2.9340
29.0000	5.3881	2.9344
30.0000	5.4264	2.9347
31.0000	5.4619	2.9351
32.0000	5.4948	2.9354
33.0000	5.5254	2.9357
34.0000	5.5538	2.9359
35.0000	5.5803	2.9362
36.0000	5.6050	2.9364
37.0000	5.6279	2.9366
38.0000	5.6494	2.9368
39.0000	5.6694	2.9370
40.0000	5.6882	2.9372
41.0000	5.7057	2.9374
42.0000	5.7221	2.9375

43.0000	5.7376	2.9376
44.0000	5.7520	2.9378
45.0000	5.7656	2.9379
46.0000	5.7783	2.9380
47.0000	5.7902	2.9381
48.0000	5.8014	2.9382
49.0000	5.8120	2.9383
50.0000	5.8219	2.9384

C.4. Summarized Matlab Output for Reactor 2

Table 20. Average Effluent Metronidazole Concentrations for Reactor 2 at Various Operating Conditions

Treating a solution of metronidazole with an initial concentration of 6 μM , and an alkalinity of 75 mg/L at a flow rate of 2.0 L/s. Model predictions obtained utilizing a value for the reaction rate constant between metronidazole and the hydroxyl radical, k_6 , of $1.98 \times 10^9 \text{ M}^{-1}\cdot\text{s}^{-1}$. All other rate constants and quantum yield values as listed in Table 5. Extinction coefficient of typical tap water used.

Reactor Radius (mm)	Residence Time (s)	Influent H_2O_2 Concentration (mg/L)			
		25	50	75	100
50	8.3	5.60	5.45	5.38	5.35
100	37	5.43	5.27	5.23	5.22
150	84	5.44	5.33	5.31	5.33
200	150	5.50	5.42	5.42	5.45
250	235	5.56	5.50	5.51	5.54

Notes:

All reported average effluent metronidazole concentrations in μM . Average effluent concentration calculated utilizing the trapezoidal rule.

Concentration in bold represents the lowest average effluent concentration observed.

Table 21. Average Effluent H_2O_2 Concentrations for Reactor 2 at Various Operating Conditions

Treating a solution of metronidazole with an initial concentration of 6 μM , and an alkalinity of 75 mg/L at a flow rate of 2.0 L/s. Model predictions obtained utilizing a value for the reaction rate constant between metronidazole and the hydroxyl radical, k_6 , of $1.98 \times 10^9 \text{ M}^{-1}\cdot\text{s}^{-1}$. All other rate constants and quantum yield values as listed in Table 5. Extinction coefficient of typical tap water used.

Reactor Radius (mm)	Residence Time (s)	Influent H_2O_2 Concentration (mg/L)			
		25	50	75	100
50	8.3	0.734	1.47	2.20	2.93
100	37	0.733	1.47	2.20	2.93
150	84	0.733	1.47	2.20	2.93
200	150	0.733	1.47	2.20	2.93
250	235	0.733	1.47	2.20	2.93

Notes:

All reported average effluent H_2O_2 concentrations in mM. Average effluent concentration calculated utilizing the trapezoidal rule.

C.5. Calculation of Average Effluent Concentrations from Matlab Output

Average effluent concentrations of metronidazole and H₂O₂ for Reactor 1 and Reactor 2 were determined utilizing the trapezoidal rule numerical integration technique. The average effluent concentration of any compound can be expressed as:

$$\overline{C_{eff}} = \frac{\iint C_{eff} r \cdot dr \cdot d\theta}{\iint r \cdot dr \cdot d\theta} = \frac{2\pi \int C_{eff} r \cdot dr}{2\pi \frac{1}{2} r^2 \Big|_{R_i}^R} = \frac{2 \int C_{eff} r \cdot dr}{R^2 - R_i^2} \quad (C.7)$$

Therefore, the trapezoidal rule was used to solve:

$$I = \int C_{eff} r \cdot dr \quad (C.8)$$

Applying the trapezoidal rule yields:

$$I = \int C_{eff} r \cdot dr = \sum \frac{(r_{i+1} - r_i)(C_{eff,j+1} r_{i+1} + C_{eff,j} r_i)}{2} \quad (C.9)$$

The value of I is then substituted into Equation C.8 to determine the value of $\overline{C_{eff}}$.

Below is an example of the calculation of the average effluent metronidazole concentration of Reactor 1 with a radius of 50 mm and an influent H₂O₂ dose of 100 mg/L.

r	C_{eff}	$C_{eff}r$	I_i
17	4.557	77.47	
18	4.666	83.99	80.73
19	4.766	90.54	87.27
20	4.856	97.11	93.83
21	4.937	103.69	100.40
22	5.012	110.27	106.98
23	5.080	116.85	113.56
24	5.143	123.43	120.14
25	5.200	130.01	126.72
26	5.253	136.58	133.30
27	5.302	143.15	139.87
28	5.347	149.70	146.43
29	5.388	156.25	152.98
30	5.426	162.79	159.52
31	5.462	169.32	166.06
32	5.495	175.83	172.58
33	5.525	182.34	179.09
34	5.554	188.83	185.58
35	5.580	195.31	192.07
36	5.605	201.78	198.55
37	5.628	208.23	205.01
38	5.649	214.68	211.45
39	5.669	221.11	217.89
40	5.688	227.53	224.32
41	5.706	233.93	230.73
42	5.722	240.33	237.13
43	5.738	246.72	243.52
44	5.752	253.09	249.90
45	5.766	259.45	256.27
46	5.778	265.80	262.63
47	5.790	272.14	268.97
48	5.801	278.47	275.30
49	5.812	284.79	281.63
50	5.822	291.10	287.94
		$I = \Sigma I_i$ ($\mu\text{M}\cdot\text{mm}^2$) =	6108.3
		$R^2 - R_i^2$ (mm^2) =	2211
		$\overline{C_{eff}}$ (μM) =	5.53

Therefore, the average effluent concentration of metronidazole is 5.53 μM .

**APPENDIX D – Multi-Lamp UV Reactor: Simulation Model
Development, Matlab Code, and Selected Output**

D.1. Background Calculations

For the multiple UV lamp reactor, as described in Section 3.1.2, the LVREA at any position in the reactor can be expressed as the sum of the contributions from all the lamps in the system. For Reactor 3, there are four lamps centered at $(0.5R, 0)$, $(0, 0.5R)$, $(-0.5R, 0)$, and $(0, -0.5R)$. As a result, for any location within the reactor, the total LVREA can be expressed as:

$$A = A_1 + A_2 + A_3 + A_4 \quad (D.1)$$

where A_1, A_2, A_3 and A_4 represent the LVREA due to lamps 1, 2, 3 and 4, respectively, and, based on the relationship shown in Equation 27, can be expressed as follows:

$$A_1 = \mu_s q_o \frac{R_i}{\sqrt{(x-0.5R)^2 + (y)^2}} e^{-2.303\mu_s(\sqrt{(x-0.5R)^2 + (y)^2} - R_i)} \quad (D.2)$$

$$A_2 = \mu_s q_o \frac{R_i}{\sqrt{(x)^2 + (y-0.5R)^2}} e^{-2.303\mu_s(\sqrt{(x)^2 + (y-0.5R)^2} - R_i)} \quad (D.3)$$

$$A_3 = \mu_s q_o \frac{R_i}{\sqrt{(x+0.5R)^2 + (y)^2}} e^{-2.303\mu_s(\sqrt{(x+0.5R)^2 + (y)^2} - R_i)} \quad (D.4)$$

$$A_4 = \mu_s q_o \frac{R_i}{\sqrt{(x)^2 + (y+0.5R)^2}} e^{-2.303\mu_s(\sqrt{(x)^2 + (y+0.5R)^2} - R_i)} \quad (D.5)$$

The outer radius of the quartz sleeve, R_i , was taken to be 17×10^{-3} m for all lamps used in Reactor 3.

The radiant energy flux at the outer surface of the quartz sleeve of each lamp, q_o , was calculated based on the UV lamp output of 36 W, and the outer surface area of the quartz sleeve:

Surface area of quartz sleeve:

$$S = 2\pi R_i L = 2\pi(17 \times 10^{-3} m)(1.2m) = 0.128m^2 \quad (D.6)$$

For each lamp in Reactor 3:

$$q_o = \left(\frac{36W}{0.128m^2} \right) \left(\frac{J/s}{W} \right) \left(\frac{mol\ photon_{254nm}}{4.713 \times 10^5 J} \right) = 5.97 \times 10^{-4} \frac{mol\ photon}{m^2 \cdot s} \quad (D.7)$$

The extinction coefficient of the aqueous solution was assumed to be constant for all locations within the photoreactor, and was calculated based on the extinction coefficient of tap water and in the influent concentration of H₂O₂. The UV absorptive properties of metronidazole were neglected due to its low influent concentration, and the influent concentration of H₂O₂ was used because it was assumed that very little H₂O₂ would be consumed, resulting in an almost uniform concentration of H₂O₂ throughout the reactor. Based on the above assumptions, the solution extinction coefficient, μ_s (m⁻¹), to the base 10, for the solution in the reactor can be written as:

$$\mu_s = \mu_w + \varepsilon_{H_2O_2} C_{H_2O_2,inf} = 10.0 + 1.86 C_{H_2O_2,inf} \quad (D.8)$$

where μ_w is the extinction coefficient of average tap water, in m⁻¹, and $\varepsilon_{H_2O_2}$ is the molar absorptivity (mM⁻¹m⁻¹) of H₂O₂, and $C_{H_2O_2,inf}$ is the influent concentration (mM) of H₂O₂.

D.2. Matlab Code Development – Reactor 3

Presented below is code for Matlab files “reactor3main.m”, which calls the predictor/corrector method to solve the set of ODE’s in file “reactor3model.m”.

For reference, concentrations of compounds in the reaction model are represented as follows:

- C_{RH} is represented as y(1);
- $C_{H_2O_2}$ is represented as y(2);
- $C_{\bullet OH}$ is represented as y(3);
- $C_{HO_2\bullet}$ is represented as y(4);
- $C_{HCO_3^-}$ is represented as y(5);
- $C_{CO_3^{2-}}$ is represented as y(6);
- $C_{\bullet CO_3}$ is represented as y(7).

The reaction rate constants and extinction coefficients are represented as follows:

- ϕ_1 is represented as phi1, and ϕ_7 is represented as phi7.
- k_2 is represented as k2, k_3 is represented as k3, etc.; and

Other parameters, as outlined in Section B.1, are represented as follows in the Matlab code:

- A is represented as A;
- A_1 is represented as A1, A_2 is represented as A2, etc.;
- q_o is represented as q0;
- μ_s is represented as mu.

In the file “reactor3model.m”, the final seven lines of code represent the chemical reaction model equations presented in Section 3.3. As an example, Equation 32 in Section 3.3, incorporating the relationship presented in Equation 26, can be written as:

$$\frac{\partial C_{RH}}{\partial \tau} = -R_{RH} = -k_6 C_{RH} C_{\bullet OH} - \phi_7 A f_{RH} = -k_6 C_{RH} C_{\bullet OH} - \phi_7 A \frac{\epsilon_{RH}}{\mu_s} C_{RH} \quad (D.9)$$

This equation appears as follows in the file “reactor3model.m”:

$$y(1) = -k6*y(1)*y(3)-phi7*A*2.2E2/mu*y(1) \quad (D.10)$$

All initial concentrations, as represented in the vector y_0 in the file “reactor3main.m”, are reported in mM. As such, initial H_2O_2 concentrations were converted from mg/L to mM using the molar mass of H_2O_2 of 34 mg/mmol. Initial concentrations of carbonate and bicarbonate ions are based on an alkalinity of 75 mg/L as $CaCO_3$ (see Appendix B, Section B.3).

In the file “reactor3main.m”, the value of the vector span is set to cover the retention time of within the reactor, $[0, \tau]$. The predictor/corrector method is called to solve the set of ODE’s in the file “reactor3model.m” for pairs of x - and y -coordinates, varying by 1 mm increments along each axis, for one quadrant of the reactor only. Pairs of x - and y -coordinates that fall within the location of the UV lamps were ignored. The matrix Y is created each time the predictor/correct method is called, providing the concentration profiles vs. retention time for all modeled compounds at a particular location within the reactor. The matrix Ans is used to hold the values of the effluent concentrations of metronidazole and H_2O_2 for each pair of x - and y -coordinates. Before storing the effluent concentrations in the matrix Ans , the concentration of metronidazole, $y(1)$ (or the first column of the answer matrix Y), is converted to μM .

Due to the nature of the information stored within the Ans matrix, the average effluent concentrations of metronidazole and H_2O_2 could be calculated directly by taking the average of the values stored in the Ans matrix.

CPU time required to complete simulation runs varied from 18 seconds (reactor radius of 50 mm) to 13 minutes 28 seconds (reactor radius of 250 mm) using an AMD Athlon 64 Processor 3200+.

File "reactor3main.m"

```
clear
clc

global xaxis yaxis Router

Router = 250e-3;

%span = [0 ##] <- residence time
span = [0 231.3] %span of duration of simulation

%y0 = [0.006 #### 0 0 0 .... <- Y2 initial value
y0 = [0.006 0.735 0 0 1.5 0 0] %vector of initial conditions in mmol/L

options = odeset('RelTol',1e-6,'AbsTol',[1e-6 1e-6 1e-6 1e-6 1e-6 1e-6 1e-6]);

i = 0;
j = 0;
for xaxis = 0:Router*1000;

    for yaxis = 0:Router*1000;

        if sqrt((xaxis-0.5*Router*1000)*(xaxis-0.5*Router*1000)+yaxis*yaxis)/1000 > 17e-3;
            if sqrt(xaxis*xaxis+(yaxis-0.5*Router*1000)*(yaxis-0.5*Router*1000))/1000 > 17e-3;
                if sqrt(xaxis*xaxis+yaxis*yaxis)/1000 <= Router;

                    i = i+1;
                    [t, Y]=ode15s(@reactor3model, span, y0, options);

                    Y(:,1)=Y(:,1)*1000; %convert concentration of metro into micromol/L

                    [m,n] = size(Y);

                    Ans(i,1)=xaxis;
                    Ans(i,2)=yaxis;
                    Ans(i,3)=Y(m,1);
                    Ans(i,4)=Y(m,2);

                    end
                    end
                    end

            end
        end

end

end

%Ans;
```

```
a = Ans(:,1); %x axis
b = Ans(:,2); %y axis
c = Ans(:,3); %concentration of metro in micromol/L
d = Ans(:,4); %concentration of peroxide in mmol/L

metro = mean(c) %average effluent metro concentration in micromol/L
perox = mean(d) %average effluent peroxide concentration in mmol/L

ti = 0:1:Router*1000;

[XI, YI] = meshgrid(ti,ti);

ZI = griddata(a, b, c, XI, YI);

[C,h] = contourf(XI, YI, ZI, 10);
clabel(C,h,'manual')
```

File "reactor3model.m"

```
function dy = reactor3model(t,y)
dy = zeros(7,1);    % a column vector

global xaxis yaxis Router

k2 = 3.0E4; %in mM^-1*s^-1
k3 = 6.5E6;
k4 = 1.5E3;
k5 = 1.4E7;
k6 = 1.98E6; %k of metro from model calibration
k8 = 2.0E4;
k9 = 3.7E5;
k10 = 8.0E2;

phil = 0.5;
phi7 = 0.0033; %in mmol photon^-1

%mu = (10+1.86*###) <-Initial H2O2 concentration
mu = (10+1.86*0.735); % Equation D.8

r1=sqrt((xaxis-0.5*Router*1000)*(xaxis-0.5*Router*1000)+yaxis*yaxis)/1000;
r2=sqrt(xaxis*xaxis+(yaxis-0.5*Router*1000)*(yaxis-0.5*Router*1000))/1000;
r3=sqrt((xaxis+0.5*Router*1000)*(xaxis+0.5*Router*1000)+yaxis*yaxis)/1000;
r4=sqrt(xaxis*xaxis+(yaxis+0.5*Router*1000)*(yaxis+0.5*Router*1000))/1000;

q0 = 5.97E-4; %in mmol photon/(m^2*s)
A1 = mu*q0*17E-3/r1*exp(-2.303*mu*(r1-17E-3)); %in mmol photon/(L*s),
Equation D.2
A2 = mu*q0*17E-3/r2*exp(-2.303*mu*(r2-17E-3)); %in mmol photon/(L*s),
Equation D.3
A3 = mu*q0*17E-3/r3*exp(-2.303*mu*(r3-17E-3)); %in mmol photon/(L*s),
Equation D.4
A4 = mu*q0*17E-3/r4*exp(-2.303*mu*(r4-17E-3)); %in mmol photon/(L*s),
Equation D.5

A = A1+A2+A3+A4; % Equation D.1

dy(1) = -k6*y(1)*y(3)-phi7*A*2.2E2/mu*y(1); % Equation 32

dy(2) = -phil*A*1.86/mu*y(2)-k2*y(2)*y(3)+k3*y(3)*y(3)+k4*y(4)*y(4); %
Equation 33

dy(3) = -k6*y(1)*y(3)+2*phil*A*1.86/mu*y(2)-k2*y(2)*y(3)-2*k3*y(3)*y(3)-
k5*y(3)*y(4)-k8*y(5)*y(3)-k9*y(6)*y(3); % Equation 34

dy(4) = k2*y(2)*y(3)-2*k4*y(4)*y(4)-k5*y(3)*y(4)+k10*y(7)*y(2); % Equation 35

dy(5) = -k8*y(5)*y(3)+k10*y(7)*y(2); % Equation 36
```

$dy(6) = -k_9 y(6) y(3);$ % Equation 37

$dy(7) = k_8 y(5) y(3) + k_9 y(6) y(3) - k_{10} y(7) y(2);$ % Equation 38

D.3. Summarized Matlab Output for Reactor 3

Table 22. Average Effluent Metronidazole Concentrations for Reactor 3 at Various Operating Conditions

Treating a solution of metronidazole with an initial concentration of 6 μM , and an alkalinity of 75 mg/L at a flow rate of 2.0 L/s. Model predictions obtained utilizing a value for the reaction rate constant between metronidazole and the hydroxyl radical, k_6 , of $1.98 \times 10^9 \text{ M}^{-1}\cdot\text{s}^{-1}$. All other rate constants and quantum yield values as listed in Table 5. Extinction coefficient of typical tap water used.

Reactor Radius (mm)	Residence Time (s)	Influent H ₂ O ₂ Concentration (mg/L)			
		25	50	75	100
50	5.1	5.18	4.88	4.74	4.67
100	33	4.21	3.75	3.60	3.54
150	81	4.06	3.68	3.61	3.63
200	146	4.15	3.87	3.85	3.92
250	231	4.31	4.10	4.12	4.21

Notes:

All reported average effluent metronidazole concentrations in $\mu\text{mol/L}$.

Concentration in bold represents the lowest average effluent concentration observed.

Table 23. Average Effluent H₂O₂ Concentrations for Reactor 3 at Various Operating Conditions

Treating a solution of metronidazole with an initial concentration of 6 μM , and an alkalinity of 75 mg/L at a flow rate of 2.0 L/s. Model predictions obtained utilizing a value for the reaction rate constant between metronidazole and the hydroxyl radical, k_6 , of $1.98 \times 10^9 \text{ M}^{-1}\cdot\text{s}^{-1}$. All other rate constants and quantum yield values as listed in Table 5. Extinction coefficient of typical tap water used.

Reactor Radius (mm)	Residence Time (s)	Influent H ₂ O ₂ Concentration (mg/L)			
		25	50	75	100
50	5.1	0.732	1.46	2.19	2.93
100	33	0.729	1.46	2.18	2.91
150	81	0.728	1.45	2.18	2.91
200	146	0.728	1.45	2.18	2.91
250	231	0.728	1.45	2.18	2.91

Notes:

All reported average effluent H₂O₂ concentrations in mM.

D.4. Example Concentration Profiles Within Reactor 3

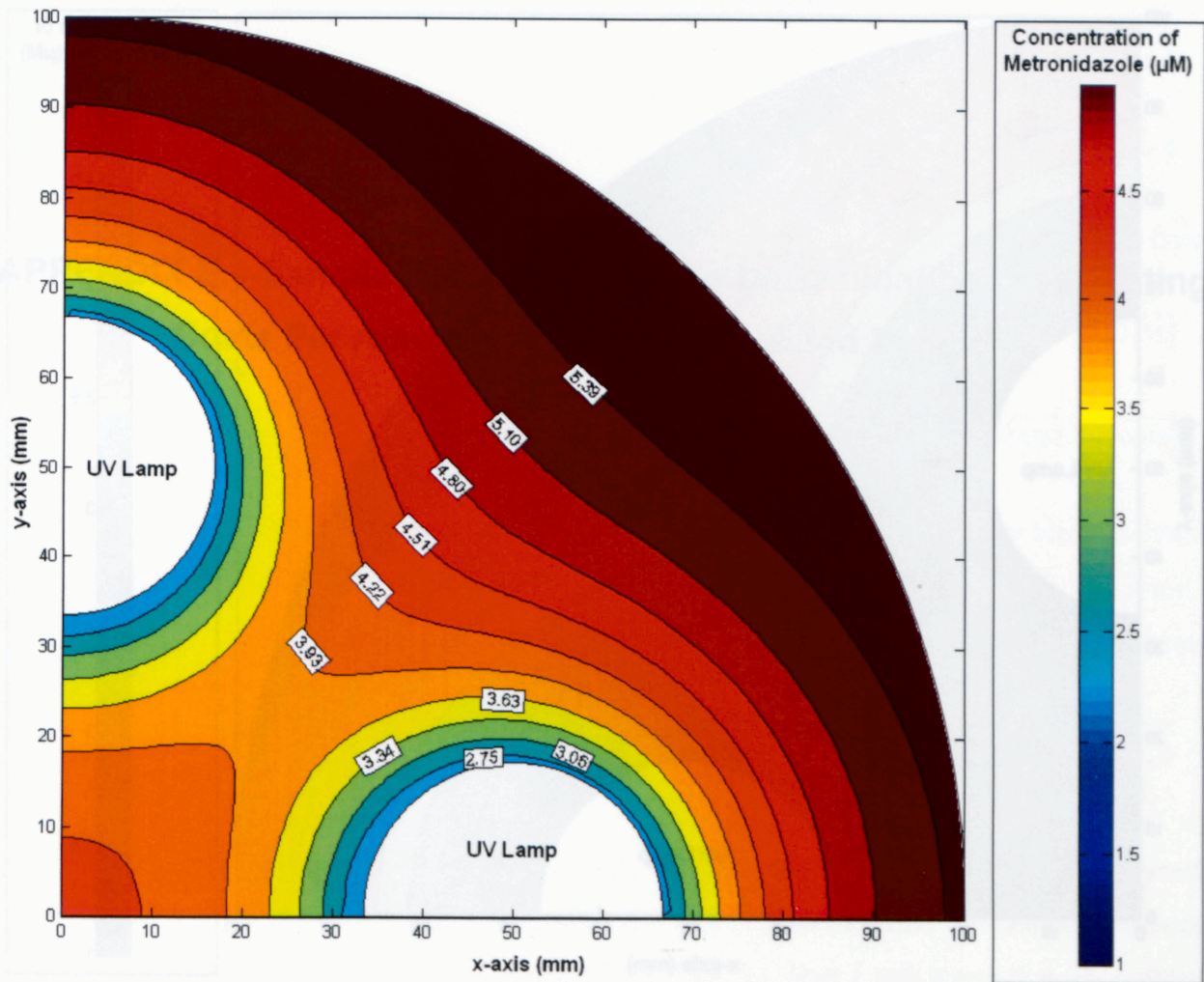


Figure 14. Metronidazole Concentration Profile for a Quadrant of Reactor 3 with $[\text{H}_2\text{O}_2]_{\text{inf}} = 100 \text{ mg/L}$ and $R = 100 \text{ mm}$ at the middle of the reactor, a distance of 1.2 m from the reactor inlet

Treatment of a $6 \mu\text{M}$ metronidazole solution with an alkalinity of 75 mg/L and pH of 6, at a flow rate of 2.0 L/s . Shown above at an equivalent residence time of 17 seconds, with an average metronidazole concentration of $4.56 \mu\text{M}$.

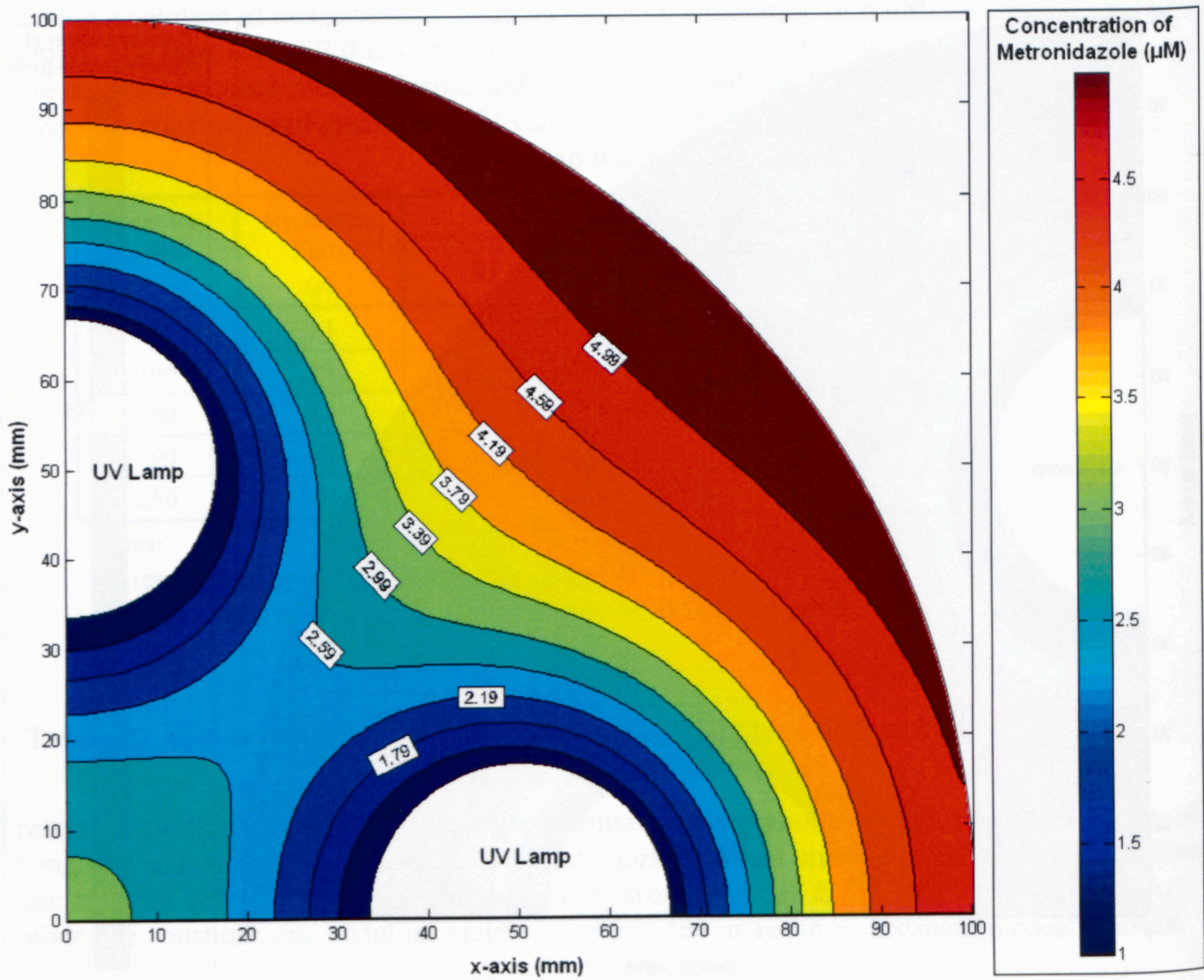


Figure 15. Metronidazole Concentration Profile for a Quadrant of Reactor 3 with $[H_2O_2]_{inf} = 100$ mg/L and $R = 100$ mm at the reactor outlet, a distance of 2.4 m from the reactor inlet
 Treatment of a 6 μ M metronidazole solution with an alkalinity of 75 mg/L and pH of 6, at a flow rate of 2.0 L/s. Shown above at an equivalent residence time of 33 seconds, with an average metronidazole concentration of 3.54 μ M.

**APPENDIX E – Sample Calculation for the Determination of Operating
Costs Per Amount of Target Compound Removed**

The following sample calculation presents the methodology used to determine the operating cost (\$/mmol metronidazole removed) for the Reactor 1 under the following operating conditions:

$$[H_2O_2]_{inf} = 25 \text{ mg/L} = 0.735 \text{ mM}$$

$$[metronidazole]_{inf} = 6 \text{ } \mu\text{M}$$

$$R = 50 \text{ mm}$$

Based on the results presented in Appendix B, for the above set of operating conditions:

$$[H_2O_2]_{eff} = 5 \text{ mg/L} = 0.734 \text{ mM}$$

$$[metronidazole]_{eff} = 5.714 \text{ } \mu\text{M}$$

Electrical costs are based on the total lamp wattage. In the case of Reactor 1, the input wattage of each UV lamp used is 75 W. Based on an operating cost of \$0.11/kWh, the electrical operating costs, S_E , to operate both lamps within Reactor 1 are:

$$S_E = 2 \left(\frac{\$0.11}{kWh} \right) (75W) \left(\frac{kW}{1,000W} \right) \left(\frac{h}{60 \text{ min}} \right) \left(\frac{\text{min}}{60s} \right) = 4.58 \times 10^{-6} \frac{\$}{s} \quad (\text{E.1})$$

Chemical costs are based on the cost for H_2O_2 , which is a function of influent H_2O_2 concentration, and the cost for NaOCl, which is a function of influent H_2O_2 concentration. From Equation 29, it is known that 1 mole of NaOCl is required to quench 1 mole of H_2O_2 . Based on a cost of \$0.14/L for a 12% (w/v) NaOCl solution, and \$1.10/kg for H_2O_2 , the chemical operating costs, S_C , are:

$$S_C = \left(\frac{\$0.14}{L \text{ NaOCl Sol'n}} \right) \left(\frac{L \text{ NaOCl Sol'n}}{120g \text{ NaOCl}} \right) \left(\frac{74.44g \text{ NaOCl}}{\text{mol NaOCl}} \right) \left(\frac{\text{mol NaOCl}}{\text{mol } H_2O_{2,eff}} \right) \left(\frac{0.734 \times 10^{-3} \text{ mmol } H_2O_{2,eff}}{L} \right) \left(\frac{2.0L}{s} \right) + \left(\frac{\$1.10}{kg \text{ } H_2O_{2,inf}} \right) \left(\frac{kg}{1,000g} \right) \left(\frac{34g \text{ } H_2O_2}{\text{mol } H_2O_2} \right) \left(\frac{0.735 \times 10^{-3} \text{ mol } H_2O_{2,inf}}{L} \right) \left(\frac{2.0L}{s} \right) = 1.82 \times 10^{-4} \frac{\$}{s} \quad (\text{E.2})$$

Therefore, the value of the ratio of operational cost to the amount of target compound removed,

F , can be calculated as follows:

$$F = \frac{S_E + S_c}{Q(C_{RH,inf} - C_{RH,eff})} = \frac{4.583 \times 10^{-6} \frac{\$}{s} + 1.825 \times 10^{-4} \frac{\$}{s}}{\left(2.0 \frac{L}{s}\right) \left(6.000 \times 10^{-3} \frac{mmol}{L} - 5.714 \times 10^{-3} \frac{mmol}{L}\right)} = 0.33 \frac{\$}{mmol} \quad (E.3)$$